Fuel Consumption and Pollutant Emissions of Spark Ignition Engines During Cold-Started Drive Cycles

Nicholas Julian Darnton

Thesis submitted to the University of Nottingham for the degree of Doctor of Philosophy,

June 1997

Contents List

Abstract

"Fuel Consumption and Pollutant Emissions of Spark Ignition Engines During Cold-Started Drive Cycles", N J Darnton

This thesis details the development and evaluation of a procedure to predict the fuel consumption and pollutant emissions of spark ignition engines during cold-started drive cycles. Such predictions are of use in the early development and optimisation of an engine and vehicle combination with regard to legislated limits on vehicle performance over defined drive cycles. Although levels of pollutant emissions are the main focus of legislation, reducing fuel consumption is also of interest and drive cycle fuel consumption figures provide a useful benchmark of vehicle performance appraisals.

The procedure makes use of a combination of engine friction models and experimentally defined correction functions to enable the application of fully-warm engine test bed data to cold-start conditions. This accounts for the effects of engine temperature on friction levels, mixture preparation and start-up transient behaviour. Experimental data to support the models and assumptions used are presented and discussed. Although not an essential part of the procedure, neural networks have been used to characterise the fully-warm engine mapping data. These are shown to provide an effective way of interpolating between engine mapping points. To facilitate the prediction of tail-pipe emissions, a simple catalyst efficiency model has been included and the complete procedure incorporated into a single software package enabling second-by-second fuel and emissions flow rates to be predicted for a given engine and vehicle combination over a defined drive cycle. This package is called CECSP or the Cold Emissions Cycle Simulation Program. The program has been designed to run on PC machines.

The procedure has been validated by application to a typical 1.8 litre medium sized vehicle driven over the ECE+EUDC drive cycle and the predictions found to be within the target accuracy of +/-5% for fuel consumption and +/-10% for engine-out emissions. Envisaged applications of the procedure to rank the sources of increased fuel consumption and emissions due to cold-starting and engine and vehicle details are outlined.

Acknowledgements

I would like to express my thanks to Professor Paul Shayler for his advice and guidance throughout my research work and during the writing of this thesis. Thanks also go to John McGhee for maintaining the rig and his help throughout the project and to the rest of the Engines Group, past and present, for their assistance and humour.

The research has been generously supported by Ford Motor Company and I would like to thank Dr Tom Ma for his enthusiasm and interest in this research.

Finally, thanks go to my family and friends for their support and encouragement during my education and, in particular, during the writing of this thesis.

Abbreviations

AFR	Air/fuel ratio by mass (measured using a UEGO sensor)
bmep	Brake mean effective pressure
CCC	Close-coupled catalyst
CECSP	Cold Emissions Cycle Simulation Program
CO	Carbon monoxide
CO_2	Carbon dioxide
DOHC	Double overhead camshaft
EC	European Community
ECE+EUDC	European drive cycle (also termed NEDC)
ECT	Engine coolant temperature
EECIV	Electronic engine control unit, version 4
EGR	Exhaust gas recirculation
EHC	Electrically heated catalyst
FID	Flame ionisation detector
fmep	Friction mean effective pressure
FTP	Federal test procedure
HC	Hydrocarbons
HEGO	Heated exhaust gas oxygen
HO	High output
IMechE	Institute of Mechanical Engineers
imep	Indicated mean effective pressure
isco	Indicated specific carbon monoxide emissions
isfc	Indicated specific fuel consumption
ishc	Indicated specific hydrocarbon emissions
$isno_x$	Indicated specific nitrous oxide emissions
LEV	Low emission vehicles
MAP	Manifold absolute pressure

MBT	Minimum advance for best torque
NEDC	New European Drive Cycle
NO_x	Nitrous oxides
PC	Personal computer
RON	Research octane number
RPM	Revolutions per minute
TDC	Top dead centre
TLEV	Transitional low emission vehicles
UBC	Underbody catalyst
UEGO	Universal exhaust gas oxygen
ULEV	Ultra low emission vehicles
ZEV	Zero emission vehicles

Nomenclature

D	Catalyst dead time (s)
F	Initial friction correction factor
L	Catalyst light-off time (s)
M_{engine}	Engine brake torque (Nm)
m_a	Mass of air induced (kg)
m_e	Mass of recycled exhaust gas (kg)
m_{inj}	Mass of fuel injected per stroke (kg)
$\dot{m}_f$	Combusted fuel mass flow rate (g/hr)
$\dot{m}_{inj}$	Injected fuel mass flow rate (kg/s)
$\dot{m}_{overall}$	Overall fuel mass flow rate (kg/s)
$\dot{m}_{unaccounted\ for}$	Unaccounted for fuel mass flow rate (kg/s)
N	Engine speed (rpm)
n_R	Number of revolutions per cycle
P	Pressure (N/m^2)
$\dot{P}$	Power (W)
$\dot{P}_{Indicated}$	Indicated power (kW)
$\dot{P}_a$	Accessory friction power loss (W)
$\dot{P}_{friction}$	Predicted friction power loss (W)
$\dot{P}_{KE}$	Power required to increase vehicle kinetic energy (W)
$\dot{P}_{prf}$	Total friction power loss (W)
$\dot{P}_{rf}$	Rubbing friction power loss (W)
$\dot{P}_{rl}$	Road load power (W)
R_{FDR}	Final drive ratio
R_{gear}	Gear ratio
r_{wheel}	Driving wheel radius (m)
T	Start temperature (°C)
V	Volume (m^3)

V_d	Displaced volume per cylinder (m^3)
V_s	Engine swept volume (m^3)
v_{veh}	Vehicle speed (km/hr)
$W_{c,i}$	Net indicated work (J)
α	Friction correction factor
γ	Delta HC constant
η_{cat}	Fully-warm catalyst conversion efficiency
η_t	Catalyst conversion efficiency at time t
η_{trans}	Transmission efficiency
ν	Kinematic viscosity (m^2/s)

Chapter 1

Introduction

1.1 Background to Thesis

Pollution of the environment by emissions from road traffic and competitive pressures to improve fuel economy are major concerns during research and development efforts on spark ignition engines. With regard to levels of emissions, vehicle performance is assessed over a drive cycle of operating conditions for which maximum limits on the masses of particular pollutants have been set by legislation. These limits have been revised downwards through a series of amendments to the legislation since the 1970's. In some cases, the test procedure and drive cycle details have also been revised over the same period. Most recently, revisions designed to give due weight to the early period of engine operation, when the engine is not fully-warm and when post-combustion systems for emissions control may not be operating efficiently, have been debated and will be fully implemented before the turn of the century.

The current European ECE+EUDC and USA FTP-75 drive cycles are designed to represent typical patterns of vehicle operation on these continents. For this reason, and because vehicles must pass tests on emission limits based on these cycles before introduction to the market, they are particularly important sets of operating conditions which manufacturers focus attention on during engine and vehicle development programs. In addition to emissions-related developments, the same cycles are used to benchmark fuel economy values. However, it is relatively late in a vehicle development program that final specifications are available for evaluation, and many critical engineering decisions must be made prior to this stage.

A technique to predict vehicle performance over drive cycles given information available relatively early on in a development programme has been investigated. This has major practical applications in, for example, screening possible design variants for potential impact on vehicle performance. At the outset of the investigation, no system was available to provide this facility. Of particular interest has been the problem of predicting the performance of vehicles during the early part of a drive cycle before the engine is fully-warm. In general terms, the objective of the investigation has been to provide a computer based system for the prediction of fuel consumption and pollutant emissions, for any specified engine, transmission and vehicle combination. The computer software which has been produced is termed CECSP (Cold Emissions Cycle Simulation Program). The experimental and theoretical studies carried out to develop CECSP, and applications of this, form the main body of the work described in the thesis.

1.1.1 European Emissions Legislation

The three main pollutant emissions produced by the spark ignition engine are:

- Carbon monoxide (CO). This is a colour free, odour free highly poisonous gas which is readily absorbed into the blood reducing its ability to supply oxygen around the body. A volumetric concentration of 0.3% can result in death in humans within 30 minutes.

- Unburned Hydrocarbons (HC). These are present as both unburned fuel and partially reacted fuel components, some of which are known to be carcinogenic. In certain conditions they react with low level ozone and nitrogen oxides to form photochemical smog.

- Nitrogen Oxides (NO and NO_2). Generally referred to collectively as NO_x since NO is readily oxidised in air to form NO_2. NO_2 is in itself a poisonous gas but, in addition, it is readily soluble in water forming nitric acid. Thus, NO_x emissions are believed to cause acid rain which is

thought to cause damage to both vegetation and buildings.

The bulk of the exhaust gases are made up of nitrogen, carbon dioxide and water. Although non-poisonous, carbon dioxide emissions are believed to contribute to the "green-house effect". These may become the focus of future emissions legislation. However, the strictest legislation deals with emissions of HC, CO and NO_x and requires manufacturers to ensure tail-pipe emissions of vehicles are no more than a prescribed limit for a carefully defined vehicle operating regime or drive cycle. The legislation defines the exact drive cycle for the vehicle performance to be assessed over and certain conditions which must apply to enable test results to be representative for different vehicles and manufacturers.

Vehicle exhaust emissions have been the focus of European legislation ever since the 1970's when a British Standard to limit 'visible' emissions was incorporated into an EC Directive [1.1]. As road traffic has increased the legislation has been tightened in response to environmental concerns and with the aim of bringing European legislation in line with the more stringent US standards. In 1985, the so-called 'Luxembourg Agreement' marked a significant step in European emissions legislation as it effectively ensured that catalytic convertors would be required to meet future emissions standards in Europe, as had been the case in the USA for several years. The agreement culminated in the adoption of EC Directive 91/441/EEC [1.2]. This directive finally brought European legislation in line with US 1983 emissions standards. US legislation has typically been led by the State of California and in September 1990, the California Air Resources Board (CARB) introduced further legislation cutting the allowed emissions of new vehicles substantially in a series of stages, as shown in Table 1.1. In Europe, new legislation and proposals aimed at tightening the regulations defined in EC Directive 91/441/EEC have already been introduced, as shown in Table 1.2. The proposed stages 3 and 4 of the European legislation, to be introduced in 2000 and 2005, are expected to bring European requirements in line with the Californian ULEV standard to be introduced in 1997. Different approaches are used to

determine the emissions levels from actual motor vehicles for comparison with the allowed limits in the United States and Europe. In the US, the Federal Test Procedure (FTP) is used while in Europe emissions are evaluated using the New European Drive Cycle (NEDC) also known as the ECE+EUDC drive cycle. Although different in detail, these two cycles both define a series of engine idling and loading repeated in a manner to define a vehicle speed characteristic representative of the typical driving behaviour experienced by production vehicles. In addition to the drive cycle profile, the start-up temperature of the engine and allowed conditioning time before emission sampling begins is carefully defined with the intention of producing a repeatable test procedure which accurately represents the relative performance of a wide range of vehicles from different manufacturers. For the purpose of this work, the NEDC has been used in accordance with current and proposed European emissions legislation already discussed.

1.1.2 The New European Drive Cycle (NEDC)

The NEDC consists of an elementary urban cycle repeated four times followed by the extra-urban cycle as shown in Figure 1.1. Each of the elementary cycles last 195 seconds and the extra-urban cycle lasts 400 seconds giving a total cycle length of 1180 seconds. The cycle is defined as a series of vehicle speed and gear number points with gear changes defined at appropriate points in the cycle, according to EC Directive 91/441/EEC. Suitable tolerances are defined in the legislation for both vehicle speed and time from start to ensure cycle repeatability is maintained to as high an accuracy as possible. Current European legislation (EC Stage 2) defines a start/soak temperature of between 20°C and 30°C and permits a period of 40 seconds of engine idling before emission sampling begins, as illustrated in Figure 1.1. Possible changes to this procedure are currently under consideration and could include the removal of the initial conditioning period and a reduction of the start/soak temperature [1.4]. CARB have already adopted cold-start CO legislation at a test temperature of -7°C for current technology vehicles although it is not yet known if the ULEV legislation will require this test

temperature. In Europe, it is thought more likely that the start/soak temperature will eventually be reduced to between 0°C and 5°C to reflect patterns of vehicle use and operating conditions in northern Europe more accurately without imposing the additional costs on industry of sub-zero test temperatures. Current proposals, however, suggest that test cycle modifications will be limited to the elimination of the 40 second conditioning period [1.5]. In addition, individual targets for HC and NO_x are to be introduced from Stage 3 onwards instead of a single target for HC+NO_x.

1.1.3 Fuel Consumption and Emissions During Cold-Start and Warm-up

The current European drive cycle includes a cold-start from a soak temperature of between 20°C and 30°C and as such is designed to represent a typical urban journey starting with a cold engine. The vehicle speed and gear number profile adopted for all light-duty vehicles does not account for variations in driving style and the different manner in which vehicles of varying performance are likely to be driven, as discussed by Andre et al [1.6]. Work done as part of the EC DRIVE program may result in a modified drive cycle format, but currently the ECE+EUDC drive cycle is believed to provide the most representative emissions performance comparisons between vehicles and as such is used extensively in the work presented in this thesis. Given that all European vehicles are assessed over the same drive cycle under the same operating conditions, techniques for reducing total emissions production over this drive cycle are of paramount interest to manufacturers. Whilst pollutant emissions are of primary importance, fuel consumption is of increasing interest and provides a useful benchmark for vehicle performance appraisals. Work done at the University of Melbourne [1.7] indicates that for hot-start operation the main influences on fuel consumption and exhaust emissions are vehicle acceleration and speed, revealing the importance of overall vehicle mass and choice of transmission ratios when applied to the fixed vehicle speed profile of the ECE+EUDC drive cycle. However, the primary area of concern in the current drive cycle is the initial period following the cold-start when various effects combine to give both poor fuel economy and increased

emission levels. This period contributes significantly to actual overall vehicle pollution in northern Europe. It has long been established that vehicle exhaust emissions from vehicles fitted with catalytic convertors are at their highest in the period immediately following a cold-start before catalyst light-off occurs, and that the driving conditions which yield the greatest adverse effects on emissions are at low ambient temperature and during urban driving [1.8]. Results from the United States Department of Energy show that vehicles used for short cold-start trips consume fuel at a much higher average rate than during long trips, and that the effect is magnified with decreasing ambient temperatures [1.9]. Furthermore, averaged over weekday trips in the 100 largest metropolitan areas in the United States, fuel consumption is between 13% and 17% higher than it would be if fuel consumption rates during engine warm-up were those of fully-warm vehicles [1.10]. Approximately one third of all motor vehicle travel in the United States consists of trips no more than ten miles in length [1.11]. A similar picture exists in Europe, where the bulk of weekday travel occurs in urban areas and starts with a cold engine. In fact, according to Andre, approximately one third of all journeys start with a cold engine (coolant and oil temperatures below 30°C) and a similar proportion are completed before the engine is fully-warm [1.12]. Thus the cold-start element of the European drive cycle is of vital significance to the overall fuel consumption and emissions produced over the cycle period, since the relative contribution of pollutants emitted during vehicle warm-up has been magnified due to the outstanding performance of modern catalytic convertors nearly eliminating pollutants emitted from fully-warm engines. This is most important when considering tail-pipe exhaust emissions, particularly those of HC, as more than 80 per cent of these are generated in the warm-up phase before the catalytic convertor has reached its normal operating temperature [1.13]. The principle sources of HC emissions in the exhaust pipe have been reviewed by Heywood et al [1.14]. These can be summarised as follows:

- Release of HC from narrow crevice volumes within the cylinder where the combustible mixture escapes burning because the flame cannot penetrate into these narrow volumes.

- Flame quenching by the cold cylinder walls, resulting in the appearance of a thin layer of unburned mixture adjacent to the relatively cold surfaces in the combustion chamber.
- Absorption of fuel hydrocarbon components into thin oil layers in certain parts of the cylinder before combustion takes place and subsequent desorption at a later stage in the cycle.
- Leakage past the exhaust valve between compression and combustion. This effect is particularly significant in high mileage vehicles where worn valves and valve seats can lead to significant leakage.
- Presence of liquid fuel on the combustion chamber walls during early seconds of engine operation after a cold-start escaping combustion and passing directly into the exhaust stream. Further work by Heywood [1.15] suggests that liquid fuel films around the inlet valve can last for periods in the region of 60 seconds after a 20°C start.
- Work by Shayler et al [1.16] suggests that poor mixture preparation in the inlet manifold due to injector location and intake geometry can lead to a degree of mixture stratification in the cylinder resulting in some fuel rich mixture escaping combustion and entering the exhaust pipe.

Each of the above mechanisms have a different effect on total HC emissions depending on the operating conditions and state of the engine with the result that HC emissions are poorly understood and difficult to predict, particularly in the period immediately following a cold-start.

1.2 Aims of Work

The aims of developing CECSP and the associated procedures to apply this are to predict fuel and engine-out emission mass flow rates on a second-by-second basis for the ECE+EUDC drive cycle and other patterns of operating conditions which might be specified. The procedure was to require only fully-warm engine mapping data to characterise the engine under consideration and the vehicle was to be defined by inputing appropriate definition parameters. As such, the procedure was intended to provide a means of determining to within a target

accuracy of 10% both the expected fuel consumption and engine-out (also termed feedgas) emission levels expected for a given engine/vehicle combination and the effects on these values of changing the various engine, vehicle and drive cycle variables modelled.

For a cold-start drive cycle, fuel consumption and engine-out emissions, particularly those of HC, are influenced by the increased friction levels and fuel enrichment associated with the cold-start and warm-up process. Engine-out emission production mechanisms, particularly those for HC emissions, are involved and complex. Tail-pipe emissions are influenced by the time taken for the catalyst to reach its normal operating temperature and by the conversion efficiency of the catalyst itself. In addition, actual vehicle and drive cycle details, such as total weight, transmission ratios and aerodynamics, will influence the total fuel consumption and emission levels. Thus, improvements in vehicle drive cycle emission performance can come from many different areas of both engine and vehicle design. The prediction procedure was intended primarily to enable the effects on total fuel consumption and engine-out emissions of HC, CO and NO_x of changing various vehicle and drive cycle parameters to be examined for both a fully-warm and cold-started drive cycle. Once engine-out emissions have been predicted, tail-pipe values can be calculated from basic knowledge of catalyst light-off and conversion performance.

CECSP uses fully-warm steady-state dynamometer data to characterise the engine fuel and emissions performance for the required operating conditions imposed by the drive cycle under consideration. In general, engine maps are produced for fully-warm operating conditions, which are most easily controlled and provide the bulk of the information needed for engine development. In addition, these maps are usually available at an early stage of engine development and so predicting drive cycle performance from such maps will enable drive cycle performance of pre-production vehicles to be assessed early in their development period. Figure 1.2 shows a brief outline of the procedure. A simple road load

model is used to deduce engine speed and brake load from a given vehicle and drive cycle description. An engine thermal model is used to predict engine friction levels on a second-by-second basis throughout the drive cycle for both a fully-warm start and a cold-start enabling indicated loads to be calculated, and then the fully-warm indicated engine map is used to deduce instantaneous fuel and emission mass flow rates. The emissions mass flow rates then need to be adjusted to account for the expected changes during engine warm-up and both the fuel and emissions flow rates adjusted to account for the transient effects associated with a cold-start. This procedure relies on several assumptions and engine models derived from experimental data. Figure 1.3 shows the inputs required and a brief summary of the route to achieve the desired outputs.

1.3 Thesis Content

This thesis deals with the various concepts and models which need to be combined to produce the final drive cycle prediction procedure. The following sections detail each of these and how this thesis covers the work done in developing the procedure.

1.3.1 Engine Mapping

The prediction procedure outlined in Figure 1.2 is based on the assumption that fully-warm engine mapping data will be used to characterise the engine under consideration. Fully-warm data is generally available even at an early stage in engine development. In order to use this to determine fuel and emissions mass flow rates at non-fully warm operating conditions the effects of differences between fully-warm and warm-up conditions on performance must be accounted for. A key step towards this is to recast the engine data, based on the rationale given in Chapter 4, into indicated operating conditions. The indicated mean effective pressure (imep), defined as the total work done by the engine is calculated from the brake mean effective pressure as:

$$imep = bmep + fmep \quad (1.1)$$

where fmep is the friction mean effective pressure. Thus, if the fmep at each point in the cold-start drive cycle is determined, it should be possible to infer the fuel and emissions flow rates from the fully-warm engine map, providing the effect of engine temperature on the relationship between indicated operating conditions and exhaust flow rates can be defined. Although not essential, in this application a neural network has been used as a simple way of characterising the engine map and interpolating between the fixed fully-warm engine mapping points to determine fuel and emissions mass flow rates at each point in the drive cycle. Chapter 2 deals with the engine mapping data processing and details the application and optimisation of the neural network to characterise the engine map.

1.3.2 Predicting Cold-Start Fuel Consumption and Emissions

In order to apply the fully-warm indicated operating map to the indicated load profile of the cold-start drive cycle, the effect of both engine operating temperature and the transient effects of start-up on the indicated engine operating map has to be established. Chapter 4 deals with the influence of engine coolant temperature on fuel consumption and the development of a model to predict the increase in fuel consumption during and immediately following a cold-start. Chapter 5 deals with the corresponding effect on engine-out exhaust emissions with particular attention being paid to the increase in HC emissions during the early minutes of engine operation. When applying the fully-warm engine map to the cold-started drive cycle, the engine management calibrations for parameters such as spark timing and EGR rate are, for simplicity, assumed to be identical to the fully-warm calibration.

Predicting the increased engine friction and engine temperature distribution during the cold-started drive cycle is achieved by using a program for modelling engine thermal systems called PROMETS [1.17] previously developed at the University of Nottingham. Chapter 6 details the basic structure and validation of

this model and its application to the drive cycle prediction procedure. Chapter 7 outlines the combination of the various elements of the prediction procedure that comprise CECSP.

1.3.3 Assessment of Model Performance

Chapters 8 and 9 detail applications of the CECSP software. The flexibility of the prediction software is investigated and its application to various possible engine/vehicle development programs illustrated. The effect of changes to engine/vehicle details such as total vehicle mass, transmission ratios and engine management strategy are discussed and possible future applications of the procedure suggested. Initially developed to predict engine-out emissions, the extension to predict tail-pipe emissions and account for appropriate after-treatment considerations is considered and the implication of the various proposed drive cycle changes investigated. The use of the software to prioritise the principle sources of emissions during the ECE+EUDC drive cycle, and possible areas of emissions reduction, is demonstrated.

1.4 Contribution of Thesis to Engine Development

The main objective of the work presented in this thesis was to develop a simple prediction procedure, based on fully-warm dynamometer test-bed data, to predict to within a target accuracy of 10% the total fuel consumption and engine-out emissions produced for a typical drive cycle. The work has resulted in the production of a software package (CECSP) which predicts fuel and emissions mass flow rates at each point in a defined drive cycle for given engine fully-warm mapping data and defined vehicle characteristics. The procedure requires no cold engine data and assumes that fully-warm engine calibration settings apply throughout the drive cycle, and as such provides a useful approximation of expected drive cycle performance for a loosely defined engine and vehicle combination. The procedure enables the relative effects of changing many engine and vehicle parameters to be examined and as such could be used to prioritise areas of performance improvement during vehicle development. In addition, the

requirement of fully-warm engine mapping data only means that the procedure can be used at an early stage of engine development to predict expected drive cycle results before engine and vehicle design parameters are fixed and before experimental measurements can be taken.

Chapter 2

Characterising Engine Mapping Data Using Neural Networks

2.1 Introduction

Details of how fully-warm engine performance maps have been exploited in the modelling of cold-started drive cycle conditions will be described in later chapters. As a precursor to this, general trends in fully-warm steady-state engine behaviour and how these can be characterised in a suitable form are described here. In particular, the use of neural networks to relate independent and dependent engine state variables is considered. Although this is not an essential part of the model representing the physical processes involved, this form of data handling plays an important role in enabling efficient use of the model.

The major operating variables that influence spark ignition engine performance are engine speed, load, air/fuel ratio (AFR), spark timing and exhaust gas recirculation rate (EGR) [2.1]. The engine mapping data used in the work presented here has been derived from engines mapped with production engine management strategies. Hence the spark timing and EGR rate for a given engine speed, load and AFR during fully-warm operation are fixed by the strategy and so the engine variables of interest are limited to these three. The major part of this chapter deals with characterising engine mapping data in terms of just engine speed, load and AFR and assumes that the spark timing and EGR rate are determined by the engine management strategy, since engine data in this format was readily available. However, in order to provide a more complete picture of engine map characterisation, the effect of changing the spark timing and EGR rate calibrations is also be considered here. This requires a much larger and more

complex engine map database but such an engine map could then be used to enable the effects of changing spark timing and EGR rate during a cold-started drive cycle to be assessed.

Previous work carried out by Bacon [2.2, 2.3] has demonstrated that providing patterns exist within a sequence of data values, neural networks can be used to associate these with a corresponding set of input values. Neural network computing was originally conceived as a model for the brain and, as such, neural networks comprise several interconnected processing units connected in parallel. In essence, a neural network 'learns' the relationship between input and output parameters in a process called 'training'. The trained neural network can then be used to generate output values for input patterns not included in the training data. Bacon used a neural network to emulate certain elements of a current engine control strategy and found the interpolation and extrapolation accuracy to be high. In particular, the neural network approach was found to provide a significant time saving when compared to the standard control algorithm development times. Work by Stevens et al [2.4] demonstrated the use of neural networks to determine relationships between engine-out emissions and engine state variables and concluded that very accurate predictions of engine performance could be made providing the engine database was sufficiently large to characterise the engine performance map. Hence, neural networks provide a simple, time saving, alternative to regression analysis to characterise engine mapping data. In the work presented in this thesis a neural network has been optimised to predict fuel consumption and emissions as a function of engine speed, load and AFR. In addition, work has been carried out to investigate the possibility of using a neural network to simulate a complete engine map with engine speed, load, AFR, spark timing and EGR rate as the inputs. The characteristics of the engine maps used are given below. In addition, a brief description of neural networks and an overview of their application to engine mapping is given. A comprehensive introduction to the theory and application of neural network processing techniques can be found in publications by Rumelhart and McClelland [2.5-2.7].

2.2 Engine Map Characteristics

The engine mapping data are generally available as a series of steady-state fully-warm brake load sweeps at a range of engine speeds and AFRs. The engine performance parameters of interest here are fuel, HC, CO and NO_x mass flow rates. In order to keep the amount of data to be handled to a minimum the range of engine speeds and loads covered by the mapping data was restricted to that imposed by the ECE+EUDC drive cycle. By way of illustration, the results used in this chapter are taken from a 1.8 litre Ford Zetec engine. This 4-valve per cylinder engine is representative of engines currently in service and is designed to operate at stoichiometric mixture setting at most operating conditions. First, the influence of operating conditions for fixed tail-pipe AFR mixture calibration is considered. Figures 2.1 and 2.2 show a typical dataset plotting fuel and emissions against engine speed and brake load for stoichiometric AFR operation and with spark timing set to MBT (Minimum advance for Best Torque). Fuel mass flow rates increase with both engine speed and load in proportion to air mass flow rate increases, to maintain a constant stoichiometric tail-pipe AFR. Similarly, CO mass flow rates increase uniformly with both engine speed and load because CO concentrations are effectively dependent only on the AFR, which is constant. HC and NO_x emissions behave less uniformly due to the variation in volumetric concentration with both engine speed and load. Consequently, the HC and NO_x mass flow rates do not follow the fuel mass flow rate variations as closely as the CO flow rates.

A more detailed picture of the effect of operating conditions on engine-out emissions can be obtained by considering emission concentrations. Again considering only stoichiometric mixture settings, the effect of engine speed and indicated load on HC emissions concentrations is shown in Figure 2.3. The HC formation mechanisms, discussed in Chapter 1, are sensitive to both engine speed and load. Whilst the way engine speed and load effect the various formation mechanisms is difficult to describe in quantitative terms the observed trends are attributable to a trade-off between combustion temperature and in-cylinder and

exhaust residence times [2.1]. Increasing engine speed at constant indicated load results in increased gas temperatures in both the expansion and exhaust strokes due to the reduced significance of heat transfer from the cylinder. This results in more oxidation of unburnt HC which more than offsets the reduced residence time in the cylinder and exhaust system. Consequently, unburnt HC emissions decrease with increasing engine speed. Similarly, when increasing indicated load at constant engine speed, gas temperature increases offset the effect of reduced residence time resulting in a slight decrease in HC emissions.

Figure 2.4 shows the effect of engine speed and brake load on NO_x emissions and shows it to be the opposite of that for HC emissions. NO_x concentrations increase both with increasing engine speed and indicated load. As discussed above, increasing both engine speed and indicated load results in increased combustion temperature due to the reduced significance of heat transfer. In addition, increases in in-cylinder pressure result in increased combustion temperature and these effects combine to have a direct effect on NO_x emissions which are extremely sensitive to combustion temperature.

The engine data presented in Figures 2.1 to 2.4 were all obtained with a stoichiometric tail-pipe AFR. The third and final engine variable of interest in the engine maps to be characterised here is AFR, since emission concentrations are particularly sensitive to this parameter. Figure 2.5 [2.1] shows (not to scale) the variation of HC, CO and NO_x emissions of a typical spark ignition engine with AFR. HC emissions decrease as the AFR is progressively increased and more and more of the injected fuel is oxidised. However, eventually the mixture becomes too lean to burn and partial misfiring occurs causing the HC emissions to rise again. CO emissions also reduce with increasing AFR as combustion becomes increasingly complete and the carbon in the fuel is increasingly oxidised to CO_2. This effect is particularly significant when the AFR is richer than stoichiometric as oxidation is limited by lack of oxygen and so any increase in oxygen levels will significantly affect the completeness of combustion. As mentioned above,

NO_x emissions are governed by combustion temperature and so peak when the AFR is just lean of stoichiometric when the combustion temperature is at its highest. NO_x emissions then reduce uniformly with AFR either side of this peak.

The combined effects of engine speed, load and AFR on the emissions produced by a spark-ignition engine is that engine emissions performance maps are more complex than the fuel consumption map. In order to characterise these engine performance variations with engine speed, load and AFR a neural network has been used to 'learn' the experimental engine data and enable the interpolation of fuel and emissions flow rates at points within the boundaries defined by the experimental data.

The engine data considered so far has been obtained with MBT spark timing and no exhaust gas recirculation. Both these variables, like AFR, are generally fixed by the engine management strategy. However, if a complete engine map is to be simulated the effect of all the engine operating variables on fuel and emissions flow rates must be considered.

The spark timing in an engine cylinder determines at what point in the engine cycle combustion begins. If combustion starts too early the work transfer from the piston at the end of the compression stroke on the combusting gases is too large, and results in an excessively high in-cylinder gas temperature causing pre-ignition of the remaining air/fuel mixture in a phenomenon often called 'knock'. If combustion starts too late, the peak cylinder pressure is reduced and the expansion stroke work transfer from the gas to the piston decreases [2.1] resulting in reduced brake torque. Consequently, MBT spark timing gives the maximum brake power and minimum brake specific fuel consumption. Deviations from MBT spark timing influence fuel consumption and emissions performance through changes in combustion gas temperature and exhaust gas temperature. Retarding spark timing from the optimum (reducing the spark advance relative to TDC) results in lower combustion temperatures and higher

exhaust gas temperatures because combustion takes place later in the expansion stroke of the engine. Therefore, retarding spark timing relative to MBT reduces NO_x emissions (due to reduced combustion temperature) and also reduces HC emissions (due to increased exhaust gas temperatures).

Exhaust gas recirculation (EGR) is used to reduce NO_x emissions. The system involves recycling a fraction (typically up to 30%) of the exhaust gases from the exhaust to the intake system. This gas then acts, along with the normal residual gas fraction from the previous engine cycle, as a diluent resulting in reduced combustion temperature without significantly affecting the combustion AFR. Here, the EGR rate is defined as:

$$EGR(\%) = \left(\frac{m_e}{m_a + m_e} \right) \times 100 \qquad (2.1)$$

where m_e is the mass of recycled exhaust gas and m_a the mass of induced air. Increasing the EGR rate reduces NO_x emissions due to decreased combustion temperature but also reduces the combustion rate making stable combustion more difficult to achieve. The amount of EGR a particular combustion chamber design can tolerate depends on its combustion characteristics, the speed and load, and the in-cylinder AFR. Typically, EGR rates in the range 15-30% are the maximum a spark ignition engine will tolerate [2.1]. As a result of the decreased burn rate and combustion and exhaust temperatures, HC emissions increase with increasing EGR. As the EGR limit of an engine is approached the increase in HC emissions is significant due to the reduction in combustion stability.

2.3 Neural Network Description and Application

The previous section outlines the effects of the main engine variables of interest here on fuel and emissions mass flow rates. The following gives a brief description of neural networks and how they have been applied to characterise the typical engine mapping data discussed above.

Figure 2.6 shows an illustrative example of a generalised neural network. The network is constructed of a series of interconnected units or nodes. In this example the units are arranged in three groups which by convention are referred to as the 'input', 'hidden', and 'output' layers. There may be any number of hidden layers, although most problems use a single hidden layer [2.5]. Each node in the input layer is connected to each of the nodes in the hidden layer. Likewise, each of the hidden layer nodes is also connected to each of the output layer nodes. There are no direct connections between the input and output nodes. Each of the connections has a weight term associated with it, which determines how strongly the incoming data value is transmitted to the node in the next layer. Networks are trained by adjusting the strengths of the connections between nodes in order to correlate the input and output patterns. Each node may be represented by three sections, as shown in Figure 2.7. The input to a node is calculated as:

$$\text{input}_i = \sum_j w_{ij}\text{output}_j + \text{bias}_i \qquad (2.2)$$

w_{ij} is the weight on the connection between nodes j to i, output_j is the output from node j, and j is the number of nodes that are connected to the input side of node i. The bias is in effect an additional weight term which can be learned just like the other weights by treating it as the weight from a unit that always gives an output of 1. When a set of inputs is applied to the network an activation value is calculated for each node in the network. For the input layer, the activation value for each node is calculated from the network input applied to it. In the hidden and output layers the activations are calculated from the current values of activations and weights in the appropriate connected layer. Thus, the activations of the input layer and weights connecting input and hidden nodes are used for the hidden layer activation calculation.

An individual unit's output is related to its inputs via an activation function. It is a requirement of many training methods that this function is both continuous and differentiable, and that its output is constrained between defined limits, usually

0 and 1. For these reasons the sigmoid function is normally employed, and the activation a_i is thus:

$$a_i = \text{output}_i = \frac{1}{(1+ e^{-\text{input}_i})} \tag{2.3}$$

The calculation of the output proceeds through all the units of each layer simultaneously, starting with the input layer and finishing with the output layer. The activation is computed for each unit in the input layer and the activations for the next layer are then calculated from the known connection weights and activations of the previous layer. This process is carried out for each layer until the output layer is reached and the network outputs calculated. Providing each layer is fully calculated before the next layer is started, this method of propagating the signals forward through the network mimics the desired parallel processing.

During the training process, the network learns to associate the required outputs with the defined inputs in the training data. Details of the training process used are given by Bacon [2.2] and summarised in Table 2.1. Several procedures are available for modifying the weights during network training. The most common of these, and the one used here, is the 'Back Propagation' or BP method. This method adjusts the weights that contribute significantly to the error calculated between the desired and actual output values in order to reduce the error. The training patterns are presented to the network randomly and each complete pass of the training samples is called an epoch. The number of iterations, or epochs, used during training can be set to an absolute number or, alternatively, the process may be set to iterate until the total error for all the input patterns in the training set is below a pre-defined threshold value. This total error is calculated as the sum of the squared errors in each of the outputs for all the patterns in the training dataset. Once the error threshold is reached, the weight values represent an optimised solution of the relationship between the input and output pairs in the training data. The accuracy of the solution can then be assessed by direct

comparison of the desired and actual output values for each input pattern.

2.3.1 Network Configuration to Predict Fuel and Emissions Flow Rates

The network configuration to predict fuel consumption, HC, CO and NO_x emissions from engine speed, imep and AFR inputs requires a three node input layer and a four node output layer. The network inputs were limited to these three because the bulk of the engine data available were obtained with MBT spark timing and calibrated EGR rates. It is generally accepted that a certain degree of trial and error is required when selecting a neural network configuration for a particular problem [2.6]. Of particular interest here was the size of the hidden layer and the number of training epochs to use in order to provide the most accurate solution. The training time is sensitive to both hidden layer size and the number of training epochs and so a trade-off exists between network accuracy and network training time.

In order to determine the optimum size of the hidden layer and the minimum number of training epochs to provide the desired training accuracy, a series of network configurations were examined. Figure 2.8 shows the effects of hidden layer size and number of training epochs on the correlation coefficient between predicted and target outputs. The engine data used were for a 1.8 litre Ford Zetec engine, as shown in Figures 2.1 and 2.2, and consisted of around one hundred input patterns covering the range of engine speeds from idle to 4000 rpm in steps of 500 rpm, and brake loads from 0 to 120 Nm in steps of 10 Nm, all at stoichiometric AFR. To determine the accuracy of output values, for data examples used during training, and separately for other examples not used during training, the dataset was split into two sets of cases. The training data set consisted of around 80% of the total number of input and output pattern pairs and was used to train the neural network. The remaining data patterns were not used to train the network but were used after training to confirm the accuracy of the network predictions at 'unseen' data points. The prediction accuracy at these points was of particular interest because these represent the drive cycle operating

conditions at which fuel and emission flow rates need to be inferred from the training data. The training data was scaled to lie in the range 0.1 to 0.9 as the network can only manipulate input and output values within a range of 0 to 1. Scaling the data between 0.1 and 0.9 avoids the network having to predict values at the extreme limits of 0 and 1 which would require extreme connection weights between nodes. Simple linear regression analysis was then used to determine the correlation coefficient between predicted and target output values. All the network preparation and results processing together with the network training have been carried out on an IBM compatible 486 PC. The results for fuel mass flow rates are given in Figure 2.8 and indicate that, for this database configuration, the optimum hidden layer size is 20 nodes and the best training accuracy is obtained after 10,000 training epochs. Predicted and target scaled fuel and emission mass flow rates for the training and validation data are shown in Figures 2.9 to 2.12. The closest agreement between target and predicted values can be seen to occur for fuel mass flow rates but in all cases the prediction accuracy is within +/- 10%. The prediction accuracy at the 'unseen' validation points is as good as that at data points used to train the network.

Additional work has been carried out to investigate if the neural network approach used here could be extended to account for changes in the spark timing and EGR calibrations used on the test engine. This involved training a neural network with five inputs, instead of three, on a much bigger database. The engine data used were for a 1.6 litre Zetec engine and, although the data did not cover the complete range of values required during engine calibration, it did enable the possibility of using a neural network to predict the effect of spark timing and EGR rate on engine emissions performance to be examined. The network used had five input nodes and a hidden layer size of 80. The engine database consisted of around 1600 data points, all of which were used to train the neural network. The results of the network training are shown for HC and NO_x emissions in Figures 2.13 and 2.14 respectively. The prediction accuracy is generally within +/-10%, as for the simpler engine map, which suggests that a neural network is

capable of characterising the more complex engine map successfully. The trained neural network was then used to demonstrate the effect of both EGR rate (Figure 2.15) and spark timing relative to MBT (Figure 2.16) on HC and NO_x emissions. The predictions reflect the expected trends (discussed above) in engine performance.

2.4 Discussion and Conclusions

Before fuel consumption and emission mass flow rates at each point in the ECE+EUDC drive cycle can be determined, a full engine map covering all possible operating conditions has to be inferred from a much smaller set of fully-warm engine data. For the work in this thesis, the engine operating variables of interest are engine speed, brake and hence indicated load, and AFR. Other engine variables, such as spark timing and EGR rate, are determined by the engine mapping data and are fixed by the control strategy on the test engine. Initially, fuel and emissions flow rates have been predicted from engine speed, load and AFR information for fully-warm engine mapping data with a fixed spark timing and EGR rate calibration.

In order to characterise the engine mapping data, a neural network has been used to 'learn' the engine map and enable fuel and emissions flow rates to be determined at all points within the boundaries of the engine mapping data. A degree of trial and error is required when optimising the configuration of a network to obtain the best training performance and this resulted in the selection of a 20 node hidden layer and a minimum of 10,000 training epochs for this application. Such a network is capable of predicting fuel and emissions flow rates to within +/-10% of the training data using engine speed, load and AFR as inputs. The network prediction accuracy at operating conditions from within the range of engine speeds and loads covered by the training data is equally good. This suggests that fuel and emissions mass flow rates can be predicted to within +/-10% for all operating conditions bounded by the data used to train the neural network.

The possibility of extending the neural network approach to a more complicated engine map, using spark timing and EGR rate as additional input variables, has been investigated. A single engine map of this type was available and this data did not include the complete range of operating conditions likely to be experienced over a cold-started drive cycle. This has limited the scope of the investigation. However, the results obtained are encouraging. A modified neural network appears to be capable of predicting the expected trends within the database. This suggests that the technique of characterising engine performance data with neural networks could be used successfully to account for deviations from the fully-warm spark timing and EGR rates during a cold-started drive cycle. However, before such an extension to the envisaged drive cycle prediction procedure can be achieved, further work is required to optimise the neural network set-up and more engine data for network training and validation required. Increasing the number of inputs to the neural network is likely to require a larger hidden layer to enable the network to learn the more complicated engine map and consequently increases the processing time needed to train and interrogate the network. Furthermore, the effect of increasing the complexity of the engine map is likely to result in a reduction in prediction accuracy and may result in the advantages of using a neural network, compared to regression analysis, being negated.

Chapter 3

Fuel Consumption and Emissions Studies: Literature and Test Facility Description

---

3.1 Introduction

The effect of reduced engine operating temperature on indicated specific fuel consumption and emissions is important. When the engine is operating at conditions other than fully-warm, indicated operating conditions will differ for a given brake operating condition. This is due primarily to higher engine friction loads during engine warm-up. In addition, reduced engine temperatures will adversely affect mixture preparation conditions in the inlet port. These will influence emissions levels particularly, but may also have a small effect on fuel consumption. These influences need to be taken into account when applying fully-warm engine data to warm-up operating conditions. Examining how this should be done is the subject of this and the subsequent three chapters. Here, a review of the relevant literature is presented, the implications are described, and the associated needs for experimental work defined. The experimental facilities used in the subsequent investigation are described later in the chapter.

3.2 Fuel Consumption and Emissions Literature

The starting point for fuel consumption predictions during engine warm-up is the corresponding point on the fully-warm indicated operating engine map. During the period immediately following a cold-start there is a difference between the amount of fuel injected and the amount of fuel burned, as accounted for by exhaust gas analysis. Indeed, current engine strategies inject approximately five times the required fuel during the first one or two cycles at room temperature to get the engine started as soon as possible [3.1]. According to Shayler et al [3.2]

only 25-30% of the injected fuel is in vapor form inside the engine cylinder during the first few cycles of engine cranking. During the subsequent warm-up period a degree of fuel enrichment is used to ensure sufficient fuel vaporizes to facilitate stable combustion. This additional fuel causes accordingly large amounts of liquid fuel to be deposited on the intake port walls and in the engine cylinder. In addition, it has been shown [3.3] that hydrocarbons present in the gasoline are observed in the crankcase oil and that fuel related hydrocarbons in the sump oil can reach 1.35% by mass [3.4]. Hence, in additional to any mixture preparation effects on indicated specific fuel consumption during warm-up this additional 'lost' fuel has to be accounted for when predicting cold-start fuel consumption.

Pollutant emissions are more sensitive than fuel consumption to changes in mixture preparation. Previous work by Shayler et al [3.5] investigated the influence of fuel injection system details on exhaust emissions at fully-warm steady-state operation. They concluded that system detail changes influenced emissions by affecting mixture preparation. In particular, mixture inhomogeneity in the cylinder at the start of combustion is believed to result in a degree of stratification of the air/fuel mixture. Much other work at fully-warm steady-state operating conditions has investigated the influence of various injector designs, locations and injection timing strategies on mixture preparation, including techniques to determine droplet sizes using laser imaging [3.6]. Most spark ignition engines have individual solenoid controlled valves (injectors) which deliver fuel into the engine inlet of each cylinder. This arrangement for fuel delivery is known as multi-point injection. Early multi-point injection systems operated all injectors simultaneously. Later systems with computer controlled injection use sequential injection timing, meaning that injection can be timed to occur at the same point in the cycle for each cylinder. Such systems have formed the basis for work investigating the effect of fuel injection parameters on mixture preparation and the associated effects on pollutant emissions. For example, Nogi et al [3.7] concluded that reducing the diameter of spray droplets and preventing

fuel from concentrating in the intake valve promotes vaporisation, reduces fuel concentration on cylinder walls, and prevents reductions in engine performance. However, the bulk of the literature available has concentrated on fully-warm steady-state operation and not on the vital warm-up phase of interest here, where mixture preparation variations are believed to be more significant. The bulk of the literature available concentrates on the sources of emissions of unburnt hydrocarbons. These sources are: crevice volumes, oil layer absorption and desorption, incomplete combustion, flame quenching and air fuel ratio abnormalities [3.8]. During engine starting and warm-up, these mechanisms can produce particularly high levels of HC emissions. Of particular importance is the influence of poor mixture preparation under these conditions. Work resulting from a collaborative research project investigating the sources of unburnt hydrocarbon emissions [3.9] in cold engines has also shown the importance of minimising in-cylinder crevice volumes and optimising valve timing. In addition, work to investigate the effect of varying coolant flow to vary engine warm-up, inparticular cylinder liner warm-up time, suggested that coolant flow should be minimised to enhance warm-up and reduce wall quench effects. Andrews et al [3.10, 3.11] have shown that coolant and lubricant temperatures influence HC emissions significantly. Work by Guillemot and Gatellier [3.12] investigated the influence of coolant temperature on HC emissions, employing a dual system cooling the cylinder head and block independently. Their results indicated that the cylinder head temperature influences the HC emissions. They also concluded that mixture preparation, absorption/desorption and crevice volume effects were greatly reduced with increasing coolant temperature. The effect of coolant temperature on emissions formation mechanisms is still not fully understood. HC emissions have been shown to be dependent on engine coolant temperature, but the effect on CO and NO_x emissions is less well documented. However, additional work by Andrews et al [3.13] investigating the transient warm-up behaviour of two Ford engines, detected a strong dependence of NO_x emissions on engine coolant temperature concluding that NO_x emissions increased during engine warm-up due to the appreciable time taken for the combustion process to

achieve its maximum flame temperature. Likewise, Lee [3.14] observed similar qualitative trends in emission levels with coolant temperature, using a single cylinder engine operating at constant speed and part throttle operation. Lee concluded that increasing coolant temperature from 65°C to 100°C decreased HC emissions by around 10%, increased NO_x emissions by around 10% and increased CO emissions by around 5%. Hence, knowledge of the variation of steady-state emission levels with engine coolant temperature during engine warm-up is required when using fully-warm emissions data to predict emissions levels at lower engine temperatures.

In addition to the variation of steady-state emission levels with engine coolant temperature, the effect of the initial engine start-up transient on each of the three emissions needs to be considered. Both CO and NO_x emissions are closely related to the actual air/fuel mixture burnt in the combustion process whereas HC emissions result primarily from the air/fuel mixture left unburned at the end of each expansion stroke. As such, HC emissions are particularly sensitive to the fuelling strategy during engine start-up. HC emissions increase during cold-starting because the fuel vaporisation is insufficient [3.15]. As a result, excessive amounts of fuel need to be injected to enable sufficient fuel to vaporise to form a combustible mixture at the spark plug. Indeed, according to Shayler et al [3.2], at 16°C only 25-30% of the injected fuel is in vapour form inside the cylinder during the first few cycles of cranking. This extra fuel causes accordingy large amounts of liquid fuel to be layered on the surfaces of both the intake port and the engine cylinder [3.16]. Hence, although the combustible mixture may be close to the desired stoichiometric air/fuel ratio in the period immediately following a cold start, the HC emissions are much higher than would be associated with this mixture strength due to the large amounts of liquid fuel which do not take part in the combustion process. Much work has been carried out to both attempt to visualise the behaviour of the liquid fuel deposited on the engine intake and combustion surfaces [3.17] and to reduce the amount of liquid fuel that does not take part in the combustion process. Takeda et al [3.18]

investigated general fuel behaviour during cold-start and warm-up and concluded that to reduce engine-out HC emissions it is important to reduce intake port wall-wetting and cylinder wall-wetting simultaneously. Injection system details are important if wall-wetting is to be minimised and various studies have been carried out to determine the effect of both injection timing and injector type on wall-wetting and engine-out HC emissions [3.19-3.22]. However, the investigation into engine hardware configurations is beyond the scope of the work presented in this thesis. This has made use of standard production engines and fuelling strategies.

3.3 Experimetal Test Set-up and Procedure

Engine data presented in the subsequent two chapters of this thesis were acquired using an engine test facility built for a previous research project. The installation consists of three main parts: the engine and management system, the monitoring and control equipment, and the engine data acquisition system. It is convenient to desribe these at this point in the thesis for future reference.

3.3.1 Test Engine and Management System

The test engine used in this work was a 1989-specification Ford 2.0 litre DOHC 8V engine, details of which are given in Table 3.1. This engine is a standard production four cylinder with multi-point fuel injection as used initially by the Ford Sierra and Granada ranges and currently by certain models in the Ford Scorpio range. The test engine was mounted at its original points onto a steel frame via rubber vibration dampers, the frame being mounted onto steel rails sunk into the concrete base of the engine test bed. Figure 3.1 shows the general layout of the test rig within the test laboratory. Fuelling and spark timing were controlled using the Ford EECIV engine management system, shown schematically in Figure 3.2. The system uses a hot wire anemometer to determine air mass flow rate, an Electronic Distributorless Ignition System (EDIS) and sequential fuel injection with conventional single spray solenoid injectors. A standard Ford EECIV calibration console connected to the engine management

system enabled changes to the calibrated AFR and spark timing strategy to be made and various management signals to be logged on the PC based engine controller. Standard 95 RON unleaded gasoline was used throughout the engine testing. Measurements of AFR were made using an NTK MO-1000 AFR meter, the UEGO sensor of which was mounted in the exhaust downpipe approximately 1m from the exhaust ports.

3.3.2 Engine Monitoring and Control Equipment

The engine was coupled to a Froude EC38TA eddy-current dynamometer via a Ford MT-75 five-speed gearbox, fourth gear of which gave a 1:1 gear ratio. Dynamometer load was determined by a Froude HD70B control module enabling the engine to be run at either constant speed or constant brake torque. In all tests, the dynamometer control was used to set engine speed with brake torque being adjusted by means of a stepper motor connected to the throttle linkage.

The rig cooling system enables the engine to be cooled to temperatures as low as -10°C and the engine coolant as low as -25°C. The engine oil and coolant circuit is shown schematically in Figure 3.3. Oil and coolant flow was directed either through the heat exchangers activated by computer controlled solenoid valves or to the Drakes refrigerated water chiller.

When soaking-down the engine the gate valves to the coolant heat exchanger were closed and those to the chiller opened. Refrigerated coolant, a 50/50 mixture of water and glycol antifreeze, was then circulated through the engine. As shown in Figure 3.3, the engine could be covered by a removable insulating blanket manufactured to fit over a steel frame enclosing the complete engine. The refrigerated coolant is pumped by the chiller pump through a standard automotive radiator and then through the engine block and cylinder head through the standard water jacket and thermostat bypass loop. The radiator was used to chill the air enclosed by the insulating blanket drawn up through the radiator by the fan mounted above the radiator. A second parallel path allowed coolant to circulate

through a fabricated copper coil located in the sump to cool the engine oil. Using this configuration, the engine oil and coolant temperatures could be reduced to -10°C from ambient temperature in around 3-4 hours.

When the engine was at the desired temperature, the insulating blanket was removed and the gate valves to the heat exchanger opened and those to the chiller closed. In this configuration, the engine water pump was used to circulate the coolant through the thermostat bypass during warm-up and through the coolant heat exchanger once the thermostat was open. Cooling water was circulated through the heat exchanger and the dynamometer and returned by a centrifugal pump to a Carter fan-assisted cooling tower in the service yard outside the test laboratory. Before running for long periods at fully-warm operating conditions an oil heat exchanger was fitted to the oil filter inlet to prevent overheating, cooling water again coming from the external cooling tower.

Certain engine tests (detailed in chapter 5) required steady-state running at non-fully-warm operating conditions. This was achieved by removing the thermostat and thermostat bypass loop. This enabled the engine to be force-cooled using either the chiller circuit (for coolant temperatures below ambient) or the heat exchanger circuit (for coolant temperatures between ambient and fully-warm).

A schematic of the engine test facility monitoring and control system is shown in Figure 3.4. A list of the equipment used in the control and monitoring system is given in Table 3.2. The digital input/output card was used to switch the relays for the oil and coolant solenoid valves, and to index the throttle stepper motor. Table 3.3 lists the various temperatures monitored using the calibrated thermocouple board together with the analogue signals logged using the ADC board. Engine-out emissions concentrations measurements were made using an Horiba MEXA-324 GE analyser for CO emissions and Signal Series 3000 and 4000 analysers for HC and NO_x emissions respectively, the sample lines being

located in the exhaust downpipe alongside the NTK AFR sensor.

3.3.3 Engine Data Acquisition

Engine data acquisition was carried out on two separate PC systems. The first system uses the rig control PC to log specified engine parameters selected from the temperatures and analogue signals displayed by the rig control and monitoring system. The second system was used to capture cylinder pressure data from cylinder number one and calculate imep.

The imep system is based on an Amplicon PC226 data acquisition card installed in an IBM-compatible 486-33 PC. The PC226 card was triggered using a one degree crank angle signal obtained from a Hohner Series 3000 optical shaft encoder, mounted on the engine block connected to the crankshaft via a flexible coupling.

In addition to the one degree trigger signal, the shaft encoder also produced a once-per-revolution marker pulse. This marker pulse was aligned to cylinder one TDC using the polytropic exponent method described by Douaud and Eyzat [3.23]. Compression TDC was determined by comparing pressure data at successive TDC samples.

Cylinder pressure from cylinder one was acquired using a Kistler 6121 piezo-electric pressure transducer, flush mounted in the cylinder head. The transducer signal was amplified using a Kistler 5007 charge amplifier with a standard 180kHz filter. As the cylinder pressure signal obtained from the pressure transducer was not absolute a reference procedure was required. This involved offsetting the cylinder pressure data between the exhaust and induction strokes when both the inlet and exhaust valves are open to the manifold absolute pressure. Manifold absolute pressure was measured using a Setra 280E absolute pressure transducer connected to the inlet manifold using 4mm diameter polypropylene tube. In order to suppress any fluctuations in the pressure, the tube

was approximately 5m long.

The hardware configuration of the 486-33 PC enabled about 200 consecutive cycles of engine data to be acquired. However, repeatable imep results were obtained from averaging pressure data from 10 consecutive cycles. In this thesis, the imep is defined as the work delivered to the piston over the entire four strokes of the cycle, per unit displaced volume. As defined is equation 3.1, the imep is calculated over a crank angle window of 720° between consecutive non-firing TDCs of the same cylinder.

$$\text{imep} = \frac{1}{V_d} \int_{\theta=TDC}^{\theta=TDC+720} PdV \qquad (3.1)$$

where P is the cylinder pressure at crank angle θ, V_d is the displaced volume per cylinder, and dV is the change in cylinder volume between crank angle θ and $\theta+d\theta$.

3.4 Conclusions

This chapter reviews the literature relevant to the fuel consumption and emissions studies carried out in subsequent chapters. In addition, details of the experimental hardware used are given. The tests performed using this hardware, and the results obtained, are detailed in the appropriate chapters.

Chapter 4

Predicting Fuel Consumption From Fully-Warm Data

4.1 Introduction

In this chapter, consideration is given to how fuel consumption can be determined from engine data taken at fully-warm operating conditions. Two aspects of this are covered in the following. The first concerns the relationship between indicated specific fuel consumption and indicated operating conditions. The assumption made is that this will be independent of differences between warm-up and fully-warm engine thermal states, and experimental studies have been carried out to examine and support this. This second concerns the differences between the amount of fuel injected and fuel combusted. This difference can be significant during cold engine operation. The amount of fuel injected is the appropriate value for fuel consumption calculations but it is the fuel combusted that is relevant to considerations of indicated performance.

Fully-warm engine mapping data are generally obtained at constant tail-pipe AFR. At fully-warm steady-state operation, the tail-pipe AFR gives an accurate measure of the overall in-cylinder AFR since all the fuel in the cylinder is vaporised. However, in the period immediately following a cold-start the tail-pipe fuel mass flow rate does not account for any liquid fuel stored in the engine cylinder and lubricating oil. During the warm-up period the overall fuel mass flow rate is thus:

$$\dot{m}_{overall} = isfc.\dot{P}_{indicated} + \dot{m}_{unaccounted\ for} \qquad (4.1)$$

where:

$$isfc = \frac{\dot{m}_f}{\dot{P}_{Indicated}} \tag{4.2}$$

isfc is in g/kWhr when $\dot{m}_f$ is the combusted fuel mass flow rate in g/hr and $\dot{P}_{Indicated}$ the indicated power in kW. Consequently, when predicting the overall fuel mass flow rate during engine warm-up two effects have to be accounted for. The work presented here details the investigation into these effects. Throughout the work the tail-pipe AFR has been determined using a UEGO sensor mounted in the exhaust system. Recent work by Shayler et al [4.1] suggests that such a sensor records an AFR that is leaner than the true tail-pipe AFR in the early stages of engine warm-up due to the high concentrations of unburnt HC emissions in the exhaust gas stream. In this period, the UEGO sensor only accounts for fuel that has been combusted in the engine cylinder and not the unburnt fuel also present as unburnt HC emissions. However, during steady-state operation, both at fully-warm conditions and during force-cooled running when unburnt HC emissions are much lower, the UEGO sensor was found to give an accurate measure of the tail-pipe AFR. Consequently, when determining the overall fuel mass flow rate according to equation (4.1), the isfc is determined from the combusted AFR recorded by the UEGO sensor and the 'unaccounted for' fuel term includes the proportion of the injected fuel present in the exhaust gas stream as unburnt hydrocarbons, which are not accounted for by the UEGO sensor. The investigation of the fuel unaccounted for term is described in the second part of this chapter. The first part reports the investigation of the effect of engine coolant temperature on the indicated specific fuel consumption term.

4.2 Effect of Coolant Temperature on isfc

Tests were carried out to investigate the effect of changing engine coolant temperature on indicated specific fuel consumption over a range of engine operating conditions. The tests were carried out as a series of fixed engine speed

and throttle position warm-up runs, with engine data logged on a second-by-second basis throughout the warm-up. The experimental data were obtained using the engine test rig described in Chapter 3. Before each test the engine was run at fully-warm temperatures and the engine speed and brake load fixed using the dynamometer and throttle stepper motor controls. The engine was then stopped, with the engine speed and throttle position fixed, and allowed to cool down to 20°C. The coolant control valves were then switched to allow coolant from the chiller to be circulated around the engine and the engine coolant brought down to -25°C. The insulating blanket was used to aid the cooling process and left in position until the oil sump temperature fell to -10°C. Once cool, the insulating blanket was removed and the coolant control valves switched to allow the engine water pump to circulate coolant through the heat exchanger once the thermostat opened. Cylinder pressure data were acquired at regular intervals during the warm-up and corresponding imep values calculated by the acquisition software. Imep values were produced at approximately 50 second intervals due to the need to average cylinder pressure data over several cycles and because the imep calculations require intensive use of the 486 PC's processor. Table 4.1 shows the test conditions used and Table 4.2 lists the imep readings and corresponding time from start of test for one test condition. Two second-by-second fuel mass flow rates were recorded for each test. Fuel injected was determined from EECIV fuel injector pulsewidth from the calibration console and fuel combusted from the UEGO sensor tail-pipe AFR and EECIV measured air mass flow rate.

The observed effect of engine coolant temperature on isfc is shown in Figure 4.1. The results show isfc plotted against imep at engine coolant temperatures between -10°C and 80°C at engine speeds of 1750rpm and 2400rpm. At each test point, isfc is calculated from the measured imep and the tail-pipe detected fuel mass flow rate from the measured airflow and UEGO AFR. During each warm-up test the fully-warm tail-pipe AFR was set at stoichiometric using the EECIV calibration console. Initial data immediately following the engine start-up was

discarded as in this period accurate control of the tail-pipe AFR was not possible. This essentially replicates a cold-start in a current production vehicle where a HEGO sensor, operating on the same principle as a UEGO sensor, provides feedback to the engine management system to maintain a stoichiometric AFR in a process known as closed loop fuelling. According to Figure 4.2, the input isfc, calculated from the mass of fuel injected, decreases rapidly and converges to the UEGO sensor determined tail-pipe isfc value as the engine warms-up and the input AFR tends towards the stoichiometric tail-pipe AFR. The tests indicate that, by careful control of engine fuelling, a near stoichiometric tail-pipe AFR can be maintained once the coolant temperature has reached -10°C. From this point onwards, isfc calculated from the combusted fuel mass flow rate using a UEGO sensor remains approximately constant independent of coolant temperature. The scatter in the isfc data in Figure 4.1 is of the order of 2% and within this scatter there is no definable trend in isfc with ECT.

4.3 'Unaccounted For' Fuel During Warm-Up

In addition to the constant AFR warm-up tests, tests were carried out using the standard EECIV cold-start fuelling strategy to vary the AFR during engine warm-up. As before, a series of fixed engine speeds and throttle positions were used (Table 4.3) and cylinder imep measurements were recorded during the warm-up period to enable indicated specific fuel consumption (isfc) values to be calculated. These tests were used to investigate the relationship between fuel injected and fuel burnt during the warm-up process, and so the same injected and UEGO detected fuel flow rate measurements as for the constant AFR tests were recorded to enable 'unaccounted for' fuel during warm-up to be calculated.

The data presented above suggest that tail-pipe isfc is only weakly dependent on ECT during engine warm-up. However, Figure 4.2 indicates that a substantial difference between fuel injected and fuel burnt exists in the period immediately following engine start-up. This difference is due to fuel being deposited on the combustion chamber surfaces and being absorbed into the lubricating oil during

the early stages of engine warm-up. In addition, in the period immediately following start-up the UEGO sensor used to detect the AFR of the exhaust gases fails to account fully for unburnt fuel in the form of HC emissions present in the tail-pipe. Consequently, when determining fuel consumption during engine warm-up from fully-warm engine data, knowledge of the additional fuel required to maintain a stoichiometric AFR as detected by the UEGO sensor is important. The second set of engine warm-up tests, using the standard fuelling strategy, were used to investigate the behaviour of this 'unaccounted for' fuel during engine warm-up. Figure 4.3 shows a typical warm-up test result for AFR and fuel mass flow rate during engine warm-up and the resulting 'unaccounted for' fuel calculated as the difference between fuel injected and fuel detected by the UEGO sensor in the tail-pipe. At fully-warm conditions, any residual difference between fuel supply and exhaust fuel flow rate was attributed to calibration errors and zeroed by adjusting the air mass flow rate calibration. The results appear to show a near exponential decrease of 'unaccounted for' fuel from an initial peak. As reported elsewhere, a proportion of this fuel is believed to be due to in-cylinder storage of fuel on cold combustion chamber surfaces [4.2, 4.3]. Recent work by Shayler et al [4.1] has investigated the behaviour of 'unaccounted for' fuel during the warm-up period and attempted to define the relative proportions of fuel lost to the lubricating oil and stored in fuel films in the engine cylinder, but such an investigation was beyond the scope of the work presented here.

4.3.1 Characterising 'Unaccounted For' Fuel

In order to predict fuel consumption during engine warm-up and the period immediately after start-up from fully-warm data, characterising the behaviour of the observed 'unaccounted for' fuel detailed above is important. Work to investigate the behaviour of this fuel under cold-start conditions has resulted in the development of a simple exponential function to simulate the observed experimental behaviour [4.4]. The tests were carried out on a Ford 1.8 litre 16V Zetec engine over a wide range of operating conditions. The amount of 'unaccounted for' fuel at any point in the warm-up period as a percentage of the

fuel supplied can be expressed as:

$$\text{Unaccounted For Fuel} = A.\exp\left(\frac{\Delta ECT}{-\beta}\right) \times 100 \qquad (4.3)$$

where ΔECT is the difference between the instantaneous ECT and the initial coolant start temperature.

The A value defines the initial peak of the 'unaccounted for' fuel and has been found to depend on the following:

i) Initial start temperature

Tests have indicated that a reduction in engine start temperature increases the magnitude of A. This is thought to be due to the increased amount of liquid fuel entering the combustion chamber as a result of reduced vaporisation within the intake port. Wall wetting in the combustion chamber will be more significant due to the combination of increased amounts of liquid fuel entering and the lower wall temperatures. This fuel behaviour has been observed photographically elsewhere [4.5] and the liquid fuel films found to remain in the cylinder for a considerable portion of the warm-up [4.6].

ii) Fuel Injected

The amount of fuel injected per stroke is a function of air charge and AFR. Increasing the amount of fuel injected increases the magnitude of A as the increased fuel mass in the intake port is believed to result in more liquid fuel entering the cylinder.

iii) Engine Speed

Increasing the engine speed has been found to reduce the magnitude of A. This is thought to be due to increased air mass flow rates resulting in better air/fuel mixing and fuel atomization and consequently reducing the

amount of wall wetting in the engine cylinder.

A mathematical expression for A has been defined from experimental data and is a function of engine speed, fuel injected per stroke and start temperature, as shown below.

$$A = m_{inj}(-0.2N + 1300 - 6T)^2 \qquad (4.4)$$

where N is the engine speed in rpm, T the initial start temperature in °C and m_{inj} the fuel injected per stroke in kg.

The β value is defined as the 'unaccounted for' fuel temperature constant and has been found to depend on the following two parameters:

i) Start temperature

Decreasing the start temperature was found to decrease the β value. A lower start temperature is believed to result in a larger quantity of liquid fuel in the cylinder and consequently more time is needed for the coolant and wall temperature to rise sufficiently to vaporise this fuel.

ii) Fuel injected per stroke

The amount of fuel injected is believed to strongly influence the amount of liquid fuel in the cylinder. Consequently, a longer time is required to heat up the coolant and cylinder walls to vaporise this fuel resulting in a larger β value with increased fuel injected per stroke.

Once again, experimental data were used to derive a function to define β as shown below [4.4]:

$$\beta = \frac{1}{[0.51+(0.012T)+(-0.00011T^2)]}+(120000m_{inj}) \qquad (4.5)$$

Using equations (4.3)-(4.5) an 'unaccounted for' fuel fraction can be determined during a warm-up test. Figure 4.4 shows measured and predicted 'unaccounted for' fuel curves for two warm-up tests from -15°C on the 2 litre DOHC 8V engine with different engine speeds, brake loads and AFR control during warm-up. Whilst, in both cases, the fully-warm AFR was 14.2:1 the AFR strategy during warm-up was different. The test in Figure 4.4a was run using the standard EECIV determined cold-start AFR strategy while the data in Figure 4.4b was obtained with constant tail-pipe AFR during warm-up. These tests illustrate the significance of the 'fuel injected' term in the model as with the standard EECIV fuel enrichment strategy the 'unaccounted for' fuel fraction is much more significant.

4.4 Discussion and Conclusions

The data presented in this chapter suggest that the relationship between isfc and imep is only very weakly dependent on ECT when fuel mass flow rates are calculated from exhaust gas analysis. Assuming this weak dependence to be negligible enables fully-warm fuel mass flow rate data to be applied to non-fully-warm operating conditions, providing indicated operating conditions are used to correlate cold operating conditions with fully-warm conditions. In this way engine friction considerations are accounted for. If fully-warm and cold-start engine indicated operating conditions are not available, an engine friction model is required to recast the engine brake operating conditions into indicated operating conditions. Such an engine model and its application is discussed in Chapter 6 of this thesis.

The above assumption only applies to fuel flow rates calculated from tail-pipe AFRs which closely represent the fuel involved in combustion and do not always equate to the fuel mass injected. Thus, in order to determine the total fuel mass flow rate during non-fully-warm conditions, the difference between fuel injected and fuel detected by exhaust gas analysis in the period following a cold start has to be accounted for. A simple model has been developed at Nottingham

University to characterise this 'unaccounted for' fuel fraction [4.4]. This has been found to depend upon engine start temperature, mass of fuel injected per stroke and engine speed and decays exponentially with increasing ECT.

The 'unaccounted for' fuel fraction can be more accurately described as the fraction of fuel supplied which is not accounted for by the UEGO sensor in the exhaust, and is believed to be due to a combination of several engine warm-up effects. Liquid fuel films have been shown to form in the intake port and on the intake valves and liquid fuel may be temporarily stored within the combustion chamber. Several studies [4.2, 4.3, 4.5] have shown this occurs in the period immediately following engine start-up. The in-cylinder films have been observed to last for several minutes after engine start-up, but do eventually vaporise as the cylinder wall temperature rises. In addition, liquid fuel has been shown to pass the piston rings and mix into the engine lubricating oil [4.7] and up to 1% of the fuel injected during the first 20 minutes of a light-load warm-up test from room temperature was detected in the lubricating oil. This fuel is then believed to return to the cylinder via the crankcase breather system at a near undetectable rate. A further fraction of the liquid fuel in the cylinder is thought to pass directly into the exhaust system as unburnt hydrocarbons. After combustion has been completed and the in-cylinder pressure decreases during the exhaust stroke, some of the fuel wall-wetting in the cylinder is vaporised as unburnt hydrocarbons [4.8] with the result that the cold-start HC emissions are greatly increased in the period when liquid fuel is present in the engine cylinder. Shayler et al [4.1] have shown that in this period the UEGO sensor does not fully account for these hydrocarbons and records an AFR that is lean of the true tail-pipe AFR. As a result, the 'unaccounted for' fuel fraction includes a proportion of the injected fuel that passes undetected down the exhaust tail-pipe. The relationship between 'unaccounted for' fuel and the unburnt hydrocarbon emissions during cold-starting is considered in the following chapter of this thesis and is of particular importance when applying fully-warm HC emissions data to cold-start indicated operating conditions.

In conclusion, it can be seen that fully-warm fuel flow rate data can be recast to represent cold-start conditions and engine warm-up. This requires a combination of accounting for engine friction changes during engine warm-up by using indicated operating conditions, and predicting the 'unaccounted for' fuel in the period immediately following engine start-up. In order to predict the percentage of injected fuel that is unaccounted for in the exhaust system, knowledge of the overall injected fuel mass flow rate is required. When applying predictions to fully-warm engine data to determine the percentage increase in fuel consumption associated with 'unaccounted for' fuel, the overall injected fuel mass is not known. Consequently, an iterative approach has to be applied with the initial 'unaccounted for' fuel percentage being calculated by assuming that the fuel injected is the same as the fuel detected in the exhaust pipe. A new fuel injected mass flow rate can then be calculated and the procedure repeated. After two such iterations the change in predicted instantaneous 'unaccounted for' fuel as a percentage of fuel injected is less than 0.5%, and the 'unaccounted for' fuel percentage assumed to have converged.

Chapter 5

Predicting Emissions From Hot Test Bed Data

5.1 Introduction

Indicated specific engine-out emissions are more sensitive than fuel consumption to changes in air/fuel mixture preparation and in-cylinder temperature variations during engine warm-up, as discussed in Chapter 3. In addition, for a period after cold start-up, HC emissions are further influenced by the consequences of poor fuel utilisation [5.1]. This chapter deals with how the treatment of fuel consumption, described in the previous chapter, can be adapted to enable the prediction of emission levels during cold running. Firstly, the effect of reduced engine coolant temperature on the steady-state engine-out indicated specific emission levels is examined and then the additional effect of engine start-up transients on engine-out HC emissions is considered. The objective of the work has been to develop a simple technique for scaling fully-warm engine-out emission levels to account for changes in mixture preparation during warm-up and the effect of engine start-up transients in the period immediately following a cold-start. As such, the individual sources of the three pollutant emissions under consideration at fully-warm operating conditions are not of primary importance but the likely mechanisms that influence changes during warm-up are. The possibility of predicting the effect of engine coolant temperature changes on HC, CO and NO_x emissions during steady-state operating conditions and the additional effect on HC emissions of the transient period immediately following a cold start have been investigated. Of particular interest was the possible link between the increase in HC emissions due to engine start-up and the observed discrepancy between the amount of fuel injected and the amount of fuel burnt as accounted for by exhaust gas analysis described in the previous chapter.

5.2 Experimental Test Set-up and Procedure

Engine test data have been obtained from a 2 litre DOHC 8V engine installed on the test rig described in Chapter 3, and from a Ford 1.8 litre HO Zetec engine installed on an identical test facility. Two sets of experiments have been carried out. The first to establish how mixture preparation effects arise under relatively stable thermal conditions produced by force-cooling the engine. The second was to investigate the link between 'unaccounted for' fuel and HC emissions in the transient period immediately following engine start-up.

The effect of ECT on indicated specific emissions has been investigated under stable thermal conditions maintained by force-cooling to limit the rate of engine warm-up. This enables steady-state emissions data to be taken at coolant temperatures down to 0°C. Force-cooling entailed removing the engine thermostat and continuously circulating refrigerated coolant through the engine. By careful control of coolant flow rates and chiller temperature settings, ECT could be held at any temperature between 0°C and 85°C for up to 10 minutes. Before an emission reading at each temperature was finalised, the emissions data were allowed to settle to a steady-state value after each step change in temperature. This ensured that any transient effects due to sudden temperature changes and cold-starting did not influence the results, and took about 5 minutes to achieve. At a given test temperature engine data were logged on a 5 second interval basis and imep readings recorded to enable indicated specific emissions (in g/kWhr) to be calculated. Each warm-up test was carried out with a fixed throttle position and UEGO sensor measured tail-pipe AFR giving an approximately constant imep during warm-up. Table 5.1 shows the range of operating conditions tested for the 2 litre DOHC 8V engine and the additional tests carried out on the 1.8 litre HO Zetec engine.

5.3 Predicting the Effect of ECT on Indicated Specific Emissions

To examine if the effects of mixture preparation on engine-out emission levels could be characterised by a relatively simple function of ECT, the experimental

indicated specific emissions data were plotted against ECT in Figure 5.1. At each ECT value, the absolute emission value is divided by the corresponding fully-warm value to give an ECT Correction Factor. The data presented in Figure 5.1 are from the full range of test conditions defined in Table 5.1, and demonstrate that, when normalised to values obtained at fully-warm operating conditions, the indicated specific emissions are strongly correlated to ECT. For each of the pollutants of interest, a simple function of ECT has been defined to characterise the correction factor required to define indicated specific emissions to within +/-5% of the observed values. This function is independent of engine speed, indicated load and AFR to within this level of accuracy and experimental repeatability. The three ECT Correction Functions for the three indicated specific emissions are defined in Appendix A.

Previous work by Shayler et al [5.2] described studies of the relationship between emissions and operating conditions and fuel injection system details. They showed how many of the effects on emissions could be explained on the basis of mixture inhomogeneity within the cylinder at the time of combustion. In the work presented here, ECT is believed to provide a direct indication of mixture preparation conditions in the intake port, which in turn give rise to varying degrees of mixture inhomogeneity within the cylinder and consequently to variations in emissions from values at the corresponding fully-warm engine state.

Emission concentrations for the 2 litre DOHC 8V engine against AFR for one operating condition are shown in Figure 5.2. With reference to this, the lower isco emissions observed during warm-up are believed to be due to the bulk of the cylinder mixture being leaner than the overall AFR during the warm-up period. Figure 5.1 suggests that CO emissions at 20°C are between 5%-10% lower than those for the corresponding fully-warm operating conditions, irrespective of engine speed, load and tail-pipe AFR when normalised.

Ishc emissions are relatively high during the warm-up period. Figure 5.1 shows

that ishc emissions are approximately 30% higher when the coolant temperature is 20°C, compared to the fully-warm case.

Isno$_x$ emissions were found to be around 30% lower at 20°C than at the corresponding fully-warm condition, again independently of engine speed, indicated load and overall tail-pipe AFR. Figure 5.2 indicates that the NO_x emissions are influenced by the AFR of the lean part of the stratified mixture, but the changes in NO_x emissions cannot be entirely due to this, since the same dependence on ECT was observed regardless of whether the engine was run lean or rich of the AFR producing peak NO_x. It is likely that the reduction in NO_x emissions is more significantly influenced by the lower combustion temperatures during engine warm-up than by mixture stratification.

The mechanisms that produce these trends are likely to arise in any engine but whether or not the simple ECT correction functions presented here are adequately representative is an open issue and requires further work. However, additional data were obtained from a Ford 1.8 litre HO Zetec engine to confirm that the above functions were representative for this engine, since data from this engine were to be used in the drive cycle evaluation procedure, described in Chapter 7. Figure 5.3 shows experimental data from the Zetec engine plotted in the same ECT correction factor format as for the 2 litre DOHC 8V engine data. Figure 5.3 also shows the model predicted correction factors obtained from the DOHC data and indicates that the same trends in emissions occur on the Zetec engine. The Zetec data were derived from only three tests all at an engine speed of 2000 rpm and imep of 8.3 bar at tail-pipe AFRs of 12:1, 14.7:1 and 17:1. Despite the limited amount of data available, the general agreement with the ECT Correction Functions derived from the DOHC data is generally good suggesting that the trends observed and modelled are generic to other engine types.

5.4 Predicting the Effect of Engine Start-Up Transients on HC Emissions

In addition to the force-cooled tests, experiments were carried out to investigate

the relationship between 'unaccounted for' fuel in the period immediately following cold start-up and the increased HC emissions in this period. These tests were carried out using the standard EECIV cold-start fuelling strategy. Once again, a series of fixed engine speeds and throttle positions were used (Table 5.2) and cylinder imep measurements recorded during engine warm-up. The coolant circuit was the standard production circuit with the standard thermostat unit fitted.

Figure 5.4 shows HC mass flow rates during two fixed throttle warm-up tests. The measured HC mass flow rate is that determined from exhaust concentrations and fuel and air mass flow rates logged throughout the test period. The predicted HC mass flow rate is calculated from the fully-warm steady-state value at the end of the warm-up test and is corrected to account for mixture preparation effects, using the ECT functions described above, and for changes in tail-pipe AFR during warm-up by interpolation using fully-warm AFR data. Since each test was carried out at near constant indicated load, the HC mass flow rate at each point in the warm-up, neglecting mixture preparation effects, could be calculated from the fully-warm HC mass flow rate scaled according to AFR. This was done using simple linear interpolation based on fully-warm engine data at corresponding indicated operating conditions and a range of tail-pipe AFRs. This HC mass flow rate was then scaled according to ECT to account for mixture preparation changes to give the predicted HC mass flow rate during engine warm-up. This mass flow rate can be seen to be significantly lower than the measured HC mass flow rate in the early seconds after engine start-up.

The difference between the measured and predicted HC mass flow rates, termed the 'Delta HC Flow Rate', is closely related to the 'unaccounted for' fuel behaviour described in Chapter 4, as shown in Figures 5.5 and 5.6. Figure 5.5 shows the results from three warm-up tests at an engine speed of 1750 rpm and a range of fully-warm engine brake loads with a start temperature of -15°C. The relationship between Delta HC and 'unaccounted for' fuel is relatively insensitive to engine

load, engine speed and start temperature as indicated by Figure 5.6. This shows the results for a series of warm-up tests with a range of engine speeds, engine loads and start temperatures, detailed in Table 5.2. Linear regression on these data gives:

$$\Delta HC = \gamma(\dot{m}_{inj} - \dot{m}_{exh}) \qquad (5.1)$$

where γ has a value of 0.33. $\dot{m}_{inj}$ is the fuel mass flow rate injected and $\dot{m}_{exh}$ the fuel mass flow rate determined by exhaust gas analysis with the UEGO sensor. Similar engine data obtained at Nottingham University from a Ford 1.8 litre 16V HO Zetec engine demonstrate the same linear relationship [5.3]. However, in this case the value of γ was found to be 0.5 which suggests that γ is dependent on engine type. The DOHC engine data correlation has been used to predict total HC mass flow rates during engine warm-up and the methodology detailed below. The details and implications of the work using the Zetec engine data [5.3] are discussed later in the chapter.

For the 2 litre DOHC 8V engine examined, equation (5.1) gives a good first approximation to the increase in HC emissions during the period immediately following engine start-up, believed to be primarily due to liquid fuel films in the engine intake and cylinder. Using this relationship and the 'unaccounted for' fuel model described in Chapter 4, an additional HC mass flow rate during engine warm-up due to cold-starting was predicted for each of the warm-up tests carried out. The total HC mass flow rate at any point during the warm-up was predicted by summing the fully-warm value at the corresponding AFR corrected for mixture preparation effects and an additional 'Delta HC' term, calculated from equation (5.1). Figure 5.7 shows the results of two such tests, which correspond to the data presented in Figure 5.4. These tests demonstrate that the simple linear correlation with 'unaccounted for' fuel enables a good approximation to the actual HC mass flow rate in the early seconds of engine warm-up to be made from the fully-warm HC mass flow rate for the engine examined.

5.5 Discussion

The experimental data presented in this chapter were obtained to illustrate the effects of reduced engine temperature on indicated specific emissions under steady-state conditions and the additional effect of engine start-up transients on HC emissions. These two phenomena are essentially coupled together as, in reality, both occur simultaneously during the standard engine start and warm-up. However, in order to predict the engine-out emissions at non-fully-warm operating conditions from fully-warm data the two effects have been separated and examined independently.

The effect of mixture preparation on the engine-out indicated specific emissions have been characterised by three functions defining a correction factor to scale fully-warm emission values for engine coolant temperatures down to 0°C. Indicated specific emissions have been used in order to compensate for the effect of increased engine friction at lower engine temperatures. The three functions were obtained by curve fitting to experimental data obtained from the 2 litre DOHC 8V engine test rig. The data indicate that the effect of ECT on each of the indicated specific emissions is independent of engine speed, indicated load and tail-pipe AFR when the emissions are normalised to the corresponding indicated operating conditions at fully-warm. Indicated specific CO emissions were found to be around 5%-10% lower at 20°C than at fully-warm and to increase linearly with ECT despite the tail-pipe AFR remaining the same at all ECT values. Conversely, indicated specific HC emissions decreased with increasing ECT and were in the region of 30% higher at 20°C than at fully-warm. Indicated specific NO_x emissions increased with increasing ECT and were around 30% lower at 20°C than at fully-warm. This behaviour is believed to be due to a degree of charge stratification in the cylinder due to mixture preparation changes in the intake system. Mixture preparation conditions in the intake port and HC emissions particularly are known to be very sensitive to ECT [5.4, 5.5] but the mechanisms governing the effects of ECT on emissions are less well understood. The tests presented here were carried out with a constant tail-pipe AFR measured

by a UEGO sensor which is believed to give an accurate measure of the overall in-cylinder AFR during steady-state operating conditions under force-cooled running [5.6]. Hence, even with a constant overall in-cylinder AFR, the degree of charge stratification decreases and the combustion AFR becomes progressively richer as mixture preparation improves with increasing ECT. This results in the observed increase in CO emissions and the corresponding decrease in HC emissions as the unburnt mixture fraction decreases. Figure 5.8 shows HC and NO_x correction factors plotted against CO correction factor during the warm-up phase with typical experimental data points, and shows HC emissions decreasing and NO_x emissions increasing during engine warm-up. Similar trends in HC and CO emissions have been observed qualitatively elsewhere [5.7, 5.8]. Lee's results are particularly interesting as he found that increasing ECT from 65°C to 100°C decreased HC emissions by around 10%, increased NO_x emissions by 10% and decreased CO emissions by less than 5%.

While the charge stratification theory outlined initially by Shayler et al [5.2] appears to hold for both CO and HC emissions, the behaviour of NO_x emissions is less clear. CO emissions are, in effect, a direct measure of the combusted AFR and HC emissions are primarily due to the remaining uncombusted and poorly oxidised fuel. NO_x emissions, like CO emissions, are heavily influenced by the combustion AFR and as such would be expected to either increase or decrease according to whether the combusted AFR was rich or lean of the peak NO_x AFR. However, the additional effect of changing combustion temperature during warm-up is believed to out-weigh any effect of charge stratification, since NO_x emissions were always observed to increase during warm-up independently of AFR. Similar trends in NO_x emissions have been observed by Andrews et al [5.8] and Russ et al [5.9] and explained in terms of increasing combustion temperature.

Both CO and NO_x emissions are directly linked to the AFR of the combusted in-cylinder mixture at all times in the warm-up process. Thus, isco and $isno_x$ at all points in the warm-up can be determined by scaling the fully-warm indicated

specific emissions to account for mixture preparation as described above. However, HC emissions arise primarily from fuel that does not take part in combustion and as such are particularly sensitive to any additional fuelling needed in the period immediately following a cold start. Consequently, an additional increase in HC emissions occurs over and above that associated with mixture preparation changes during this transient period.

The additional increase in HC emissions is believed to be due to liquid fuel films existing in the engine cylinder in the early seconds after engine start-up. The build-up of these fuel films and additional absorption of fuel into the lubricating oil [5.10] contributes to the 'unaccounted for' fuel behaviour described in Chapter 4 of this thesis. Various studies [5.11-5.13] have shown the existence of liquid fuel films in the engine cylinder and a significant fraction of this fuel is believed to pass directly into the exhaust system as unburnt hydrocarbons [5.14]. After combustion has been completed and the in-cylinder pressure decreases during the exhaust stroke, a proportion of the fuel wall-wetting in the cylinder is vaporised as unburnt hydrocarbons. The data for the 2 litre DOHC 8V engine presented in this chapter suggest that around 33% of the fuel 'unaccounted for' based on exhaust measurements made with a UEGO sensor is actually present as unburnt hydrocarbons in the exhaust system but passes the sensor undetected. Similar work on a Ford 1.8 litre HO Zetec engine [5.3] suggests that, for this engine, the additional HC emissions account for 50% of the UEGO 'unaccounted for' fuel fraction. Additional work on this engine [5.6] has attempted to identify the various sources of apparent fuel loss which result in the overall 'unaccounted for' fuel observed. Three sources of 'unaccounted for' fuel can be identified. Firstly, the UEGO sensor is demonstrated to record an AFR which is lean of the overall in-cylinder AFR during engine warm-up. This is because the UEGO sensor fails to fully account for the high proportion of unburnt hydrocarbons present in the period immediately following a cold start. As the warm-up proceeds and the HC concentration decreases, the UEGO sensor records an AFR which is progressively closer to the overall in-cylinder AFR. For the Zetec engine

examined, Shayler et al defined a UEGO sensor correction factor to scale the UEGO AFR to that calculated by analysis of all the exhaust gas products of combustion. This correction factor is specific to the engine examined and the same procedure cannot be applied to the DOHC engine data presented in this chapter since the rig instrumentation did not enable measurements of the carbon dioxide and oxygen concentrations in the exhaust gases needed to calculate the exhaust AFR. Consequently, for the DOHC engine data, the contribution of UEGO sensor errors to the total 'unaccounted for' fuel cannot be accurately defined and the 'unaccounted for' fuel, characterised from experimental data in Chapter 4, includes fuel, in the form of unburnt HC, undetected by the UEGO sensor.

Predicting the amount of fuel stored temporarily in the engine cylinder and absorbed into the lubricating oil is difficult. After correcting the UEGO sensor AFR during warm-up, Shayler et al [5.6] estimate the relative proportions of fuel stored and fuel lost by analysis of the HC and UEGO corrected 'unaccounted for' fuel curves during warm-up, but once again, the lack of an accurate UEGO correction function for the DOHC engine prevents a similar analysis here. However, the fact that the additional HC contributes 33% of the total 'unaccounted for' fuel on the DOHC engine and that this fraction is around 50% on the Zetec engine, given that the additional HC mass flow rate is similar for both engines, suggests that the proportion of fuel lost to the lubricating oil is greater for the DOHC engine. This is believed to be consistent with the comparitively more modern design and construction of the Zetec engine.

Because the UEGO sensor does not provide an accurate overall AFR during the early period of engine warm-up, the 'unaccounted for' fuel predicted by the exponential functions detailed in Chapter 4 will give an over estimation of the additional fuel required when predicting cold-start fuel consumption from fully-warm engine data. However, using the UEGO sensor to determine the 'unaccounted for' fuel is consistent with current vehicle technology which relies

on a similar sensor, the HEGO sensor, to maintain an assumed stoichiometric AFR during both warm-up and fully-warm operation. In reality, such a sensor will maintain a tail-pipe AFR that is slightly rich, in the region of one air/fuel ratio, of stoichiometric in the period when the exhaust hydrocarbons are high and not fully-accounted for by the exhaust mounted sensor. In addition, using such a sensor here enables the definition of a simple function to relate excess exhaust hydrocarbons during warm-up to the UEGO predicted 'unaccounted for' fuel detailed in Chapter 4.

5.6 Conclusions

In order to investigate the possibility of predicting engine-out emissions during cold-starting and engine warm-up two sets of warm-up tests have been carried out. The first set of tests involved force-cooling the engine to establish near steady-state engine conditions at non-fully warm temperatures and constant tail-pipe AFR. These tests suggest that, unlike indicated specific fuel consumption, indicated specific emissions are strongly dependent on ECT. The data suggest that fully-warm indicated HC, CO and NO_x emissions can be scaled by a simple ECT Correction Function to account for changes in mixture preparation due to reduced coolant temperatures during engine warm-up. Indicated specific emissions were used to remove the effect of increased engine friction at lower engine temperatures enabling the effect of mixture preparation to be assessed independently.

Changes in emissions with ECT have been explained in terms of charge stratification due to poor vaporisation in the intake system and reduced combustion temperatures due to reduced in-cylinder metal temperatures.

The relationship between the additional HC emissions immediately following start-up and the 'unaccounted for' fuel in this period has been investigated. Experimental data indicate that a simple linear relationship exists between the additional HC over that predicted by poor mixture preparation and 'unaccounted

for' fuel measured using a UEGO sensor, such that the additional HC is around 33% of the 'unaccounted for' fuel at any time during the warm-up.

Similar work at Nottingham University [5.6] suggests that, in the period immediately following a cold start, the UEGO sensor does not fully-account for unburnt hydrocarbons in the exhaust pipe resulting in a measured AFR that is lean of the actual tail-pipe AFR. Consequently, the 'unaccounted for' fuel predicted based on UEGO measurements provides an over-estimate of the fuel stored in the engine cylinder and absorbed in the lubricating oil. Experimental data suggest that, for the engine examined, around 33% of the fuel unaccounted for by the UEGO sensor is actually present as unburnt hydrocarbons in the exhaust pipe.

Chapter 6

Engine Thermal Model to Predict Friction Characteristics

6.1 Introduction

Both fuel consumption and emissions are affected by changes in thermal conditions during engine warm-up. In order to apply the developments and results described in the preceding chapters, a means of predicting how thermal conditions vary from engine start-up onwards is required. This involves the use of an engine thermal model developed at the University of Nottingham called PROMETS which, amongst other things, provides the facility to predict engine frictional losses and oil and coolant temperature variations. The indicated mean effective pressure (imep), defined as the total work delivered to the piston over the entire four strokes of the engine cycle per unit displaced volume, is calculated from the brake mean effective pressure as:

$$\text{imep} = \text{bmep} + \text{fmep} \tag{6.1}$$

where fmep is the friction mean effective pressure due to rubbing friction in the engine and ancillary friction losses such as the water and oil pumps. This chapter gives a brief description of the thermal model employed and details its application to the work presented in this thesis. A more detailed description is given elsewhere [6.1].

Increased frictional losses are responsible for a significant part of the increase in fuel consumption of a cold engine. Sorrell and Stone [6.2] found that combustion chamber wall temperatures rose rapidly to their steady-state values, indicating that reduced thermal efficiency due to cold cylinder walls is not a significant

cause of increased fuel consumption during warm-up. Work by Haahtela et al [6.3] investigated the warm-up behaviour of a 1.3 litre engine starting at -10°C. Figure 6.1(a) shows the measured motoring frictional losses as a function of oil temperature. The excess motoring losses were attributed to the increased viscosity of the cold engine oil. Figure 6.1 (b) shows that the effect of oil temperature on frictional losses is different for various engine components. Temperature was found to have the greatest influence on the crankshaft group, which includes the crankshaft, connecting rod, piston and rings. It was also estimated that the fuel flow rate required at -10°C is 85% higher than that required by a fully-warm engine. Much work has been done to investigate the effect of engine oil viscosity on engine cranking, starting and warm-up fuel economy [6.4-6.7], but little work relates to the prediction of frictional losses during the period between start-up and fully-warm.

6.2 Modelling Engine Friction Using PROMETS

The PROMETS software package enables engine oil, coolant and metal warm-up rates to be predicted for a defined set of engine operating conditions. Thermal analysis of the engine structure is based on the lumped capacity approach. The engine is divided into elements, each of which has a spatially uniform temperature, a given thermal capacity, and is thermally coupled to adjacent elements and to any adjacent heat sinks. Energy balance equations are formed for each element and temperatures obtained by solving appropriate sets of simultaneous equations. In the version of PROMETS used here, 36 elements are used to represent the engine structure around one cylinder of the 1.8 litre Zetec engine and 30 elements for the 2 litre DOHC 8V engine. The additional six elements in the Zetec case are used to define the additional intake and exhaust valves in this engine configuration.

The friction model in PROMETS is used to predict the increase in imep caused by higher friction losses during engine warm-up. In determining friction losses, it is important to clarify the component sources that are included in the

calculation. In this thesis, imep is defined as the net imep or the work delivered to the piston over the entire four strokes of the cycle, per unit displaced volume. As such, it follows that:

$$\text{imep} = \text{bmep} + \text{rfmep} + \text{amep} \tag{6.2}$$

where rfmep is the rubbing friction mean effective pressure and amep the accessory mean effective pressure.

The friction model developed by Patton et al [6.8] is used to predict the rubbing friction and accessory mean effective pressure terms for fully-warm engine states. The effect of the bore, the stroke, the number of cylinders, the number and size of bearings and the valve train configuration are accounted for. The bearings group includes friction from the main bearings, con-rod bearings and camshaft bearings. The piston groups includes friction from piston and piston rings and the valve train group is made up of friction from the cam followers and valve actuator mechanisms. The accessory friction is the sum of oil pump, water pump and alternator friction. The correlations used to define these terms are given for reference in Appendix B.

In the implementation of the friction model used by PROMETS, the net indicated work, $W_{c,i}$, is determined over the whole engine cycle as:

$$W_{c,i} = \oint P.dV \tag{6.3}$$

and imep is calculated as:

$$\text{imep} = \frac{W_{c,i}}{V_s} \tag{6.4}$$

where V_s is the swept volume. Consistent with these definitions, the total friction losses described hereafter are only the sum of the rubbing friction loss and accessory friction loss and are independent of pumping losses during the

induction and exhaust strokes of the cycle.

Power and mean effective pressure (mep) are related by:

$$\dot{P} = mep.V_s . \frac{N}{n_R} \tag{6.5}$$

where n_R is the number of revolutions per cycle and N the engine speed in revolutions per second. In the following, the total friction power loss is denoted by $\dot{P}_{prf}$, the rubbing friction loss by $\dot{P}_{rf}$, and the accessory friction power loss by $\dot{P}_a$. These terms are related by:

$$\dot{P}_{prf} = \dot{P}_{rf} + \dot{P}_a \tag{6.6}$$

6.2.1 Friction Power Losses During Steady-State

The total friction power loss, $\dot{P}_{friction}$ predicted using the Patton et al model [6.8], is split into four components so that the frictional generated heat can be distributed as heat sources within the thermal analysis of the engine.

$$\dot{P}_{friction} = \alpha(a+b+c+d)\dot{P}_{prf} \tag{6.7}$$

where:

$$a+b+c+d=1 \tag{6.8}$$

where the coefficients a to d represent the proportions of the steady-state friction losses for the valve train, the bearings, the piston, and the accessory components respectively. The factor α is used to compensate for discrepancies between measured friction losses and the friction losses predicted by the model. Experience of applying the model [6.9] indicates that α is typically 1.34 for a four cylinder engine. Table 6.1 lists the predicted friction losses for each component source of the 2 litre DOHC 8V engine running at 3000 rpm and 30 Nm brake

load. It can be seen that piston friction accounts for the largest proportion of the total friction losses, and is dependent on gas pressure.

6.2.2 Friction Power Losses During Warm-Up

For other than fully-warm running conditions, the effect of oil temperature on viscosity and hence friction losses is taken into account by introducing a correction factor. This is used to scale the instantaneous friction loss in proportion to values at the same running condition for fully-warmed up conditions. The correction is given by:

$$\dot{P}_{warm\text{-}up} = \left(\frac{\nu}{\nu_{ref}} \right)^{n} \dot{P}_{f} \qquad (6.9)$$

where the reference viscosity is for a temperature of 90°C and ν is the viscosity at any time during warm-up, whose dependence on absolute temperature T_{abs} is calculated using the Walther equation [6.10]:

$$\ln(\ln(\nu+0.6)) = c_1 + c_2 \ln T_{abs} \qquad (6.10)$$

where c_1 and c_2 are constants determined from the oil viscosity specification. The reference oil temperature is that at the inlet to the oil pump and is taken as being representative of the mean sump oil temperature. The index n has been determined experimentally to be typically 0.19-0.24 [6.9]. Not all of the friction loss dissipated as heat goes into the lubricating oil. The majority is transferred to adjacent parts of the engine structure or piston. During the development of PROMETS the split between the proportion transferred to the surrounding structure and the proportion which heats the oil directly has been established by trial and error to best match measured temperature characteristics on a number of engines. Typically, about 10% of the friction power is dissipated directly to the oil.

In the version of PROMETS used here, heat transfer from the gas side to the engine structure is described by a model which partly utilises the Taylor and

Toong correlation [6.11] for heat rejection rate to the coolant under fully-warm operating conditions. The calculation depends upon the mass flow rate of fuel induced which, during warm-up, will be higher than for fully-warm operating conditions at the same brake load and speed conditions due to the higher friction levels. Thus the increased fuel flow rate must be estimated to enable a prediction of warm-up and friction characteristics. This estimation is only used to generate the engine warm-up profile and, as such, only a relatively crude estimate is required. This is achieved by assuming that the indicated specific fuel consumption at the warm-up temperature (say 20°C) is equal to that at 90°C and thus that:

$$\dot{m}_{f,20°C} = \frac{\dot{m}_{f,90°C}}{\dot{P}_{f,90°C}+\dot{P}_b}\,(\dot{P}_{f,20°C}+\dot{P}_b) \qquad (6.11)$$

where $\dot{P}_f$ is the friction loss at the relevant temperature indicated by the subscripts and $\dot{P}_b$ is the brake power.

6.3 Validation of Friction Model

Previous experimental work by Christian [6.12] investigated the warm-up and friction prediction accuracy of PROMETS for a Ford 1.1 litre Valencia engine over the temperature range from 20°C to 90°C using SAE 10W/30 engine oil. In addition to the experimental work, Christian validated the above procedure for determining friction power losses during engine warm-up using published friction data for a 1.3 litre Volkswagen engine [6.3]. He found that the difference between measured and predicted friction power losses was always less than 20% for temperatures between -10°C and 100°C and concluded that the above correlations provided an adequate friction prediction for PROMETS. In essence, equation (6.9) provides a useful approximation to describe the overall effect of oil viscosity on friction power losses for the entire engine, but further work is required to determine how accurate this approximation is over a wider range of test conditions.

In order to determine if the above relationships are valid over wider temperature and viscosity ranges additional tests were carried out using the 2 litre DOHC 8V engine test rig described in Chapter 3 of this thesis. The test facilities enabled start/soak temperatures down to -10°C to be used giving a much wider range of oil viscosity. To further extend this viscosity range, a series of tests were carried out with SAE 20W/50 oil and the effect of the value of the index n observed. The oil viscosity variation with absolute temperature was calculated using equation (6.10) and the variation for the two test oils is shown in Figure 6.2. The tests were carried out as fixed throttle free warm-up tests with start/soak temperatures of -10°C and +20°C with constant stoichiometric input AFR. Table 6.2 shows the range of operating conditions and start/soak temperatures used.

Figures 6.3 and 6.4 show measured and predicted friction power losses and measured and predicted oil and coolant warm-up temperatures for two typical tests with start/soak temperature of 20°C and -10°C respectively, and demonstrate close agreement between measured and predicted values. Of particular interest are the friction power losses in the period immediately following engine start-up. During this period the friction is much higher and reduces more rapidly than is predicted by equation (6.9). Such behaviour indicates that the viscosity of the oil at pump inlet temperature does not fully account for friction level changes immediately following start-up. In the version of PROMETS used here, a linear drop in friction power has been incorporated into the friction power loss representation. The friction power loss at engine start-up is assumed to be 1.5 times the value predicted by equation (6.9). After 50 seconds, the friction power losses are assumed to be fully-dependent on oil viscosity and are then calculated directly from equation (6.9). While the linear drop in friction representation provides a good approximation to the friction behaviour for the 20°C start the approximation is less accurate for the -10°C start where the initial friction factor (F) is greater than 1.5 times the value predicted by equation (6.9) and takes longer than the allowed 50 seconds to decay. In order to develop a more representative

model of the initial start-up friction behaviour additional cold-start tests have been carried out on the 2 litre DOHC 8V engine and additional engine test rigs at the University of Nottingham. This work is ongoing, but initial results suggest that an exponential decay function provides a more accurate model of the initial friction behaviour. The initial friction factor F is modelled as:

$$F = 1 + Xe^{\left(-\frac{t}{\tau}\right)} \qquad (6.12)$$

where t is the time from engine start-up and X and τ are determined from experimental data. Initial work on a range of engines suggests that X is dependent on engine start/soak temperature and τ on engine speed and oil viscosity. Figure 6.5 shows the predicted friction behaviour using this function for the two cold-start tests detailed above. Equation (6.12) can be seen to provide a more accurate representation of the initial fricton behaviour but canot be incorporated into the PROMETS friction model until the dependence of τ and X on engine start temperature, speed and oil viscosity have been determined.

Figure 6.6 shows ln(friction power loss ratio) against ln(viscosity ratio) for all the warm-up test data for both the 10W/30 and 20W/50 engine oils. In both cases, the deviation from the linear fit at high viscosity ratios is due to the increased engine friction immediately following engine start-up. The gradient of the linear fit to these data equates to the index n which was found to be 0.19 for the 10W/30 oil and 0.16 for the 20W/50 oil. This suggests that equation (6.9) provides a good approximation to the actual friction power loss behaviour for a given test oil and that the index n is dependent on oil type/classification. The much higher viscosity of the 20W/50 oil at low temperatures enables equation (6.9) to be validated for a larger range of viscosity ratios than would be possible with just the 10W/30 standard test oil.

6.4 Discussion

The PROMETS engine thermal model enables predictions of both engine

temperature and friction power losses to be made. The correlations used to calculate fully-warm engine friction levels are derived from the Patton et al model [6.8] and reflect the importance of basic design variables and generate a distribution of frictional dissipation throughout the whole engine.

Comparisons between measured and predicted friction power losses during engine warm-up for a Ford Valencia and, as presented here, for a Ford 2 litre DOHC 8V engine give high confidence in the technique used to scale fully-warm engine friction levels according to oil viscosity. The experimental work presented in this chapter confirms the validity of this scaling over a wider range of oil temperatures and with two different test oil specifications.

Predicting friction power losses in the period immediately following a cold-start requires an additional modification to the fully-warm friction levels over and above that described by equation (6.9). During this period, friction levels are higher than predicted by equation (6.9) and decay more rapidly, suggesting that friction levels immediately after start-up are not entirely governed by the bulk oil viscosity. Christian [6.12] suggested a linear correction function to predict this start-up friction, and the test data presented here suggests that this provides an adequate approximation to the measured friction behaviour. He postulated that the apparent independence of engine friction on oil viscosity in the first 50 seconds of engine operation was due to a lack of oil on the rubbing surfaces and the time taken to fully develop flow conditions in the engine. The exact lubrication mechanisms that result in the observed behaviour are not fully understood. Work by Hashizume and Kumada [6.13] has investigated the effect of oil flow rate on bearing temperature and it is possible that the start-up friction behaviour could be explained by differences in the oil temperature at the bearing surfaces and in the oil galleries. Additional cold-start test data from the DOHC engine test rig suggests that the start-up friction behaviour is more accurately modelled by an exponential decay function and is influenced by engine start/soak temperature and engine speed. This is believed to be due to the effects of the

initial bearing temperatures and the time taken for the bearing oil temperatures to stabilise, governed by the rate at which fresh oil is supplied to the bearing surfaces. However, further work is required to determine the way these effects combine to determine start-up friction behaviour and is currently being undertaken. Consequently, the original linear friction correction model used in PROMETS was adopted for the work presented here as it provides a good approximation to the friction behaviour, particularly when start temperatures of 20°C or higher are of interest.

Chapter 7

Application to Cold-Started Drive Cycles to Predict Fuel Consumption and Emissions

---

7.1 Introduction

The Cold Emission Cycle Simulation Program (CECSP) draws on the various models and results described in previous chapters and further components of the prediction scheme described in this chapter. The complete CECSP package enables second-by-second fuel and emissions flow rates to be predicted for a given drive cycle from a cold-start initial condition. A combination of engine friction models and mixture preparation compensation functions enable the application of fully-warm engine test bed data to cold-start conditions. Neural networks are used to characterise the fully-warm engine mapping data as described in Chapter 2.

To demonstrate the complete procedure, CECSP has been applied to the ECE+EUDC drive cycle with a 20°C start temperature and with the currently allowed 40 second idle conditioning period before emission sampling begins. A neural network is used to map fully-warm fuel and emissions mass flow rates as a function of engine speed, indicated load and AFR for the engine under consideration which is then used to interpolate fuel and emission flow rates at each point in the drive cycle. In order to predict cold-start fuel and emissions flow rates from fully-warm mapping data the PROMETS friction model is used to calculate the increased engine friction during warm-up and hence the new indicated load profile. The correlations derived in Chapter 5 are used to correct the predicted emissions values for the effect of changes in mixture preparation at low engine coolant temperatures.

In addition to predictions of engine-out emissions, tail-pipe emissions are predicted using a simple catalyst model. This enables experimental catalyst efficiencies for a given drive cycle to be used, if available, or more generally, the definition of catalyst light-off times and conversion efficiencies. When predicting tail-pipe emissions, particularly those of HC, the prediction accuracy in the early part of the drive cycle is of paramount importance as it is this period, before catalyst light-off occurs, that contributes the bulk of the total drive cycle emissions. The increased HC emissions immediately following start-up have been closely linked to differences in fuel injected and fuel combusted and to the corresponding liquid fuel puddles believed to exist in the engine cylinder during this period.

CECSP enables the user to select different combinations of engines and vehicles and to change various vehicle characteristics such as transmission ratios, wheel radius and total vehicle mass. The drive cycle to be used is defined as a series of second-by-second vehicle speed and gear number points and the start/soak temperature defined in the PROMETS friction model module of the software. The ECE+EUDC has been used during the development of CECSP. The complete vehicle speed profile for this cycle is shown in Figure 7.1 and consists of two parts, the elementary urban cycle (repeated four times) and the extra-urban cycle. For a given vehicle and drive cycle specification, engine speed variations can be defined from knowledge of rolling tyre radius and transmission ratios. The engine speed N is defined as:

$$N = \frac{v_{veh} R_{gear} R_{FDR}}{0.37699 r_{wheel}} \tag{7.1}$$

where v_{veh} is the vehicle speed(km/hr), R_{gear} the gear ratio, R_{FDR} the final drive ratio and r_{wheel} the driving wheel radius(m). The engine brake torque (M_{engine}) is then calculated by dividing the engine brake power requirement by the engine speed at each point in the cycle. Thus:

$$M_{engine} = \frac{60(\dot{P}_{rl}+\dot{P}_{KE})}{2\pi N\eta_{trans}} \qquad (7.2)$$

where:

$$\dot{P}_{rl} = F_0+F_1v_{veh}+F_2v_{veh}^2 \qquad (7.3)$$

F_0, F_1 and F_2 are coefficients determined by experiment. $\dot{P}_{KE}$ is the power required at the road wheels to increase the kinetic energy of the vehicle during acceleration. This term is set to zero when decelerating, as under these conditions energy is dissipated through the vehicle brakes and the engine is motored. This simple vehicle model enables the vehicle performance during a drive cycle to be translated into required engine performance at the engine flywheel. Figure 7.2 shows a typical example of the variations in engine brake torque and speed during the ECE+EUDC drive cycle for a medium sized vehicle. It is assumed that the over-run periods when the engine is motored can be treated as zero load points at the appropriate engine speed. Once the required engine performance over the drive cycle has been determined in this way, fuel consumption and emissions mass flow rates are inferred from fully-warm engine data modified to account for cold-start effects.

7.2 Predicting Drive Cycle Fuel Consumption and Emissions

Although not an essential part of the procedure, using neural networks to characterise engine fuel consumption and emissions performance as a function of operating conditions and calibration details has proved to be both effective and efficient, as detailed in Chapter 2. Fuel and emissions flow rates are determined by a neural network which maps fuel and emissions flow rates as a function of engine speed, indicated load and AFR. This same network can then be used to predict cold-started fuel consumption once the cold-started friction values have been calculated for each point in the drive cycle. Details of the neural network

configuration used and the training procedure employed are also detailed in Chapter 2 of this thesis. Two neural networks are used. The first maps fuel and emissions flow rates as a function of engine speed, bmep and AFR and the second uses engine speed, imep and AFR as inputs. In order to train the second network, the fully-warm mapping data has to be recast to express brake operating conditions as indicated operating conditions. This is done using the fully-warm component of the PROMETS engine friction model which is detailed in Chapter 6. Indicated mean effective pressure (imep) is calculated as:

$$\text{imep} = \text{bmep} + \text{fmep} \tag{7.4}$$

Figure 7.3 shows the steps in the prediction procedure to enable fully-warm fuel consumption and emissions values to be determined. In order to predict friction power losses at each point in the fully-warm drive cycle, approximate fuel mass flow rate values at each point are needed. Hence, the first network trained on brake operating conditions is used to determine this fuel flow rate data, enabling friction power losses to be predicted and indicated operating conditions to be defined. The second neural network is then used to determine new fuel mass flow rates and emissions mass flow rates over the drive cycle. These new fuel mass flow rates are then used to re-calculate engine friction power losses and hence indicated loads, and the network used to predict new fuel consumption and emissions values. This process is repeated until the change in predicted total drive cycle fuel used is less than 0.5%, as indicated in Figure 7.3. Generally, not more than three iterations are required to achieve this level of prediction accuracy.

Applying the procedure to a cold-started drive cycle entails the prediction of engine friction at each point in the drive cycle as the engine warms up in parallel with a time marching calculation of fuel consumption from the corresponding indicated operating conditions, as shown in Figure 7.4. The rate at which the engine structure and lubricating oil warm-up influences friction losses over the cycle, because these depend upon oil viscosity which in turn depends upon

temperature. The warm-up behaviour of the engine over the drive cycle is determined using the PROMETS engine thermal model. For each time step through the drive cycle, an iterative procedure is used to obtain a self-consistent variation of friction, indicated operating conditions and oil warm-up characteristics. Once the indicated operating conditions for the cold-started drive cycle have been determined the same neural network used to predict fully-warm fuel and emissions mass flow rates from indicated operating conditions is used to predict the cold-start values. However, in the cold-start case the values predicted by the network are not the final drive cycle flow rates, as the effects of poor mixture preparation during warm-up and initial start-up transient behaviour have to be accounted for. This is done by applying the 'unaccounted for' fuel and mixture preparation correcting functions described in chapters 4 and 5 respectively. The corrected fuel and emissions mass flow rates are then summed over the drive cycle to give the total fuel consumption and emissions produced.

To extend the prediction procedure to include predictions of tail-pipe emissions a simple catalytic convertor model has been included in the CECSP program. The model uses second-by-second catalyst conversion efficiencies for each of the three exhaust emissions to convert the predicted engine-out, or feedgas, emission mass flow rates to tail-pipe flow rates. The inputs to the catalyst model are the catalyst light-off and fully-warm conversion efficiency characteristics. After catalyst light-off, the conversion efficiency is assumed to remain constant throughout the remainder of the drive cycle.

The catalyst conversion efficiency at time t in the period between the time when the catalyst starts to become active, referred to here as the 'dead' time D, and the catalyst reaching its fully-warm efficiency, referred to here as the light-off time L, is modelled by the following function:

$$\eta_t = \eta_{cat}(1 - e^{\tau}) \qquad (7.5)$$

where:

$$\tau = -6\left(\frac{t - D}{L - D}\right) \tag{7.6}$$

η_{cat} is the fully-warm catalyst efficiency and t is the time elapsed from the start of the drive cycle. The above relationships were derived to fit the experimental data for the catalyst performance of three catalyst types and locations for a particular vehicle. Consequently, the model requires the knowledge of catalyst light-off times and conversion efficiencies for each engine/vehicle/drive cycle combination, and is not a complete model of catalyst behaviour.

7.3 Prediction Accuracy and Sources of Error

The prediction accuracy achieved by CECSP for any given application is dependent on the magnitude of various error sources from the various stages of the procedure. These can be classified as known and unknown sources of error and the way in which these combine to influence the final results can only be determined by comparisons with experimental data. The main known sources of error are the neural network/friction model characterisation of the fully-warm engine map (Chapter 2) and the temperature correction functions used to compensate for mixture preparation effects on emission levels during engine warm-up (Chapter 5). In each case, accuracy was discussed in the relevant chapter. Additional unknown errors are believed to arise as a result of engine management system details which cannot be generalised and are of concern during over-run conditions, AFR variations during throttle transients, start-up transients, and changes in engine calibration details at non-fully-warm operating conditions. This section deals with the overall prediction accuracy despite the engine management assumptions made in CECSP, by application to a Ford 1.8 litre Zetec engine in a Mondeo driven over the ECE+EUDC drive cycle in accordance with EC Stage 2 legislation requirements.

7.3.1 Treatment of Idle and Over-Run Conditions

CECSP assumes that all the over-run periods in the drive cycle can be treated as zero load idle points at the appropriate engine speeds. Fuel and emissions flow rates during over-run are thus predicted by inputing the appropriate engine speed, imep and AFR values to the neural network. The AFR during over-run is assumed to remain unchanged from the stoichiometric baseline and, as such, the over-run predictions are a simplification of the actual conditions.

In order to model over-run conditions more accurately, detailed knowledge of the fueling strategy would be required. Fueling during over-run influences HC emissions particularly, as in this period the engine is prone to poor combustion stability and misfire. Work by Boam et al [7.1] looked at HC emissions during over-run periods of the ECE+EUDC drive cycle and explained the observed behaviour in terms of features of the engine management strategy. Different engine fuelling strategies employ varying degrees of fuel cut-off during deceleration (Decel Fuel Cut-Off or DFCO) and so HC behaviour during periods of deceleration is difficult to predict. DFCO is beneficial in terms of reducing fuel consumption, CO and NO_x emissions but not HC emissions, as liquid fuel films in the inlet port cause high HC concentrations due to either a partially or completely incombustible mixture entering the cylinder. During long periods of deceleration with complete fuel cut-off, wall film dryout may occur when all the liquid fuel in the intake system has evaporated. This phenomenon results in extremely low HC emissions during this period. However, when the engine is restarted a significant proportion of the injected fuel is needed to restore the intake port wall fuel films resulting in a lean mixture entering the cylinder and possible misfire once again until the wall films are fully restored. Hence, HC emissions during over-run may be sensitive to fuelling strategy details, which are beyond the scope of this work.

Figure 7.5 shows experimental and predicted HC flow rate data for the 1.8 litre Zetec Mondeo application during the final and longest over-run in the

ECE+EUDC drive cycle. The predicted data, based on no-load idle conditions, provides a good basic approximation to the HC behaviour, but does not model the extremes believed to be caused by misfire and port wall dryout described above. Figure 7.6 indicates that only around 17% of the ECE+EUDC drive cycle is periods of deceleration and so any errors in the predictions during these periods are less significant than at all other operating conditions. This, combined with the generalised approximation of fast idle to deceleration conditions, results in the deceleration prediction performance illustrated in Figure 7.7, where deceleration fuel consumption and emissions are all predicted close to the target +/-10% accuracy.

7.3.2 Overall Prediction Accuracy

Prediction errors within CECSP come from neural network predictions, PROMETS friction model predictions and the mixture preparation compensation assumptions discussed in previous chapters. In addition, errors from the over-run and constant AFR during throttle transient assumptions are believed to exist, as well as errors resulting from the assumption that identical spark timing and EGR rates apply at both cold-start and fully-warm conditions. The errors due to both neural network engine map characterisation and mixture preparation compensation have been shown to be entirely random within the boundaries described in Chapters 2 and 5, and so predicting the error at any given point in the drive cycle is not possible. The overall prediction accuracy can be assessed by comparison with experimental data taken using a chassis dynamometer or 'rolling road'. However, such experimental data do not provide a direct comparison with predicted data due to several assumptions made in the predictions. In CECSP it is assumed that perfect mixture control maintains stoichiometric conditions throughout the drive cycle and that during over-run periods fuel and emissions mass flow rates for no-load apply at a given engine speed. Furthermore, during warm-up CECSP assumes that the same spark timing and EGR rate settings as at fully-warm apply. The only experimental data available for comparison for the engine and vehicle under consideration included a degree of fuel enrichment in

the first 50 seconds of the drive cycle and additional deviations from the desired stoichiometric AFR of around +/-0.5 AFRs at transient points in the cycle. Despite these differences, comparisons between experimental and predicted data for the 1.8 litre Zetec Mondeo indicate that both fuel and emissions drive cycle totals can be predicted to within the target accuracies of +/-5% for fuel and +/-10% for emissions. Although these target accuracy tolerances appear to be quite large, experimental fuel and emissions results are only obtainable to similar degrees of repeatability. Generally, from a range of experimental results supplied by Ford Motor Company for various engine and vehicle combinations, emissions totals varied by up to 10% and fuel consumption by up to 4% from test to test. In order to confirm that the prediction accuracies obtained when considering drive cycle totals exist over the range of conditions imposed over the drive cycle, the cumulative fuel and emissions results can be broken down into four categories: accelerations, decelerations, idles and cruises. These results are shown for fuel and HC mass flow rates in Figure 7.8 and for CO and NO_x mass flow rates in Figure 7.9. In all cases, predicted values lie within the target accuracy bands suggesting that the assumptions made do not compromise the overall prediction accuracy for this application.

7.4 Discussion

CECSP has been developed to predict fuel consumption and emissions flow rates for both fully-warm and cold-started drive cycles using a combination of neural networks and engine friction models. The data input to the procedure is fully-warm dynamometer engine mapping data covering the range of engine speeds, loads and AFRs imposed by the drive cycle. Other calibration details, such as EGR rates and spark timings, are currently determined by the form of the fully-warm data. The drive cycle is supplied as a series of vehicle speed and gear number points from which the engine speed and brake load profiles are calculated from various input parameters to define the vehicle under consideration. Thus the effect of changing both the vehicle and the engine can be investigated by changing the vehicle definition parameters or the engine mapping data. In

addition, the engine start/soak temperature at the beginning of the drive cycle can be varied. Tail-pipe emissions can be calculated from engine-out emissions using a simple catalyst efficiency model from defined catalyst conversion efficiency and light-off behaviour details for the particular engine/vehicle combination.

In order to predict cold-start fuel and emissions flow rates from fully-warm mapping data account has to be taken of the increased engine friction due to increased oil viscosity, poor mixture preparation in the intake port during engine warm-up and the initial transient behaviour of the engine in the period immediately following a cold-start. In addition, two important assumptions made in the prediction procedure are that AFR excursions during transient points in the drive cycle do not influence fuel consumption and emissions, and that zero load fuel and emission mass flow rates apply during over-run conditions. Comparisons with experimental data indicate that these assumptions allow predictions to be made to within the target accuracies of +/- 5% for fuel consumption and +/- 10% for engine-out emissions. Tail-pipe emissions can also be predicted by application of a simple catalytic convertor efficiency model enabling catalyst light-off times and conversion efficiencies to be defined. Consequently, the procedure outlined here provides the facility to investigate the likely influence of various vehicle, engine and drive cycle specification parameters on the instantaneous and cumulative drive cycle fuel and emissions mass flow rates. Furthermore, it enables possible routes to improve fuel consumption and emissions over cold-started drive cycles to be prioritised. The following chapter deals with ways in which the procedure has been used to determine these priorities.

Chapter 8

Illustration of Factors Influencing Drive Cycle Fuel Consumption and Emissions Performance

---

8.1 Introduction

The predictions of fuel and emissions flow rates detailed in Chapter 7 were computed using the assumptions that start-up effects on emissions are negligible, that mixture control is perfect and maintains stoichiometric conditions throughout the drive cycle, and that during the over-run periods of the cycle, fuel and emissions mass flow rates for no-load apply at a given engine speed. In this chapter, the extent to which these and other factors influence fuel consumption and emissions and their relative importance is investigated. As in the previous chapter, the vehicle data used were derived from a 1.8 litre Ford Zetec engine installed in a Mondeo vehicle. The data were obtained by driving the vehicle on a chassis roll dynamometer over the ECE+EUDC drive cycle with the initial 40 second conditioning period and a 20°C start temperature. The effect on the predictions made of changing various aspects of the engine/vehicle/drive cycle application used are considered. This approach has been used to rank the various sources of increased fuel consumption and emissions over the ECE+EUDC drive cycle and demonstrate the suitability of the procedure to other engine/vehicle/drive cycle combinations. Both engine-out and tail-pipe emissions are considered. Total tail-pipe emissions are particularly sensitive to emission levels in the early seconds of engine operation before the catalytic convertor becomes effective. The factors investigated are increased engine friction due to reduced engine temperature, poor mixture preparation during engine warm-up, possible AFR mixture excursions during throttle transients and cold-start transient contributions due to poor fuel utilisation immediately following a cold start.

8.2 Increased Engine Friction During Warm-Up

In order to investigate the effect of increased engine friction on total fuel consumption and emissions, comparisons were made between predictions for a fully-warm and a 20°C cold-started ECE+EUDC drive cycle. To enable the effect of engine friction alone to be assessed, the emissions mixture preparation correction functions were not applied and cold-start transient effects were assumed to be negligible. The results are shown in Table 8.1 and indicate that increased engine friction when reducing the drive cycle start/soak temperature from fully-warm to the legislated 20°C increases predicted fuel consumption by 4.5%. With the 20°C start, the oil temperature does not reach 90°C until nearly 1100 seconds of the drive cycle have elapsed, as shown in Figure 8.1. This suggests that, although the increase in engine friction is most significant in the first 400 seconds of the drive cycle, the effect of increased engine friction persists throughout most of the cycle. This is confirmed by the increased fmep, predicted by the PROMETS friction model, when compared to fully-warm (delta fmep) shown in Figure 8.2.

8.3 Poor Mixture Preparation During Warm-Up

The work presented in Chapters 4 and 5 of this thesis concerns the effect of mixture preparation changes during engine warm-up on indicated fuel consumption and emissions respectively. Indicated specific fuel consumption has been found to be only weakly dependent on engine coolant temperature down to coolant temperatures of -10°C. However, emissions concentrations and hence indicated specific emission levels are much more sensitive to mixture preparation variations. Chapter 5 details the derivation of three simple functions relating HC, CO and NO_x emissions at a given coolant temperature to the fully-warm value at the same engine operating condition. These functions apply at all operating conditions and on both the engines examined in the experimental work described to within the +/-5% target accuracy required for the drive cycle predictions. In essence, the HC emissions are around 30% higher at a coolant temperature of 20°C, NO_x emissions around 30% lower and CO emissions around 5-10% lower.

When applied to the ECE+EUDC drive cycle with a 20°C start temperature the changes in cumulative totals associated with the deterioration in mixture preparation during warm-up represent a 2.1% increase in HC and decreases of 0.7% and 1.6% in CO and NO_x respectively. Poor mixture preparation increases the HC penalty but actually reduces the CO and NO_x penalty associated with a cold start. The mixture preparation correction factors are functions of ECT and as such only apply in the period before thermostat opening occurs at around 300 seconds into the ECE+EUDC drive cycle (Figure 8.1).

8.4 AFR Mixture Excursions During Throttle Transients

During the development of the prediction procedure, the AFR over the drive cycle has been assumed to be constant and unaffected by rapid changes in charge flow rate due to throttle transients. The effect of any AFR deviations due to throttle transients on fuel consumption are expected to be insignificant since rich and lean excursions would in effect cancel each other out. However, the effect on emissions flow rates is likely to be more significant. The experimental data presented in Chapter 7 suggest that the prediction accuracy is not compromised by the assumption that throttle transients do not significantly influence emissions since each of the emission levels during periods of both acceleration and deceleration is predicted to within the overall prediction target accuracy of +/-10%, as shown in Table 8.2. However, in the experimental case presented for the 1.8 litre Zetec engine Mondeo the AFR during the drive cycle was controlled to within +/-0.5 AFRs of stoichiometric, which may not always be possible.

To take account of larger AFR excursions during transient changes in operating conditions requires a prediction of these excursions. This requires knowledge of fuel transfer behaviour in the intake port and a representation of the fuel supply control strategy which is beyond the scope and objectives of this work. However, the potential influence of such variations has been examined by imposing fixed excursions of +/-2 AFRs for two seconds at points in the cycle where rapid changes in charge flow rate or gear changes occur which represent a 'worst case'

scenario for a modern production engine. The ECE+EUDC contains 22 gear change points resulting in throttle transients and a further 80 throttle transients due to periods of acceleration or deceleration. Consequently, around 200 seconds or a sixth of the cycle is assumed to be run at a non-stoichiometric AFR when these excursions are imposed. This enables an approximate percentage change in each of the emission concentrations during the transient points to be calculated and hence the percentage change of the total drive cycle results to be determined. Figure 8.3 shows that the imposed excursions give rise to increases of 1.7% and 33.2% in HC and CO emissions, respectively, and a 7.3% decrease in NO_x emissions. The large increase in CO emissions is due to the sensitivity to AFR variations on the rich side of stoichiometric.

Although the magnitude and duration of the excursions imposed above is likely to be at least as extreme as those seen in most modern multi-point fuel injected engines, it is still possible that the resultant effects on emissions, particularly HC emissions, are conservative. In practice, rapid changes in throttle position can lead to partial or complete misfire [8.1] and this possibility has not been evaluated. However, despite the limitations when predicting emissions at transient points, CECSP can be used to illustrate the importance of good AFR control during transient changes on operating conditions.

When extending the approach of imposing AFR excursions at transient points in the drive cycle described above to tail-pipe emissions, the additional effect of AFR on catalyst conversion efficiency has to be considered. In order to both oxidise HC and CO emissions and reduce NO_x emissions a three-way catalyst requires the tail-pipe AFR to be maintained extremely close to stoichiometric [8.2], as shown in Figure 8.4. If the AFR becomes excessively rich then oxidation of HC and CO emissions is not possible and if the AFR becomes excessively lean the reduction of NO_x emissions is inhibited. Hence, when imposing the same pattern of drive cycle AFR excursions used when considering feedgas emissions, the catalyst conversion efficiency was assumed to be zero for HC and CO

emissions during rich excursions and zero for NO_x emissions during lean excursions. This generalised approach is expected to give a 'worst case' scenario but is intended to show how the procedure can be used to indicate the adverse effect on tail-pipe emissions if tight AFR control is not maintained during transient conditions. The results are shown in Figure 8.5. The modelled catalyst is electrically heated with a conversion efficiency of 98% and light-off time of 23 seconds. As is the case for the engine-out emissions, the CO increase reflects the strong dependence on AFR. The HC and NO_x tail-pipe emissions account for about 15% of the feedgas totals when the simulated mixture excursions are imposed, compared to around 2.5% over the same intervals of the cycle when mixture control is assumed to be perfect.

8.5 Cold-Start Transient Contributions

During the period immediately following a cold-start at 20°C, HC emissions are higher than would be associated solely with mixture preparation changes. An additional increase in HC occurs which is attributable predominantly to liquid fuel passing through the combustion chamber and entering the exhaust pipe. Heywood et al [8.2] have shown that liquid fuel can be present in the cylinder of a firing engine upto 60 seconds after start-up. Experimental results, detailed in Chapter 4 of this thesis, indicate a difference between the fuel injected and the fuel burned as accounted for by the UEGO sensor mounted in the exhaust tail-pipe during this initial period and suggest that typically 33% of this fuel is actually present, but undetected, in the exhaust gas stream as unburnt hydrocarbons for the Ford 2 litre DOHC 8V engine. Chapter 4 details the development and application of a model to predict this 'unaccounted for' fuel. Figure 8.6 shows the predicted 'unaccounted for' fuel percentage against time for an engine started cold at 20°C and allowed to idle. After 40 seconds of idle, currently allowed at the start of the ECE+EUDC drive cycle before emission sampling begins, the 'unaccounted for' fuel percentage has decayed to around 1%. The resultant effect on the drive cycle totals is minimal with the HC emissions increasing by a mere 0.3%. However if, as is likely in the future, the 40 second

conditioning period is removed the 'unaccounted for' fuel effect is more significant. Figure 8.7 shows the 'unaccounted for' fuel percentage and coolant temperature against time from start of the drive cycle when the conditioning period is removed and Figure 8.8 the increase in engine-out HC emissions associated with this 'unaccounted for' fuel prediction for the first 100 seconds after start-up. The total drive cycle fuel consumption increases by 0.1% and the HC emissions by a more significant 2.2%.

The increase in HC emissions occurs during the first 60 seconds of the ECE+EUDC drive cycle. Consequently, the effect on tail-pipe emissions is much more significant than on engine-out values because the catalytic convertor has not reached its peak conversion efficiency. To illustrate these effects, computations were carried out with a catalyst with an assumed efficiency of 98% and light-off times typical of various catalyst types and locations. These times were assumed to be 23 seconds for an electrically-heated catalyst (EHC), 70 seconds for a close-coupled catalyst (CCC), and 130 seconds for an underbody catalyst location (UBC). Figure 8.9 shows that in the best case, and including the effect of start-up transients on HC emissions, tail-pipe emissions are reduced to around 2.7% of the feedgas totals. Including the start-up transient HC emissions increases the best case from 2.7% to 3.5% representing a 30% increase in tail-pipe HC emissions. This clearly demonstrates the importance of transient phenomena immediately following engine start-up and shows how the catalyst model in CECSP can be used to illustrate their importance over a drive cycle.

8.6 Discussion

CECSP has been used to assess the importance to both fuel and emissions totals over the ECE+EUDC drive cycle of the various factors influencing drive cycle results. While some of these factors were shown to be of little importance when predicting engine-out emissions for the initial engine/vehicle combination examined, they are believed to be more significant when extending the predictions to other engine/vehicle applications and particularly when predicting

tail-pipe emissions.

As described in Chapter 7, CECSP predicts feedgas emissions initially and these can then be converted to tail-pipe emissions using the catalyst model described. Factors which appear to have insignificant influences on feedgas emissions cannot be disregarded when predictions of tail-pipe emissions are also required. CECSP has been used to demonstrate the significance of these effects when predicting both feedgas and tail-pipe emissions and to prioritise the factors that influence both feedgas and tail-pipe emissions over the ECE+EUDC drive cycle most significantly.

The extent to which cold-start and warm-up affects the pattern of fuel consumption and emissions is shown schematically in Figure 8.10. The relative importance of higher engine friction during warm-up, poor mixture preparation penalties and start-up transient effects due to poor fuel utilisation are summarised in Table 8.1. The baseline for comparison here is ECE+EUDC drive cycle results generated assuming the engine is fully-warm from key-on and that cold-start transient effects are zero. All results are for the Ford 1.8 litre Zetec engine installed in a Mondeo. The results indicate that increased engine friction is the main source of increased fuel consumption and feedgas emissions and that poor mixture preparation and cold-start transient effects only influence HC emissions detrimentally, and even then only by around 2%. Mixture ratio excursions throughout the drive cycle during transient changes in operating conditions have been shown to have a potentially large influence on HC and, particularly, on CO emissions.

When tail-pipe emissions are considered, poor mixture preparation and cold-start phenomena prior to catalyst light-off have substantial effects on cumulative emissions, particularly of HC. Mixture ratio excursions have a more significant effect on emissions levels than for feedgas emissions due to the sensitivity of the catalytic convertor to AFR deviations from the stoichiometric baseline. The

sensitivity of tail-pipe emissions to engine calibration details makes absolute values difficult to predict accurately, and hence the application of CECSP presented here is intended to demonstrate the significance of the various factors influencing tail-pipe emissions rather than provide absolute predictions to within the accuracy possible with feedgas emissions. Table 8.3 shows the effects demonstrated to be of primary significance to tail-pipe emissions totals over the ECE+EUDC drive cycle together with suggested actions to limit these effects.

In conclusion, this chapter demonstrates the application of CECSP to examine the influence of cold-start and engine management strategy implications on drive cycle fuel consumption, and both feedgas and tail-pipe emission levels. The illustration presented demonstrates the need to reduce engine friction levels and warm-up times to be of principal importance to minimise drive cycle fuel consumption and feedgas emissions. However, when tail-pipe emissions are considered, these priorities are overshadowed by the need for rapid catalyst light-off and good fuelling control to minimise excess fuel supply and maintain tight control of AFR excursions during transients. The following chapter goes on to detail the additional applications the CECSP prediction procedure has been used for and the appropriate changes to the model required for these applications.

Chapter 9

Model Exploitation

9.1 Introduction

In the work presented so far, CECSP has been applied to a single engine/vehicle combination driven through the ECE+EUDC drive cycle from a cold-start condition. In this chapter, other applications of CECSP are considered. Essentially, the prediction procedure developed can be used in two ways. Firstly, predictions of the effect on drive cycle performance of changing various engine/vehicle parameters for different drive cycles can be made and the likely performance of new engine/vehicle combinations in the early stages of development assessed. Such predictions require assumptions or knowledge of likely exhaust gas after-treatment performance to enable tail-pipe emissions to be predicted. Secondly, predictions of feedgas emissions can be compared with desired tail-pipe values to enable target catalytic convertor characteristics and the associated exhaust gas after-treatment system development costs to be evaluated. In both cases, the prediction of feedgas emissions is influenced by various characteristics of the complete engine/vehicle/drive cycle package and the prediction procedure can be used to investigate the effect of these characteristics on the drive cycle performance. The following details five applications of CECSP, the interpretation of results and the implications of these.

9.2 Case 1: Drive Cycle Definition Effects

In this case, CECSP is used to demonstrate the effect on fuel consumption and emission levels of the drive cycle used. The software was developed using the ECE+EUDC drive cycle, also termed the New European Drive Cycle (NEDC). However, because engine fuel consumption and emissions performance is influenced by the characteristics of the drive cycle used to determine fuel and

emissions totals, the option to use different drive cycles was considered to be important.

In the United States, the Federal Test Procedure (FTP) is used to represent typical patterns of light vehicle operation and emissions limits defined accordingly, as detailed in Chapter 1. CECSP has been used to investigate the differences between the FTP-75 and ECE+EUDC drive cycles as these are considered to be the two most important cycles in current use. Essentially both the cycles define a series of engine operating conditions thought to be typical of those experienced during normal driving behaviour, but significant differences in the definitions of the cycles exist. The ECE+EUDC drive cycle has a duration of 1180 seconds and is run continuously through two sections. The first section consists of four repeated ECE cycles and the second section of one extra-urban cycle (EUDC), the latter specifying speeds of up to 120 km/hr. The current FTP-75 cycle lasts 1877 seconds and consists of four sections. Unlike the European cycle, each section is given an assessment coefficient to determine what proportion of the emissions produced during that section will contribute to the drive cycle total. The sections are as follows [9.1]:

- Transient phase with a duration of 505 seconds and an assessment coefficient of 0.43,
- Stabilised phase with a duration of 867 seconds and an assessment coefficient of 1.0,
- Stop phase of 10 minutes,
- Repeat of the transient phase with a hot start and an assessment coefficient of 0.57.

Figure 9.1 shows a comparison of the vehicle speed profiles for the two cycles and indicates that there is a significant difference in the proportion of time spent at particular operating conditions. To make comparisons of vehicle performance over the two cycles, predictions were made using the same 1.8 litre Zetec Mondeo application used previously. Both cycles involve a start/soak temperature

of 20°C and are assumed to be run at stoichiometric AFR conditions throughout. In the ECE+EUDC case, fuel and emissions are predicted from key-on without the 40 second idle period currently allowed for Stage 2 legislation and the cycle is run continuously from start to finish. The FTP-75 cycle, however, includes a 10 minute stop phase where the engine is switched off and a degree of engine cooling and reduction in fully-warm temperature gradients in the engine structure will occur. When applying CECSP to this cycle, the temperature changes during the stop phase are assumed to be negligible and the fully-warm transient phase assumed to start with the engine in the same thermal state reached at the end of the fully-warm stabilised phase.

Coolant and oil warm-up temperature variations are given for the first 800 seconds of both cycles in Figure 9.2. The early part of the ECE+EUDC drive cycle is lightly loaded compared to the FTP-75 cycle and consequently warm-up extends for a longer period into the cycle. The effects of cold-start up persists for a similar period in both. Over the cycles as a whole, the mix of operating conditions can be broken down into periods of acceleration, deceleration and cruise conditions. A comparison of the proportions of each category is shown in Figure 9.3. The most striking difference between the two cycles is the higher proportion of transient (acceleration and deceleration periods) in the FTP-75 cycle.

The extent to which cold-start and warm-up affects the pattern of fuel consumption and emissions is shown schematically in Figure 9.4. The relative importance of higher friction during warm-up, poor mixture preparation penalties and cold-start transient effects is shown in Table 9.1. The effects of cold-starting and warm-up can be seen to be less significant for the FTP-75 cycle due to the more rapid warm-up and the assessment coefficient system for weighting the emissions flow rates from the different phases of the cycle. This, together with the high engine loads demanded by the EUDC section of the European cycle results in the fuel and emissions flow rates per kilometre on the European cycle

being higher than those for the FTP cycle, as shown in Figure 9.5. Fuel, HC and CO emissions are all increased by similar amounts due to the higher charge mass flow rate over the European cycle. However, a greater increase occurs for NO_x emissions due to the additional sensitivity of NO_x concentrations to increases in brake load.

In conclusion, CECSP has been used to investigate the differences in fuel consumption and emissions performance between the two most widely used drive cycles. The ECE+EUDC drive cycle produces significantly higher fuel consumption and emission levels for the same engine and vehicle combination than the FTP-75 drive cycle due to the higher engine load conditions imposed. Fuel, HC and CO emissions are around 25% higher per kilometre with the European cycle and NO_x emissions are 45% higher. This demonstrates the need for legislated emissions targets to be carefully matched to the vehicle test procedure and drive cycle characteristics.

9.3 Case 2: Vehicle Effects

During the development of a new vehicle, careful matching of the engine and vehicle characteristics is necessary to ensure optimum fuel consumption and emissions performance over the appropriate drive cycle. In this case, CECSP has been used to investigate the effect on drive cycle performance of changing the engine and vehicle combination to demonstrate its envisaged application to the optimisation of an engine and vehicle package. Two engines and three vehicles have been considered giving a total of six engine/vehicle combinations. The three vehicles simulated were a 900 kg 'super-mini', a 1200 kg family saloon and a 1300 kg hatchback representing Ford's Ka, Escort and Mondeo models. The two engines considered were both normally aspirated DOHC 16V units with capacities of 1.25 and 1.8 litres.

Figure 9.6 shows the effect on total fuel consumption and feedgas emissions over the ECE+EUDC drive cycle of increasing the engine size from 1.25 litres to 1.8

litres for the three vehicles considered. Increasing the size of the engine in a vehicle has only a small effect on the drive cycle torque demand as the only increase in vehicle mass is due to any increase in engine mass. However, the indicated load demand increases more substantially due to the increased engine friction levels associated with a larger engine. In addition, the larger engine is more heavily throttled to meet the required brake load demand for the drive cycle and hence operates at a lower volumetric efficiency than the smaller engine. These effects combine to increase the fuel consumption by 15-20% when the 1.8 litre engine is used instead of the 1.25 litre engine in all three vehicles. The fuel consumption penalty associated with using the larger engine decreases as the vehicle mass increases because the significance of engine friction levels and throttling losses is reduced as the brake load required to drive the cycle increases. Similar trends occur for CO emissions. HC emission levels show little sensitivity to the change in engine and this is due to the reduction in HC emissions concentrations with increasing load tending to offset the increase in charge mass flow rate. NO_x emissions are significantly reduced for all three vehicles when the engine size is increased. This is because NO_x emissions are sensitive to combustion temperature and hence increase significantly as engine load approaches its maximum. Consequently, for each vehicle, the bigger engine results in lower NO_x emissions because the drive cycle torque demand is a smaller proportion of the engine's peak torque.

Figure 9.7 shows the effect of increasing the vehicle size for a given engine capacity. Increasing the vehicle size results in a substantial increase in engine torque demand as a result of increased vehicle mass together with possible aerodynamic and rolling resistance changes. This can be seen to have the most significant effect on NO_x emissions which are particularly sensitive to increases in engine brake load. The 1.8 litre engine installed in the 1300 kg vehicle produces almost 40% more engine-out NO_x emissions than the same engine in the 900 kg vehicle despite the fuel consumption and CO emissions increasing by a much less significant 6%. Once again, HC emissions are only slightly altered and

are actually reduced for the 1200 kg vehicle compared to the 900 kg vehicle. This is again due to the reduction in HC concentrations with the increase in engine load required to drive the larger vehicle through the cycle.

9.4 Case 3: Cold-Start Temperature Effects

A major consideration when developing a new engine is friction. This determines what proportion of an engine's indicated power is available as brake power at the flywheel. To demonstrate the effect of engine friction levels on fuel consumption over a drive cycle, CECSP has been applied to a Ford 2 litre DOHC 16V engine installed in a 1300 kg, escort sized, vehicle driven over the ECE+EUDC drive cycle. Simulated cold-start drive cycles were modelled with start temperatures ranging from 20°C down to -20°C and fuel consumption results compared. Emissions flow rates were not considered as the mixture preparation correction functions have only been experimentally validated down to coolant temperatures of 0°C. A comparison of the results obtained for the 20°C cold-start and 90°C fully-warm start cases is shown in Figure 9.8 and the coolant and oil warm-up characteristics for the former case are shown in Figure 9.9. Although the coolant temperature rises rapidly the oil temperature lags substantially. In the fully-warm case the predicted fuel used was within 0.6% of the experimental value supplied by Ford Motor Company. For the 20°C cold-start cycle, the fuel consumption penalty associated with cold-start up was 4.98%. This is primarily associated with the higher fuel flow rate in the early part of the drive cycle, when the friction levels are most significantly different from the fully-warm values, although the effect of the warm-up period extends over the entire duration of the drive cycle. Figure 9.10 shows the total drive cycle fuel used and the penalty associated with cold operation for the range of start/soak temperatures examined. The fuel penalty of 4.98% for a 20°C start increases to 10.53% for a start/soak temperature of -20°C. All the predictions here are based on stoichiometric running conditions throughout the drive cycle to eliminate the additional fuel penalty associated with varying degrees and duration of fuel enrichment according to start temperature. Figure 9.11 shows how the ratio of total friction work to total indicated work for

the drive cycle (i.e friction ratio) increases as the engine start temperature is lowered. The generally high value of this ratio indicates the importance of frictional losses under the relatively light-load operating conditions imposed by the drive cycle. For the fully-warm engine case, 26% of the total friction work occurs during idle and over-run periods. The friction ratio increases from 0.39 to 0.44 when the engine is started cold at 20°C rather than fully-warm. The 5% increase in fuel consumption is a direct consequence of this increase in friction, but is not in direct proportion because the higher indicated loads affect a change in indicated specific fuel consumption (isfc). For the engine map examined, the isfc was improved, and as such partly offsets the effect of the increased friction work, as indicated by Figure 9.12.

9.5 Case 4: Engine Calibration Effects

Once an engine and vehicle combination has been specified, optimisation with respect to drive cycle performance can be achieved by changes to the engine management strategy. For example, changes to the spark timing and exhaust gas recirculation (EGR) calibrations can be made to optimise a given engine for a given vehicle. A particular engine in one car may require aggressive use of EGR in order to meet the required emissions legislation and yet, in a smaller car, the manufacturer may be able to dispense with the EGR system and reduce the vehicle costs. Consequently, it is beneficial to be able to assess the likely effects of changes to the engine calibration details on the fuel consumption and emissions performance of a given vehicle over the relevant drive cycle, as the associated cost considerations can be explored at an early stage in vehicle development.

CECSP enables the effects of changes to engine calibration details to be assessed in two ways.

i) Changing Fully-Warm Engine Data Calibration

Because the procedure uses fully-warm dynamometer data as the basis for the

predictions, any changes in the engine calibration used to obtain the fully-warm data will also be reflected in the drive cycle predictions. Consequently, changes in calibration details can be modelled by using multiple sets of engine mapping data to train the neural networks used to predict the drive cycle fuel and emissions flow rates. Such an approach has two disadvantages which limit it to giving only a first approximation to the likely effects of calibration changes. Firstly, the drive cycle calibration is fixed by the fully-warm data and so cannot be modified during the warm-up phase of the drive cycle when different spark timings and EGR rates from fully-warm may be desired. Secondly, because the neural network training errors can be up to +/-10% when predicting emissions flow rates, small differences between emission flow rates for two separate engine maps may not be accurately represented in the neural network characterisations. Hence this technique for investigating the effect of changes in engine calibration details should only be used within the context of the overall prediction accuracy and is only applicable to calibration changes that result in changes in fuel and emissions flow rates that are greater than the accuracy to which these can be predicted by the procedure.

Figure 9.13 shows the effect on the predicted fuel and emissions totals for the same engine and vehicle combination of using two different fully-warm engine maps - one with EGR and one without. While the results suggest that the use of EGR has the most significant influence on NO_x emissions, the overall prediction accuracy has to be known and accounted for before a more precise effect of EGR calibration can be determined.

ii) Changing drive cycle calibration directly

More accurate effects of changes to engine calibration details can be determined by defining the engine calibration details on a second-by-second basis throughout the drive cycle. This involves defining the calibration parameter to be investigated as an input to the neural network used to characterise the engine map and enables engine calibration variables to be changed during the drive cycle.

During the development of the prediction procedure, the defined input variables to the neural network used to define the drive cycle calibration were engine speed, indicated load and AFR. Consequently only changes in the engine AFR calibration can be assessed in this manner without changing the set-up of the software. However, modifications could be made to enable the effects of changes to spark timing and EGR rate to be assessed from a single fully-warm engine map if these were defined as additional input variables and providing that the engine map covered the range of possible values for all the input variables over the specified drive cycle.

The main industrial application of the prediction procedure to date has been to predict the effect of changes to the engine AFR calibration on drive cycle fuel consumption and NO_x emission levels. This involved defining certain areas of the drive cycle where an AFR lean of stoichiometric could be used to reduce drive cycle fuel consumption. Figure 9.14 shows the effect on fuel consumption and total feedgas emissions of running at an AFR of around 22:1 during all the cruise points during the ECE+EUDC drive cycle. It can be seen that such an AFR calibration results in a reduction in total fuel consumption of around 4% and significant reductions in both feedgas CO emissions and feedgas NO_x emissions. However, when tail-pipe emissions are considered there is a price to pay for the reduced fuel consumption. When running lean of stoichiometric a 3-way catalytic convertor as fitted to most modern vehicles cannot treat NO_x emissions due to an excess of oxygen in the exhaust gases. Consequently, although the total feedgas NO_x emissions decrease when running lean of stoichiometric, the tail-pipe NO_x emissions increase in the absence of an alternative after-treatment system to the 3-way catalytic convertor. CECSP was used to define a series of AFR calibrations to investigate the maximum reductions in fuel consumption possible and the associated requirements of an exhaust gas after-treatment system for NO_x emissions during periods of lean operation.

9.6 Case 5: Tail-Pipe After-Treatment Effects

Initially developed to predict fuel consumption and feedgas emissions, CECSP enables the definition of exhaust gas after-treatment characteristics to enable predictions of tail-pipe emissions to be made. In order to predict accurate tail-pipe emissions the catalyst model in CECSP requires catalyst data specific to the engine/vehicle/drive cycle combination which would not be available until the actual vehicle drive cycle performance could be measured. Consequently, the catalyst model is intended primarily to facilitate the investigation of the effects on tail-pipe emissions of imposed catalyst characteristics. These may be known characteristics or target values which may not yet be achievable with current catalyst technology. In the industrial application discussed above, CECSP was used to determine the required lean NO_x conversion efficiency to achieve future emissions legislation whilst achieving the maximum reduction in drive cycle fuel consumption by use of a hybrid stoichiometric/lean AFR engine calibration. A simple extension of this application of CECSP would be to determine the required after-treatment performance for a vehicle under development. This could involve engine data from engines in the early stages of production or even from simulated engine performance programs which are now becoming increasingly available.

9.7 Discussion

CECSP is intended to provide a research tool to enable the prediction of drive cycle fuel and emissions performance at an early stage in vehicle development. A wide range of possible applications are envisaged for the software in the development and evaluation of proposed solutions in the ongoing quest for reduced fuel consumption and improved emissions performance from new light-duty road vehicles. Current and future emissions legislation worldwide provide many challenges for new vehicle design engineers and result in manufacturers adapting engine/vehicle specifications to suit the intended market. Factors such as the drive cycle used to determine fuel consumption and emissions performance and the associated range of engine options that can be offered in a

given vehicle need to be considered to ensure that new vehicles comply with legislated requirements. For a given market using a given drive cycle and test procedure fuel and emissions performance can essentially be optimised in two ways: by changing the vehicle characteristics or by changing the engine and exhaust after-treatment characteristics. In CECSP, vehicle characteristics can be altered by changing parameters such as transmission ratios, vehicle aerodynamics and vehicle mass. Different engines can be mated with different vehicles to assess the significance of engine performance and the effect of both engine friction levels and engine management calibration details. Finally, a major factor influencing drive cycle emissions performance is exhaust gas after-treatment. The efficiency and location of a catalytic convertor on a vehicle significantly influences the tail-pipe emissions produced throughout a drive cycle. Initially developed to predict engine-out emissions, CECSP can be used to assess the effect of, or requirement for, exhaust gas after-treatment performance for a given engine/vehicle/drive cycle combination.

The case studies detailed above provide a brief summary of the applications considered to date and illustrate some of the important issues that need to be considered during modern engine and vehicle development. Further development work, detailed in the following chapter, will extend the scope of the existing CECSP software to cover more engineering problems.

Chapter 10

Discussion and Conclusions

10.1 Discussion

This thesis details the development and exploitation of a PC based prediction procedure, called CECSP. The aim has been to facilitate predictions of fuel consumption and emissions during cold-started drive cycles. CECSP enables the relative effects of changing several engine and vehicle parameters to be examined and so can be used to prioritise areas of performance improvement during both engine and vehicle development. Because the procedure only requires fully-warm engine mapping data it can be used at an early stage in the development process to predict expected drive cycle results before engine and vehicle design parameters are finalised. Engine development teams generally now have access to thermodynamic performance simulation codes which have been developed in-house or which are commercially available. Also early test work on prototype engines rapidly generates engine performance maps. Both simulation and experimental data tend to be for fully-warm steady-state operating conditions, and CECSP makes use of such data to predict how a given engine/vehicle combination would perform over a defined drive cycle.

CECSP has been validated by comparison with experimental data for a typical production vehicle driven over the ECE+EUDC drive cycle and the prediction accuracy found to be within the target +/-5% for fuel consumption and +/-10% for feedgas emissions. The application of CECSP to investigate and prioritise the various external factors influencing fuel consumption and emissions over drive cycles has been considered and the results and assumptions made justified and discussed. Additional applications have been considered in an attempt to illustrate

the contribution of the procedure to real engine and vehicle development situations.

10.2 Further Work

At various points in this thesis the requirement for further work to extend both the accuracy and the scope of the work presented has been highlighted. These requirements are now summarised in the context of the overall prediction procedure and the original objectives of the work.

The first area for further work concerns the use of neural networks. These have been found to provide a simple and effective way of characterising engine mapping data for use over the range of operating conditions imposed by a typical drive cycle, and have been used in preference to regression analysis. However, the neural networks used extensively here use only engine speed, load and AFR as inputs to define fuel and emissions mass flow rates as outputs. This is consistent with the original objective of the work to provide an initial prediction of the fuel consumption and emissions performance of a given engine and vehicle package over a defined drive cycle. Consequently, the drive cycle is defined in terms of a series of engine speed, indicated load and AFR conditions. Such a configuration has been shown to be capable of predicting fuel mass flow rates to within +/- 5% and emissions flow rates to within +/- 10% of experimental data but imposes fixed spark timing and EGR rate settings throughout the drive cycle. Chapter 2 shows that the neural network characterisation procedure can, in principle, be extended to map fuel and emissions flow rates as functions of spark timing and EGR rate in addition to engine speed, load and AFR, but that further work is required to determine the effect this extension has on both the prediction accuracy and the data processing time. Such an extension would enable the effects of spark timing and EGR rate changes on drive cycle performance to be investigated. Increasing the number of inputs to the neural network increases the size of the required database on which to train the neural network and consequently increases the processing time required. Since the optimisation of a

neural network setup for a given database has been found to involve a certain degree of trial and error, a significant amount of further work is required to determine the optimum network configuration for such an extension to the prediction procedure, together with the effects on the prediction accuracy that could be expected. More fundamentally, CECSP currently uses experimental engine mapping data to characterise engine performance. Ultimately, it may be possible to use a complete engine combustion model to accurately model fuel consumption and emissions and negate the current need for empirical engine data. Such engine simulation software is becoming increasingly available and provides a possibility for future development of CECSP.

The second major area of interest for further work is the period immediately following engine start-up. During the first 100 seconds after a cold-start various phenomena combine to provide uncertainty in the predictions of fuel and emissions mass flow rates. This is particularly important for emissions flow rates, as it is in this period when the bulk of the drive cycle total emissions are produced, while the catalytic convertor efficiency is low. As detailed in Chapters 4 and 5 of this thesis, a significant amount of the fuel injected into the engine intake system is not accounted for in exhaust gas analysis using a UEGO sensor, and is believed to pass undetected into both the engine lubricating oil and the exhaust system, resulting in extremely high HC emissions immediately following a cold-start. Further work is required to determine more accurately the proportions of the fuel injected that pass directly into the lubricating oil and exhaust stream and the mechanisms by which these phenomena occur. While the work presented in Chapters 7 and 8 suggests that these considerations are of little significance to the total fuel consumption and engine-out emissions predictions over a typical drive cycle, they are likely to be of much greater significance to both the instantaneous mass flow rate predictions in this period and the drive cycle tail-pipe emissions predictions.

In addition to these two areas of envisaged development, the addition of a full

catalytic convertor model to the procedure would further extend the scope of the existing software package. It is envisaged that such a model could use exhaust gas temperature predictions made by a sub-model of the PROMETS package to predict catalyst light-off behaviour for a given engine/vehicle/drive cycle combination, enabling catalyst performance and warm-up behaviour to be more accurately modelled.

The above areas of proposed further work will, it is believed, further extend the contribution of the work presented in this thesis to both engine and vehicle developent. CECSP will never ultimately be capable of modelling exactly the fuel consumption and emissions performance of an engine and vehicle combination but it is believed to provide a useful tool for predicting expected drive cycle performance to positively influence the development and optimisation of road vehicles in the future.

10.3 Conclusions

CECSP has been developed to predict fuel consumption and emissions over drive cycles starting with the engine at cold-soak temperatures. CECSP requires fully-warm test bed data to be available for the engine under consideration over the range of indicated loads and speeds imposed by the drive cycle.

Experimental data support the assumptions made when applying fully-warm data to a cold-start situation. Indicated specific fuel consumption is a function of indicated operating conditions independent of engine coolant temperature. Indicated specific emissions of HC, CO and NO_x during warm-up can be related to the corresponding fully-warm values using simple functions of engine coolant temperature to account for the deterioration in mixture preparation.

An engine friction model is used to infer indicated operating conditions from brake operating conditions. Experimental data confirm that warm-up friction power losses can be predicted by scaling fully-warm friction levels according to

oil viscosity.

CECSP has been used to investigate and illustrate the factors that influence drive cycle fuel consumption and emissions performance with the following conclusions:

Cold-start effects

- Fuel consumption and engine-out emissions, particularly of HC, are influenced most by increased engine friction levels during warm-up and poor mixture preparation.

- Cold-start transient effects due to poor fuel utilisation represent a negligible increase in fuel consumption and a very small increase in engine-out HC emissions of around 2% over the European drive cycle.

- Poor mixture ratio control during transient operating points have a potentially large influence on engine-out HC and CO emissions.

- Tail-pipe emissions are most sensitive to changes in emission levels in the period before catalyst light-off occurs immediately following a cold-start. Reductions in tail-pipe emissions are best achieved by rapid catalyst light-off and good fuel utilisation through engine calibration.

- Mixture ratio excursions influence tail-pipe emissions more than engine-out emissions due to reduced catalyst performance at AFRs rich or lean of stoichiometric. Close control of AFR during transient operating points can significantly reduce this effect.

Drive cycle effects

- Comparisons between the US FTP-75 and European ECE+EUDC drive cycles have been made. The FTP-75 cycle results are less sensitive to

changes in cold-start engine friction, poor mixture preparation and cold-start transient effects due to faster engine warm-up. In addition, the cold and hot parts of the FTP-75 cycle are weighted so that the majority of the cycle totals come from fully-warm operating conditions.

- Mixture ratio excursions have a more significant effect on the FTP-75 cycle due to a larger proportion of transient operating conditions.

Vehicle effects

- Increasing vehicle mass results in significant increases in drive cycle fuel consumption and emissions. NO_x emissions increase the most due to their sensitivity to the resulting increases in indicated load.

- Increasing engine size in a given vehicle increases fuel consumption due to increased engine friction and reduced volumetric efficiency resulting from a larger engine working at a smaller proportion of its maximum power output. NO_x emissions, however, may be reduced due to the reduction in the proportion of the engine's maximum indicated load required to drive the vehicle.

References

Chapter 1

1.1 Dunne J M and Greening P J, "European emission standards to the year 2000", IMechE Seminar on Worldwide Engine Emissions Standards and How to Meet Them, London, 25-26 May 1993.

1.2 EC Directive 91/441/EEC, OJ, L242, 1.

1.3 "Proposed Regulations for Low-Emission Vehicles and Clean Fuels", California Air Resources Board, August 13, 1990.

1.4 Hadded O, Stokes J and Grigg D W, "Low emission vehicle technology for ULEV and European stage 3 emission standards", IMechE paper C462/18/126, Autotech '93, 1993.

1.5 Dunne J M, "Status of Emissions Legislation", IMechE Seminar on Application of Powertrain and Fuel Technologies to Meet Emissions Standards, 3rd Int Seminar on Worldwide Engine Emissions Standards and How to Meet Them, 24-26 June 1996.

1.6 Andre M, Hickman A J, Hassel D and Joumard R, "Driving cycles for emissions measurements under European conditions", SAE paper no. 950926.

1.7 Watson H C, "Effects of a wide range of drive cycles on the emissions from vehicles of three levels of technology", SAE paper no. 950221.

1.8 Marshall W F and Eccleston B H, "Emissions at off-ambient

temperature", SAE paper no. 800512.

1.9 Eccleston B H and Hurn R W, "Ambient temperature and trip length - influences on automotive fuel economy and emissions", SAE paper no. 780613.

1.10 Horowitz A and Tobin R L, "The influence of urban trip characteristics on vehicle warm-up - implication for urban automobile fuel consumption", SAE paper no. 790656.

1.11 Austin T C and Hellman K H, "Passenger car fuel economy as influenced by trip length", SAE paper no. 750004.

1.12 Andre M, "In actual use car testing: 70,000 kilometres and 10,000 trips by 55 French cars under real conditions", SAE paper no. 910039.

1.13 Langen P, Theissen M, Mallog J and Zielinski R, "Heated catalytic convertor competing technologies to meet LEV emission standards", SAE paper no. 940470.

1.14 Cheng W K, Hamrin D, Heywood J B, Hochgreb S, Min K and Norris M, "An overview of hydrocarbon emissions mechanisms in spark-ignition engines", SAE paper no. 932708.

1.15 Shin Y, Cheng W K and Heywood J B, "Liquid gasolene behaviour in the engine cylinder of an SI engine", SAE paper no. 941872.

1.16 Shayler P J, Marshall W D P and Turner J, "Exhaust emissions: the influence of fuel injection system details", IMechE paper C394/015, IMechE Int Conf on Automotive Power Systems, Chester, 10-12 September 1990.

1.17 Shayler P J, Christian S J and Ma T, "A model for the investigation of temperature, heat flow and friction characteristics during engine warm-up", SAE paper no. 931153.

Chapter 2

2.1 Heywood J B, "Internal Combustion Engine Fundamentals", published by McGraw-Hill Book Company, ISBN 0-07-100499-8, 1988.

2.2 Bacon A, "Fault Diagnosis Techniques for Spark Ignition Engines", PhD Thesis, University of Nottingham, 1991.

2.3 Bacon A, Shayler P J, Ma T, "Potential for engine control using neural networks", IMechE paper C448/057, 1992.

2.4 Stevens S P, Shayler P J, Ma T, "Experimental data processing techniques to map the performance of a spark ignition engine", Proc IMechE, vol 290, 1995.

2.5 McClelland J L, Rumelhart D E, "Explorations in Parallel Distributed Processing: A Handbook of Models, Programs and Exercises", IT Press, ISBN 0-262-63113-X, 1988.

2.6 McClelland J L, Rumelhart D E, "Parallel Distributed Processing, Volume 1", IT Press, ISBN 0-262-68053-X, 1986

2.7 McClelland J L, Rumelhart D E, "Parallel Distributed Processing, Volume 2", IT Press, ISBN 0-262-63110-5, 1986

Chapter 3

3.1 Sampson A J and Heywood J B, "Analysis of fuel behaviour in the spark-ignition engine start-up process", SAE paper no. 950678.

3.2 Shayler P J, Isaacs R M and Ma T, "The variation of in-cylinder mixture ratios during engine cranking at low ambient temperatures", IMechE, Journal of Automobile Engineering, 1992.

3.3 Murakami Y and Aihara H, "Analysis of mechanism intermixing combustion products in engine oil", JSME Int. J., Series II, vol. 34, No. 4, pp.548-556 (1991).

3.4 Frottier V, Heywood J B and Hochgreb S, "Measurement of gasolene absorption into engine lubricating oil", SAE paper no. 961229.

3.5 Shayler P J, Marshall W D P and Turner J, "Exhaust emissions: the influence of fuel injection system details", IMechE paper C394/015, IMechE Int Conf on Automotive Power Systems, Chester, 10-12 September 1990.

3.6 Johansson B, Neij H, Alden M and Juhlin G, "Investigations of the influence of mixture preparation on cyclic variations in a SI engine, using laser induced fluorescence", SAE paper no. 950108.

3.7 Nogi T, Ohyama Y, Yamauchi T and Kuroiwa H, "Mixture formation of fuel injection systems in gasoline engines", SAE paper no. 880558.

3.8 Fox J W, Min K D, Cheng W K and Heywood J B, "Mixture preparation in an SI engine with port fuel injection during starting and warm-up", SAE paper no. 922170.

3.9 Boam D J et al,"The sources of unburnt hydrocarbon emissions from spark ignition engines during warm-up", IMechE paper C448/064, 1992.

3.10 Andrews G E et al, "The role of cooling water and lubricating oil temperatures on transient emissions during SI engine warm-up", IMechE paper C382/015, 1989.

3.11 Andrews G E, Harris J R and Ounzain A, "SI engine warm-up: Water and lubricating oil temperature influences", SAE paper no. 892103.

3.12 Guillemot P, Gatellier B and Rouveirolles P, "The influence of coolant temperature on unburned hydrocarbon emissions from spark ignition engine", SAE paper no. 941962.

3.13 Andrews G E, Harris J R and Ounzain A, "Transient heating and emissions of an SI engine during the warm-up period", SAE paper no. 880264.

3.14 Lee R C, "Effect of compression ratio, mixture strength, spark timing and coolant temperature upon exhaust emissions and power", SAE paper no. 710832.

3.15 Ohyama Y, Yamauchi T and Ohsuga M, "Mixture formation during cold starting and warm-up in spark ignition engines", SAE paper no. 960065.

3.16 Campbell S, Clasen E, Chang C and Rhee K T, "Flames and liquid fuel in an SI engine cylinder during cold start", SAE paper no. 961153.

3.17 Shin Y, Cheng W K and Heywood J B, "Liquid gasolene behaviour in the engine cylinder of an SI engine", SAE paper no. 941872.

3.18 Takeda K, Yaegashi T, Sekiguchi K, Saito K and Imatake N, "Mixture

preparation and HC emissions of a 4-valve engine with port fuel injection during cold starting and warm-up", SAE paper no. 950074.

3.19 Yang J, Kaiser E, Siegl W and Anderson R, "Effects of port-injection timing and fuel droplet size on total and speciated exhaust hydrocarbon emissions", SAE paper no. 930711.

3.20 Menne R J, Heuser G and Morris G D, "Potential of the new Ford Zetec SE engine to meet future emissions standards", IMechE Seminar on Application of Powertrain and Fuel Technologies to Meet Emissions Standards, 3rd Int Seminar on Worldwide Engine Emissions Standards and How to Meet Them, 24-26 June 1996.

3.21 Quader A A, "How injector, engine and fuel variables impact smoke and hydrocarbon emissions with port fuel injection", SAE paper no. 890623.

3.22 Kashiwaya M, Kosuge T, Nakagawa K and Okamoto Y, "The effect of atomisation of fuel injectors on engine performance", SAE paper no. 900261.

3.23 Douaud A and Eyzat P, "DIGITAP- An on-line acquisition and processing system for instantaneous engine data-applications", SAE paper no. 770218.

Chapter 4

4.1 Shayler P J, Davies M T and Scarisbrick A, "An audit of fuel utilisation during the warm-up of SI engines", SAE paper no. 971656.

4.2 Campbell S, Clasen E, Chang C and Rhee K T, "Flames and liquid fuel in an SI engine cylinder during cold start", SAE paper no. 961153.

4.3 Shin Y, Cheng W K and Heywood J B, "Liquid gasolene behaviour in the engine cylinder of an SI engine", SAE paper no. 941872.

4.4 Shayler P J, Duggleby P and Scarisbrick A, "Combustion stability mapping during warm-up for spark timing and mixture ratio calibrations", 6th Int EAEC Congress, Conference II, "Energy Saving and Emissions", 2-4 July 1997.

4.5 Saito K, Sekiguchi K, Imatake N, Takeda K and Yaegashi T, "A new method to analyze fuel behaviour in a spark ignition engine", SAE paper no. 950044.

4.6 Sampson A J and Heywood J B, "Analysis of fuel behaviour in the spark-ignition engine start-up process", SAE paper no. 950678.

4.7 Frottier V, Heywood J B and Hochgreb S, "Measurement of gasolene absorption into engine lubricating oil", SAE paper no. 961229.

4.8 Takeda K, Yaegashi T, Sekiguchi K, Saito K and Imatake N, "Mixture preparation and HC emissions of a 4-valve engine with port fuel injection during cold starting and warm-up", SAE paper no. 950074.

Chapter 5

5.1 Ohyama Y, Yamauchi T and Ohsuga M, "Mixture formation during cold starting and warm-up in spark ignition engines", SAE paper no. 960065.

5.2 P J Shayler, J Turner, K Ford, "Exhaust emissions: the influence of fuel injection system details", IMechE Paper C394/015, September 1990.

5.3 Davies M T, Personal Communications, University of Nottingham,

September 1996 - December 1996.

5.4 Andrews G E et al, "The role of cooling water and lubricating oil temperatures on transient emissions during SI engine warm-up", IMechE paper C382/015, 1989.

5.5 Andrews G E, Harris J R and Ounzain A, "Transient heating and emissions of an SI engine during the warm-up period", SAE paper no. 880264.

5.6 Shayler P J, Davies M T and Scarisbrick A, "An audit of fuel utilisation during the warm-up of SI engines", SAE paper no. 971656.

5.7 Guillemot P, Gatellier B and Rouveirolles P, "The influence of coolant temperature on unburned hydrocarbon emissions from spark ignition engine", SAE paper no. 941962.

5.8 Lee R C, "Effect of compression ratio, mixture strength, spark timing and coolant temperature upon exhaust emissions and power", SAE paper no. 710832.

5.9 Russ S G, Kaiser E W, Siegl W O, Podsiadlik and Barrett K M, "Compression ratio and coolant temperature effects on HC emissions from a spark-ignition engine", SAE paper no. 950163

5.10 Frottier V, Heywood J B and Hochgreb S, "Measurement of gasolene absorption into engine lubricating oil", SAE paper no. 961229.

5.11 Campbell S, Clasen E, Chang C and Rhee K T, "Flames and liquid fuel in an SI engine cylinder during cold start", SAE paper no. 961153.

5.12 Shin Y, Cheng W K and Heywood J B, "Liquid gasolene behaviour in the

engine cylinder of an SI engine", SAE paper no. 941872.

5.13 Saito K, Sekiguchi K, Imatake N, Takeda K and Yaegashi T, "A new method to analyze fuel behaviour in a spark ignition engine", SAE paper no. 950044.

5.14 Takeda K, Yaegashi T, Sekiguchi K, Saito K and Imatake N, "Mixture preparation and HC emissions of a 4-valve engine with port fuel injection during cold starting and warm-up", SAE paper no. 950074.

Chapter 6

6.1 Shayler P J, Christian S J and Ma T, "A model for the investigation of temperature, heat flow and friction characteristics during engine warm-up", SAE paper no. 931153.

6.2 Sorrell A J and Stone C R, "Spark-ignition engine performance during warm-up", SAE paper no. 890567.

6.3 Haahtela O and Decker G, "Present and future fuels and lubricants in cold climate operation", SAE paper no. 890032.

6.4 May C J and Smith C R, "The importance of lubricant low temperature performance to vehicle operation or 'Will it still go when it's 30 below?'", SAE paper no. 920024.

6.5 Henderson K O, "Low temperature performance of commercial SAE 5W-30 oils in engines and their correlation with bench tests", SAE paper no. 920650.

6.6 Caracciolo F and McMillan M L, "Effect of engine oil viscosity on low

temperature cranking, starting and fuel economy", SAE paper no. 790728.

6.7 Kytö M, "Engine lubrication in cold start-up", SAE paper no. 890033.

6.8 Patton K J, Nitschke R G and Heywood J B, "Development and evaluation of a friction model for spark ignition engines", SAE paper no. 890836.

6.9 Yuen H C R, "An Investigation of Thermal Conditions in Spark Ignition Engines", PhD Thesis, University of Nottingham, 1995.

6.10 Schilling A, "Motor Oils and Engine Lubrication", Scientific Publications (GB) Limited, 2nd edition, 1968.

6.11 Taylor C F, Toong T Y, "Heat transfer in internal combustion engines", ASME paper 57-HT-17, 1957.

6.12 Christian S J, "A Spark Ignition Engine Model for Heat Flow and Friction Characteristics", PhD Theis, University of Nottingham, 1992.

6.13 Hashizume K and Kumada Y, "A study of oil flow and temperature in journal bearings", SAE paper no. 910160.

Chapter 7

7.1 Boam D J, Clark T and Hobbs K E, "The influence of fuel management on unburnt hydrocarbon emissions during the ECE 15 and US FTP drive cycles", SAE paper no. 950930.

Chapter 8

8.1 Boam D J, Clark T and Hobbs K E, "The influence of fuel management on unburnt hydrocarbon emissions during the ECE 15 and US FTP drive cycles", SAE paper no. 950930.

8.2 Shin Y, Cheng W K, Heywood J B, "Liquid gasolene behaviour in the engine cylinder of a SI engine", SAE Paper 941872.

8.3 Heywood J B, "Internal Combustion Engine Fundamentals", published by McGraw-Hill Book Company, ISBN 0-07-100499-8, 1988.

Chapter 9

9.1 Schäfer F, van Basshuysen R, "Reduced emissions and fuel consumption in automobile engines", published by Springer-Verlag Wien, ISBN 3-211-82718-8, 1995.

Table 1.1

CARB Exhaust Emission Standards for Light-Duty Spark Ignition Vehicles [1.3]

Legislative standard	Introduced	Exhaust emissions, g/mile (Federal Test Procedure)			
		CO	NMOG[1]	NO_x	Aldehydes
	1991	7.0	0.390	0.40	-
	1993	3.4	0.250	0.40	-
TLEV[2]	1994	3.4	0.125	0.40	0.015
LEV[3]	1997	3.4	0.075	0.20	0.015
ULEV[4]	1997	1.7	0.040	0.20	0.008
ZEV[5]	1998	0	0	0	0

1 Non-Methane HC

2 Transitional Low Emission Vehicles

3 Low Emission Vehicles

4 Ultra Low Emission Vehicles

5 Zero Emission Vehicles

Table 1.2

European Emission Standards for Light-Duty Spark Ignition Vehicles [1.4]

Legislative standard	Introduced	Exhaust emissions, g/km (European light duty test cycle)	
		CO	$HC+NO_x$
Directive 91/441/EEC	1993	2.72	0.97
EC Stage 2	1996	2.2	0.5

Expected Proposed European Emissions Standards for Light-Duty Spark Ignition Vehicles [1.5]

Legislative standard	Introduction	Exhaust emissions, g/km (European light duty test cycle without 40 s idle period)		
		CO	HC	NO_x
EC Stage 3 Proposal	2000	2.3	0.2	0.15
EC Stage 4 Proposal	2005	1.0	0.1	0.08

Table 2.1

Summary of Neural Network Training Procedure (from Bacon [2.2])

Step Number	Task
1	Set all the weights in the network to random values
2	Take each input pattern in turn and, for each one, carry out steps 2(a) to 2(d)
2(a)	Apply each element of the input pattern as an input to the corresponding input unit
2(b)	Calculate the activation of the output units by progressing the activation values through the network
2(c)	Compare the actual output value or pattern with the desired output value or pattern
2(d)	Adjust the weights in the network to bring the actual output closer to the target
3	Starting again at the first input pattern, repeat step 2 until a measure of the errors in the outputs is below a defined level or until the weights values have converged to a constant value

Table 3.1

Ford 2.0 Litre DOHC 4-Stroke Engine Specification

Number of cylinders	4
Bore (mm)	86.0
Stroke (mm)	86.0
Capacity (cc)	1998
Compression ratio	10.3:1
Con-rod length (mm)	149.25
IVO (°BTDC)	13
IVC (°ABDC)	51
EVO (°BBDC)	43
EVC (°ATDC)	13
Firing order	1-3-4-2

Table 3.2

Engine Rig Monitoring and Control System Hardware

Compaq 286 PC (IBM PC-AT compatible)
Blue Chip Technology AIP-24, 12-bit analogue input card
Blue Chip Technology TIP-8, thermocouple input card
Blue Chip Technology PIO-48, programmable input/output card
RS232 serial interface
RS stepper motor driver board
Sigma Instruments stepper motor
Setra 280E 0 to 25 psia pressure transducer
NTK MO-1000 AFR meter

Table 3.3

Engine Rig Monitoring and Control System Measurements

Parameter	Instrument
Engine Condition:	
Engine Speed	Froude HD70B control module
Engine Torque	Froude HD70B control module
Throttle Position	Stepper motor drive
MAP	Setra 280E pressure transducer
AFR	NTK MO-1000 AFR meter
Fuel Pulsewidth	EECIV Calibration Console
VMAF	EECIV Calibration Console
CO Concentration (%)	Horiba MEXA-324 GE analyser
HC Concentration (1000ppm)	Signal series 3000 analyser
NO_x Concentration (1000ppm)	Signal series 4000 analyser
Temperature:	
Inlet air	K-type thermocouple
Exhaust gas	"
Engine coolant inlet	"
Engine coolant outlet	"
Engine oil inlet to filter	"
Engine oil in sump	"
Dynamometer cooling water	"

Table 4.1

Cold-Start Fixed Throttle Warm-Up Test Conditions

Constant Tail-Pipe AFR During Warm-up

Test Number	Engine Speed (rpm)	Fully-Warm Brake Load (Nm)	Tail-Pipe AFR During Warm-up
1	1750	26	14.4
2	1750	50	14.3
3	1750	80	14.4
4	1750	90	14.4
5	2400	30	14.3
6	2400	50	14.2
7	2400	75	14.3
8	2400	93	14.3

Table 4.2

Measured imep Readings for DOHC Engine During Fixed Throttle Warm-up

Test Number 2

Time From Engine Start (s)	MAP (mbar)	imep (bar)	Peak Pressure (bar)
25	424	3.82	23.60
70	438	3.91	25.71
115	446	4.08	23.19
180	454	4.10	22.97
270	467	4.09	23.38
400	484	4.07	22.91
505	488	4.05	22.16
600	489	4.04	22.15
730	489	4.03	22.01
810	490	4.03	22.78

Table 4.3

Cold-Start Fixed Throttle Warm-Up Test Conditions

EECIV Determined AFR During Warm-Up

Test Number	Engine Speed (rpm)	Fully-Warm Brake Loads Tested (Nm)
1-4	1250	30,50,70,90
5-8	1750	30,50,70,90
9-12	2400	30,50,70,90

Table 5.1

Constant AFR Force-Cooled Warm-Up Test Conditions

No Thermostat, Constant Tail-Pipe AFR during Warm-Up

i) 2 litre DOHC 8V Engine

Engine Speed (rpm)	Approximate imeps Tested (bar)	Tail-Pipe AFRs Tested
1250	3.2, 4.6, 7.3	14.5, 13.0, 17.5
1500	2.5, 3.2, 4.6	14.6, 12.0
2000	2.5, 3.2, 4.6	14.6, 12.0
2400	3.2, 4.6, 7.3	14.5, 13.0, 17.5
2500	2.5, 3.2, 4.6	14.6, 12.0

ii) 1.8 litre HO Zetec Engine

Engine Speed (rpm)	Approximate imeps Tested (bar)	Tail-Pipe AFRs Tested
2400	8.3	12.0, 14.7, 17.0

Table 5.2

Standard Fuelling Cold-Start Warm-Up Test Conditions

EECIV Determined AFR During Warm-Up

Engine Speed (rpm)	Fully-Warm Brake Loads Tested (Nm)	Start/Soak Temperatures (°C)
1250	30, 50, 70, 90	-15, 20
1750	50, 70, 90	-15, 20
2400	30, 50, 70, 90	-15, 20

Table 6.1

Predicted Friction Power Losses for the 2 Litre Ford DOHC 8V Engine Operating at 3000 rpm, 30 Nm Brake Load

Friction Components	Rubbing Friction Mean Effective Pressure (kPa)	Rubbing Friction Power Loss (W)	Percentage of Total Friction Power Loss
Main Bearing Seals	2.474	123.6	2.6%
Main Bearing Hydrodynamic Term	4.686	234.1	4.9%
Main Bearing Turbulent Dissipation Term	4.044	202.0	4.2%
Connecting Rod Bearings	4.229	211.3	4.4%
Camshaft Bearings	5.559	277.7	5.8%
Piston Body	29.400	1468.7	30.7%
Piston Rings (without gas pressure)	7.319	365.6	7.6%
Piston Rings (extra due to gas pressure)	9.724	485.7	10.1%
Valve Train Flat Follower Term	4.124	206.0	4.3%
Valve Train Oscillating Hydrodynamic Term	0.274	13.7	0.3%
Valve Train Oscillating Mixed Term	3.686	184.1	3.8%
Auxiliary Components	20.279	1013.1	21.2%
TOTAL	**95.799**	**4785.7**	**100%**

Table 6.2

Friction Warm-Up Test Conditions

Fixed Throttle Warm-Up Tests with Constant Stoichiometric Intake AFR

Engine Speed (rpm)	Fully-Warm Brake Load (Nm)	Start/Soak Temperature (°C)	Oils Tested
1000	20/50/80	-10/20	10W/30 20W/50
1500	20/50/80	-10/20	10W/30 20W/50
2000	20/50/80	-10/20	10W/30 20W/50
2800	20/50/80	-10/20	10W/30 20W/50

Table 8.1

Percentage Increases in Fuel Consumption and Feedgas Emissions Relative to Fully-Warm Start for 1.8 litre Zetec Mondeo

	Fuel	HC	CO	NO_x
Increased Friction	4.5	3.0	3.9	1.7
Poor Mixture Preparation	-	2.1	-0.7	-1.6
Cold-Start Transients	0.1	2.2	0.0	0.0

Table 8.2

Fuel Consumption and Engine-out Emissions Prediction Accuracy

Vehicle: Ford Mondeo

Engine: Ford 1.8 litre Zetec

Drive Cycle: ECE+EUDC

Other: 20°C start/soak temperature, 40 second conditioning period before emission sampling begins.

	Fuel	HC	CO	NO_x
Prediction Error(%)	0.3	1.2	-4.7	6.8

Table 8.3

Factors Influencing Tail-Pipe Emissions

Problem	**Means of Address**
Mixture Ratio Excursions	Engine Control Strategy/Calibration
Cold-Start Transients	Rapid Catalyst Light-Off/Minimum Excess Fuel Supply/Fuel Control Calibration
Friction	Low Friction Design/Fast Engine Warm-Up
Poor Mixture Preparation	Not Critical

Table 9.1

Percentage Increases in Fuel Consumption and Feedgas Emissions Relative to Fully-Warm Start for 1.8 litre Zetec Mondeo

	% Increase (ECE+EUDC/FTP-75)			
	Fuel	HC	CO	NO_x
Increased Friction	4.5/2.1	3.0/1.3	3.9/1.7	1.7/3.7
Poor Mixture Preparation	-/-	2.1/1.2	-0.7/-0.4	-1.6/-1.2
Cold-Start Transients	0.1/0.1	2.2/1.2	-/-	-/-

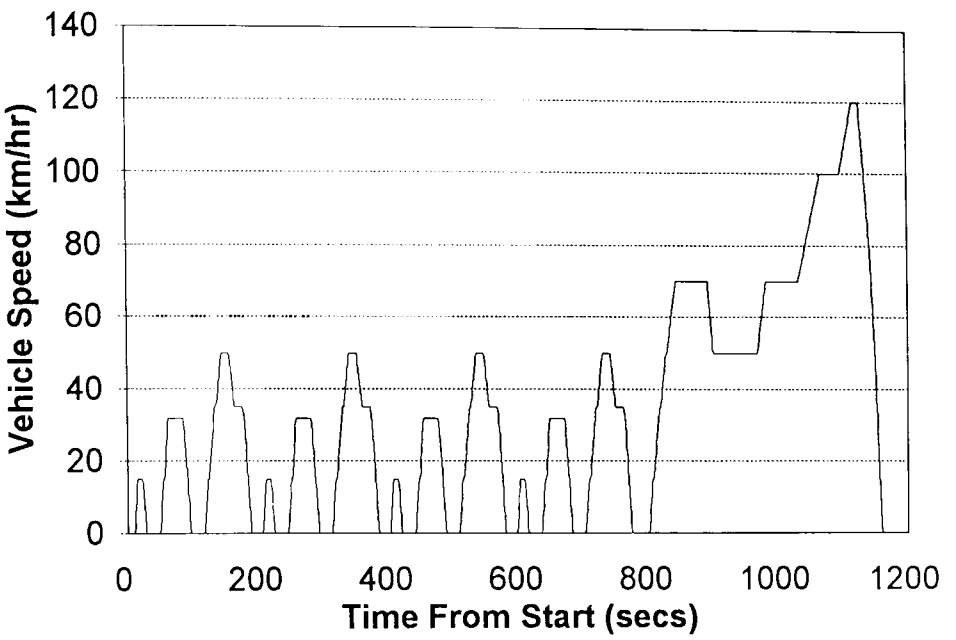

Drive Cycle Breakdown

Time(secs)	Phase
0-195	Elementary Urban Cycle No.1
196-390	Elementary Urban Cycle No.2
391-585	Elementary Urban Cycle No.3
586-780	Elementary Urban Cycle No.4
781-1180	Extra-Urban Drive Cycle

Figure 1.1
NEDC or ECE+EUDC vehicle speed vs time description

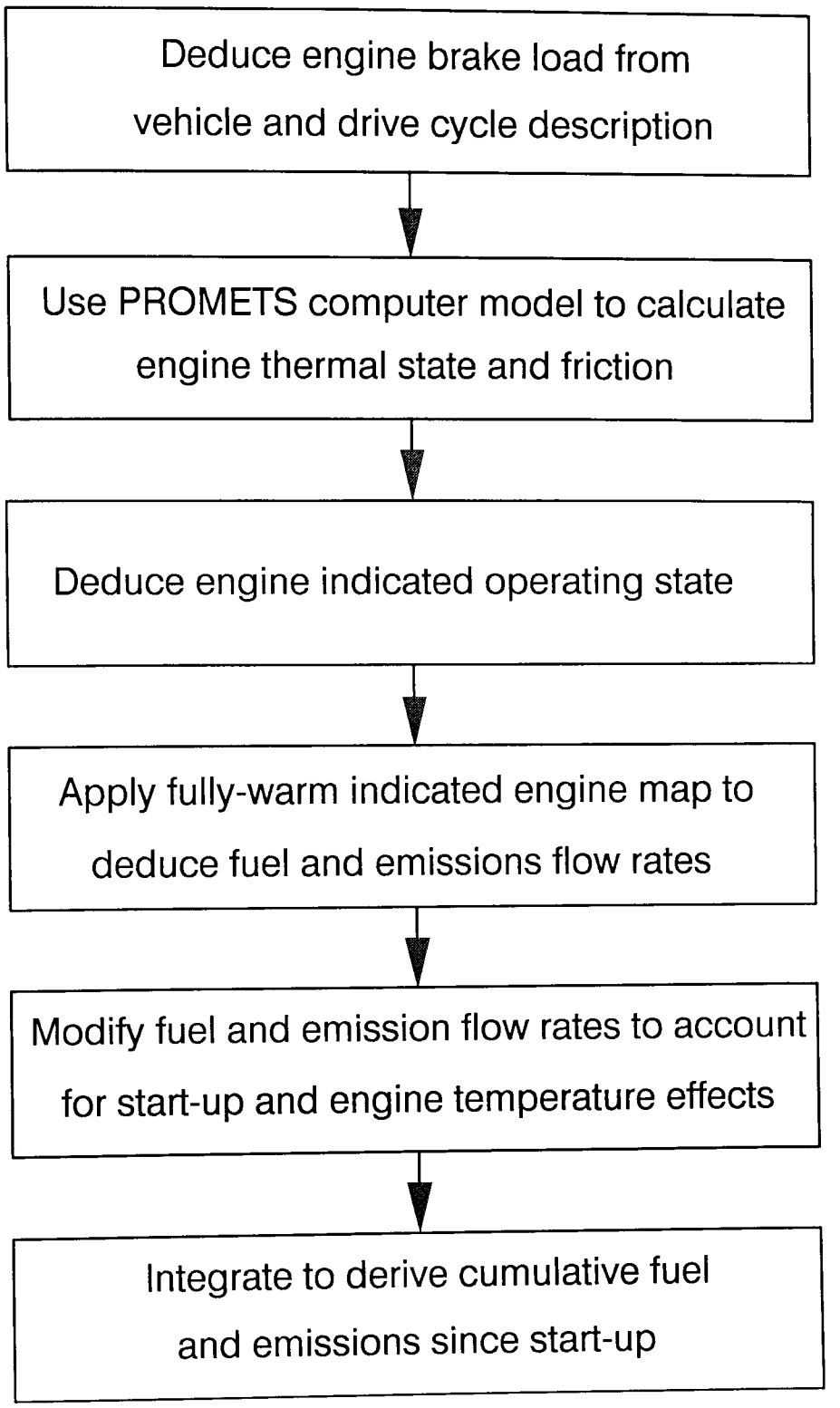

Figure 1.2
Outline of prediction procedure

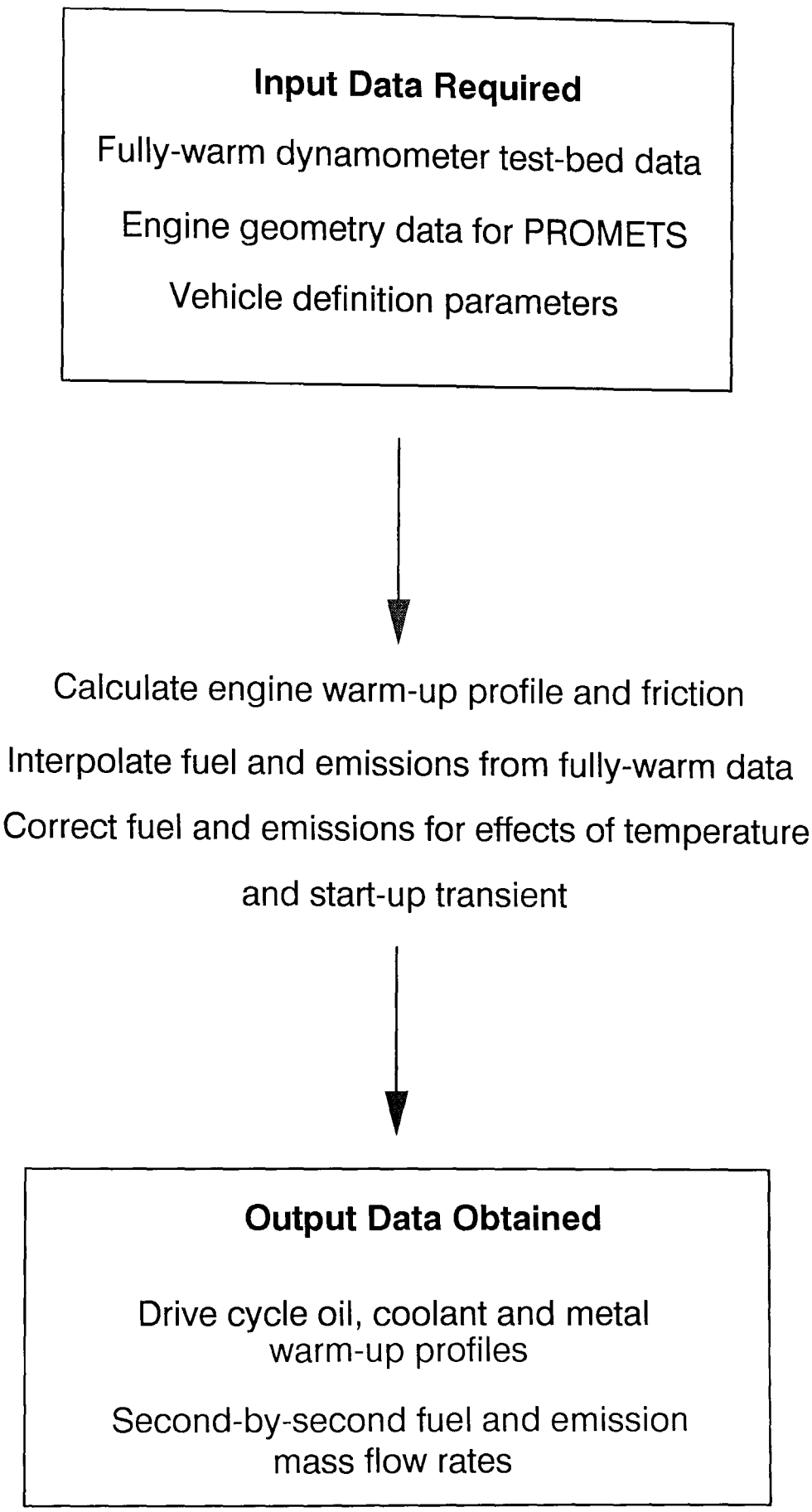

Figure 1.3
Prediction software input/output regime.

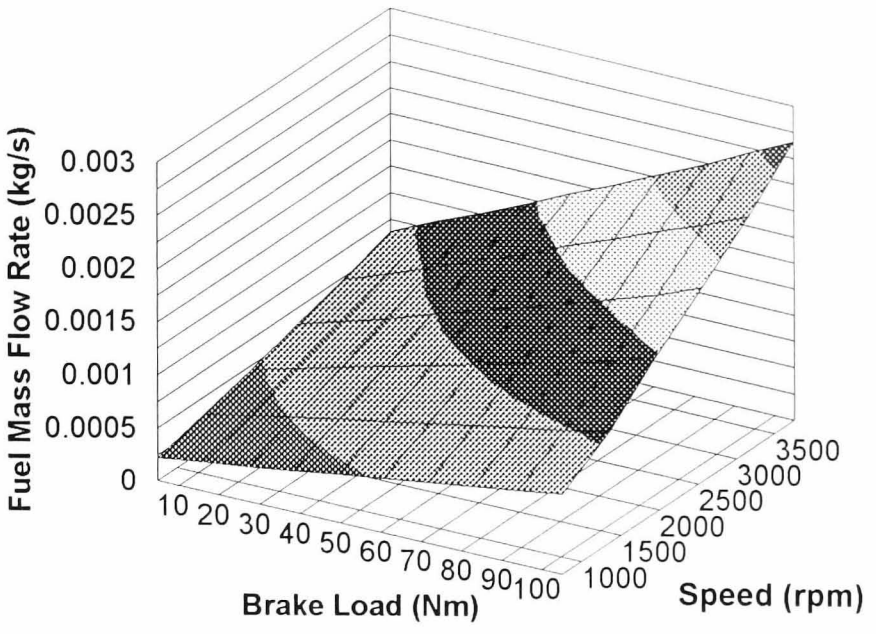

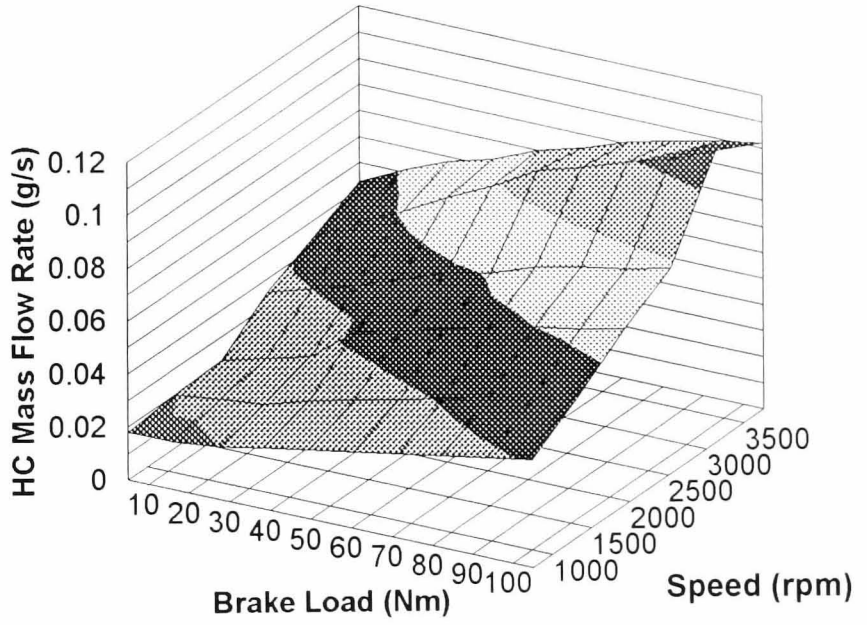

Figure 2.1

1.8 litre Zetec fully-warm engine maps for fuel mass flow rates (upper) and HC mass flow rates (lower) with stoichiometric AFR and MBT spark timing. Shading shows a range of equally spaced flow rate bands.

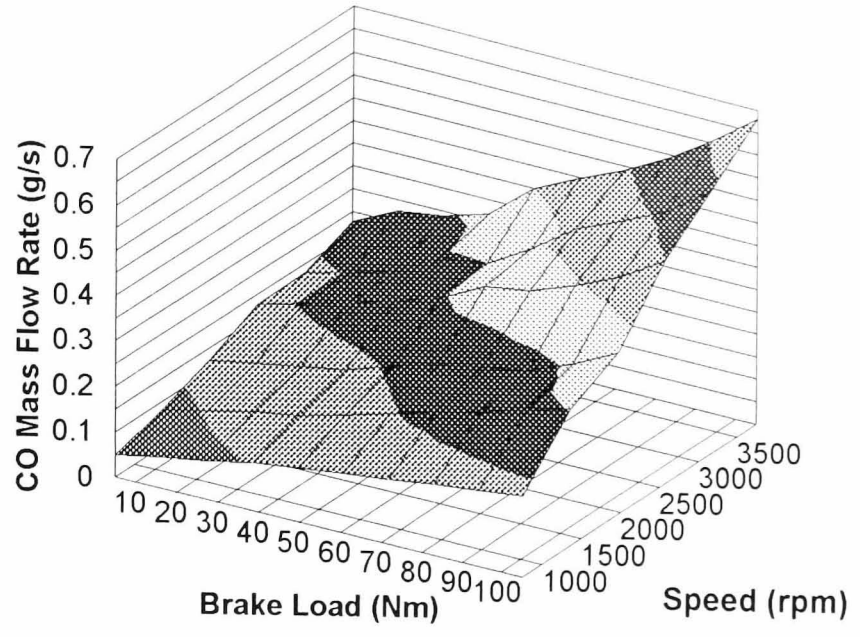

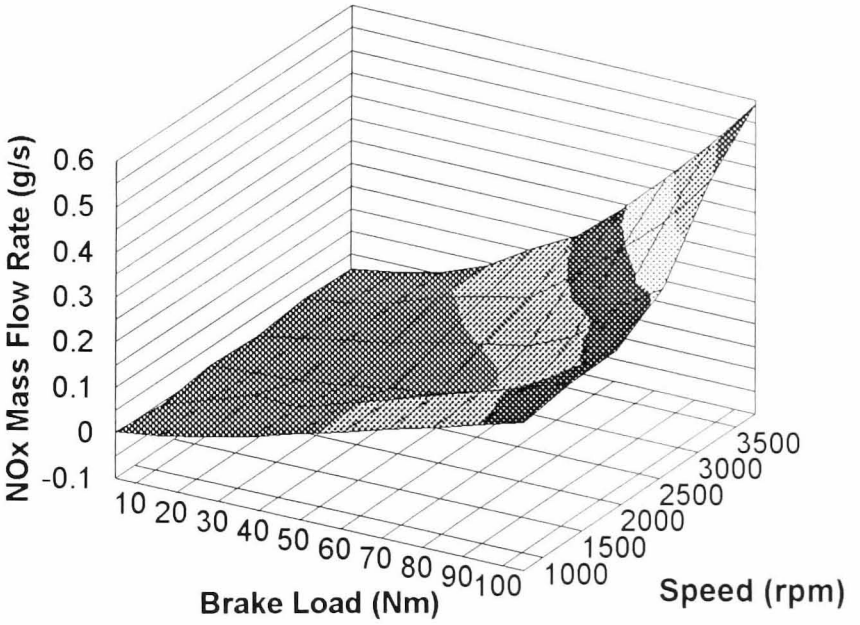

Figure 2.2
1.8 litre Zetec fully-warm engine maps for CO mass flow rates (upper) and NOx mass flow rates (lower) with stoichiometric AFR and MBT spark timing. Shading shows a range of equally spaced flow rate bands.

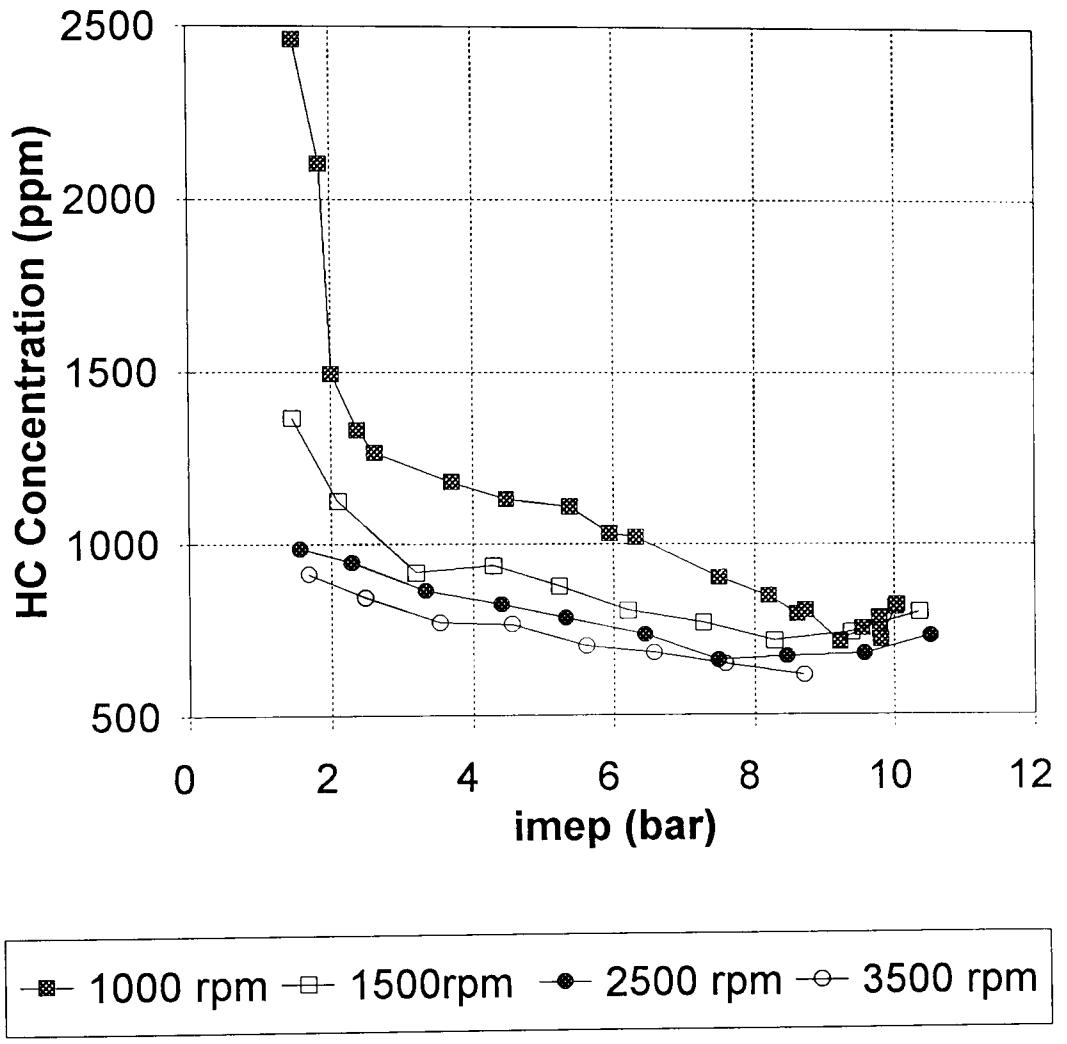

Figure 2.3
Variation of HC emissions with imep in 1.25 litre spark-ignition engine at stoichiometric AFR and without EGR at various engine speeds.

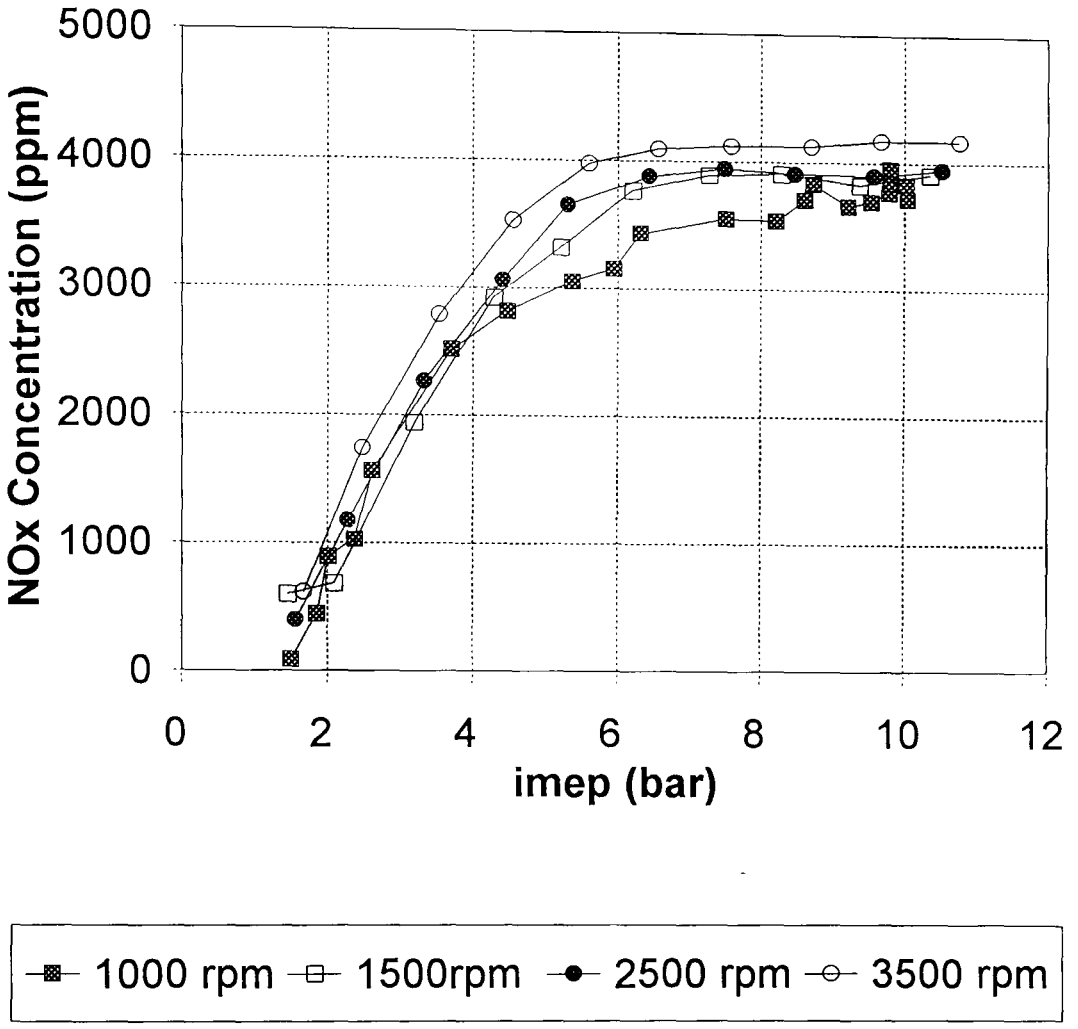

Figure 2.4
Variation of NOx emissions with imep in 1.25 litre spark-ignition engine at stoichiometric AFR and without EGR at various engine speeds.

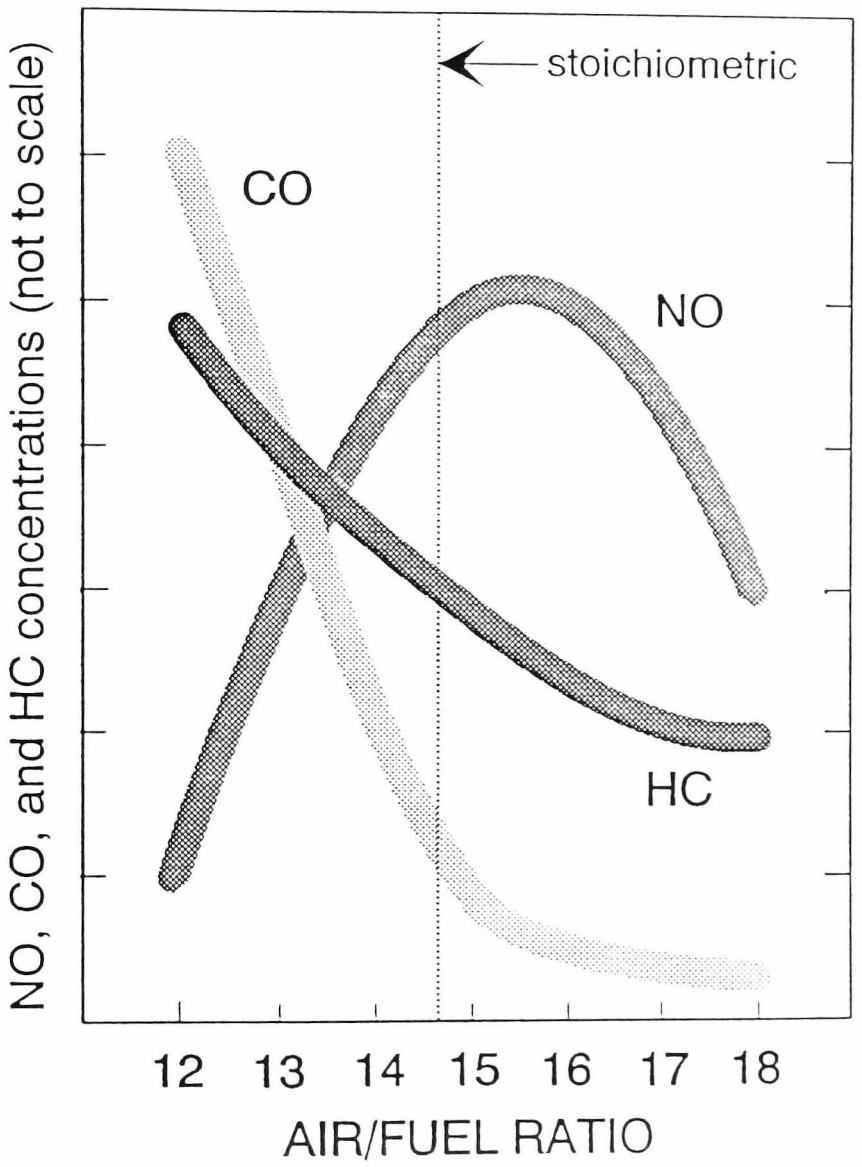

Figure 2.5
Effect of AFR on concentrations of exhaust gas pollutants [2.1].

a)

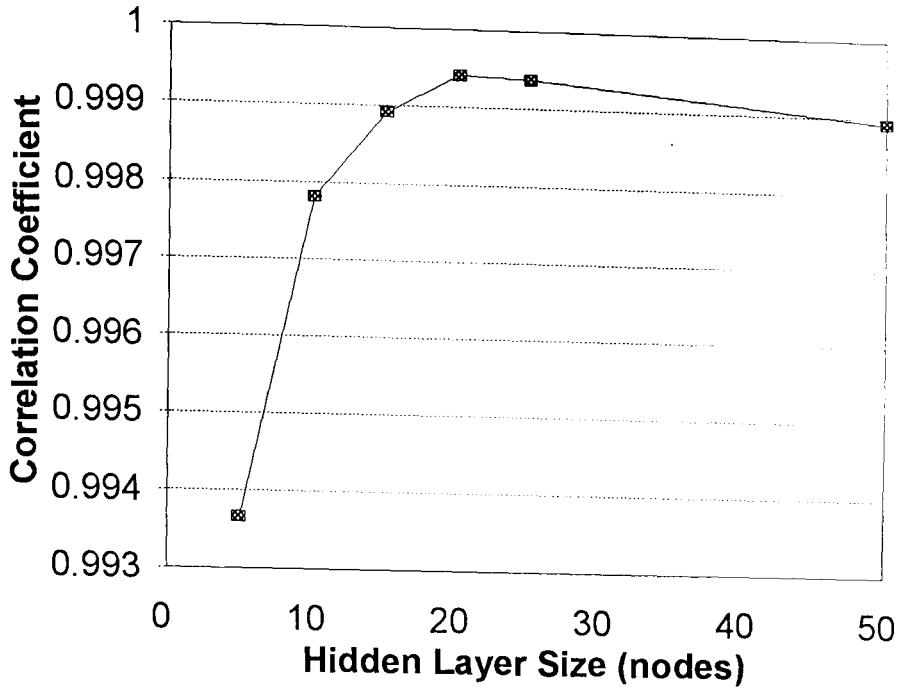

b)

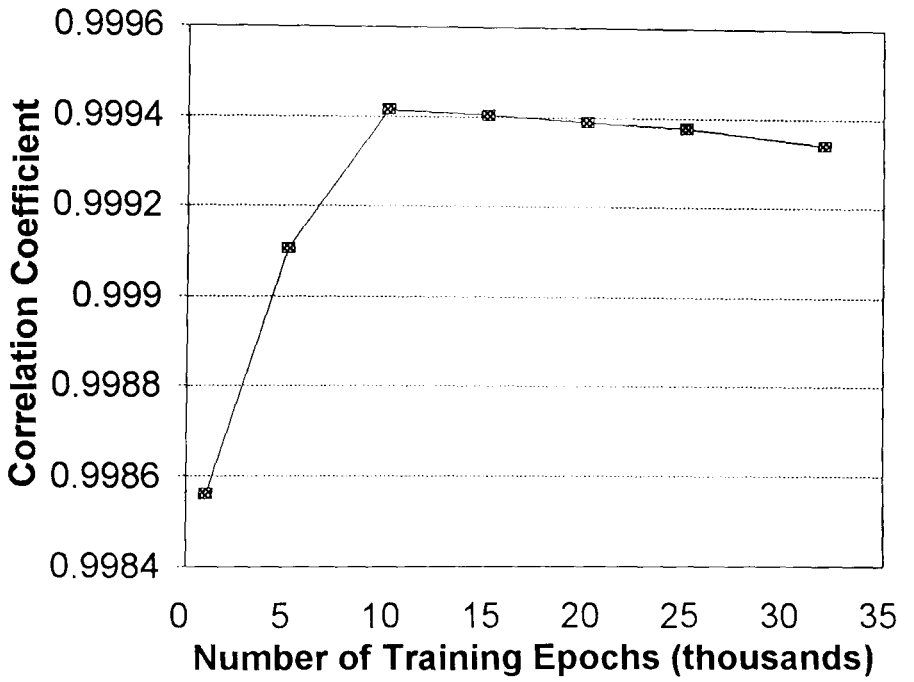

Figure 2.8

Correlation coefficients for 1.8 litre Zetec fuel mass flow rate mapping data for:

a) Range of hidden layer sizes with 10000 training epochs.

b) Range of training epochs with a 20 node hidden layer.

Fuel Mass Flow Rates:

a)

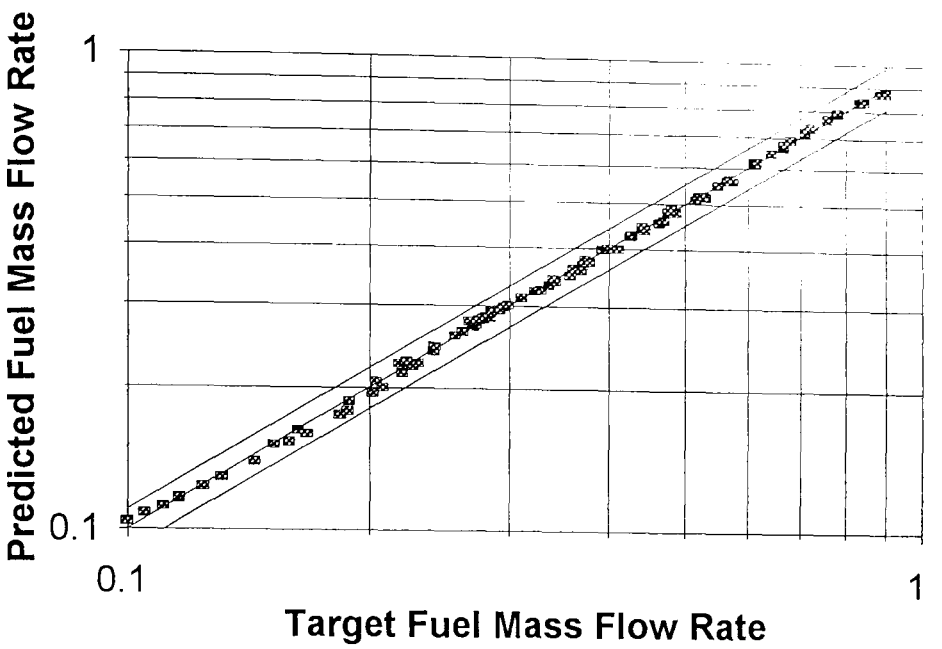

b)

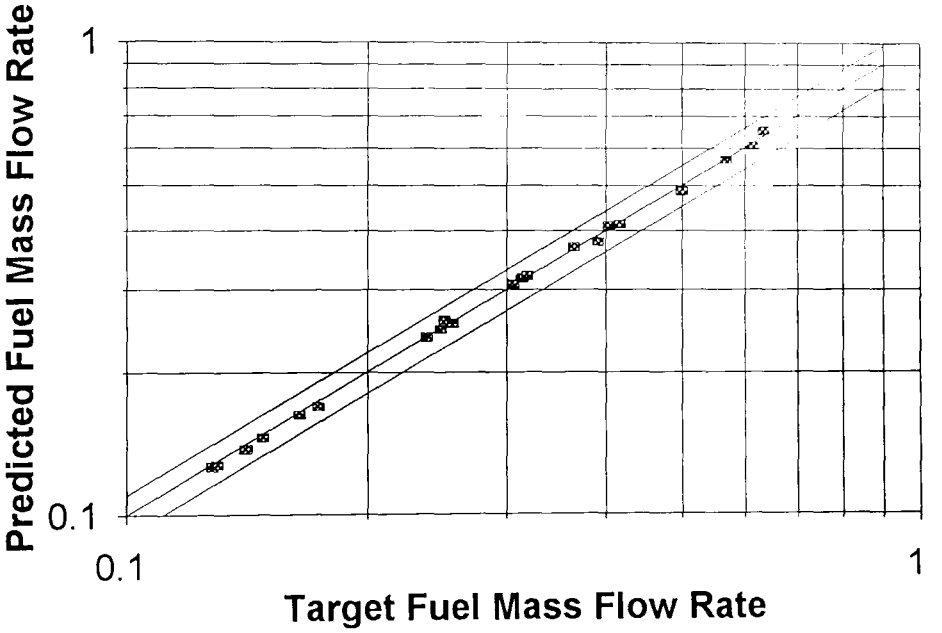

Figure 2.9
Target and network predicted fuel mass flow rates (scaled 0.1 to 0.9) from speed and load inputs showing +/- 10% error bands for:
a) Training Data
b) Validation Data

HC Mass Flow Rates:

a)

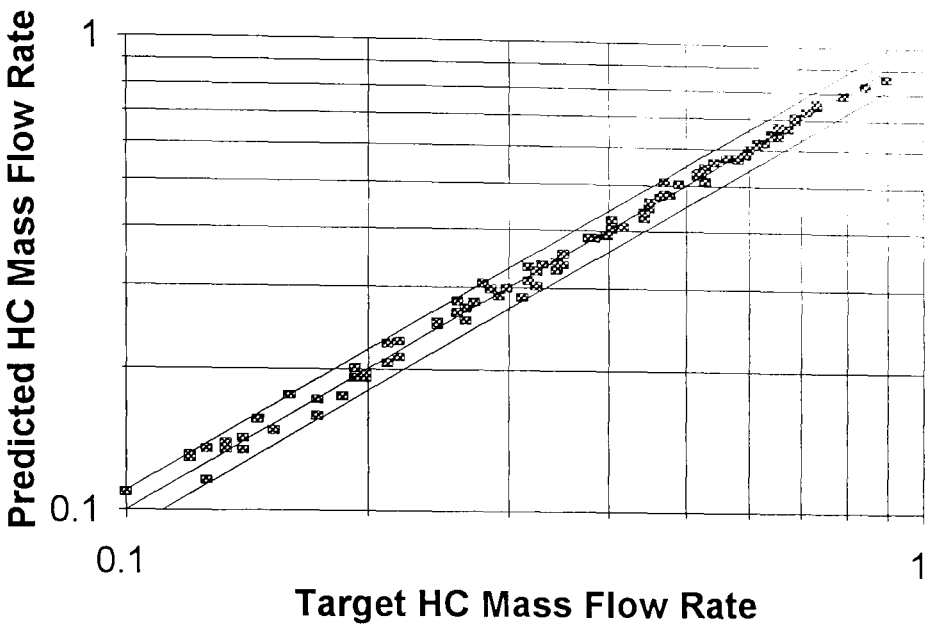

b)

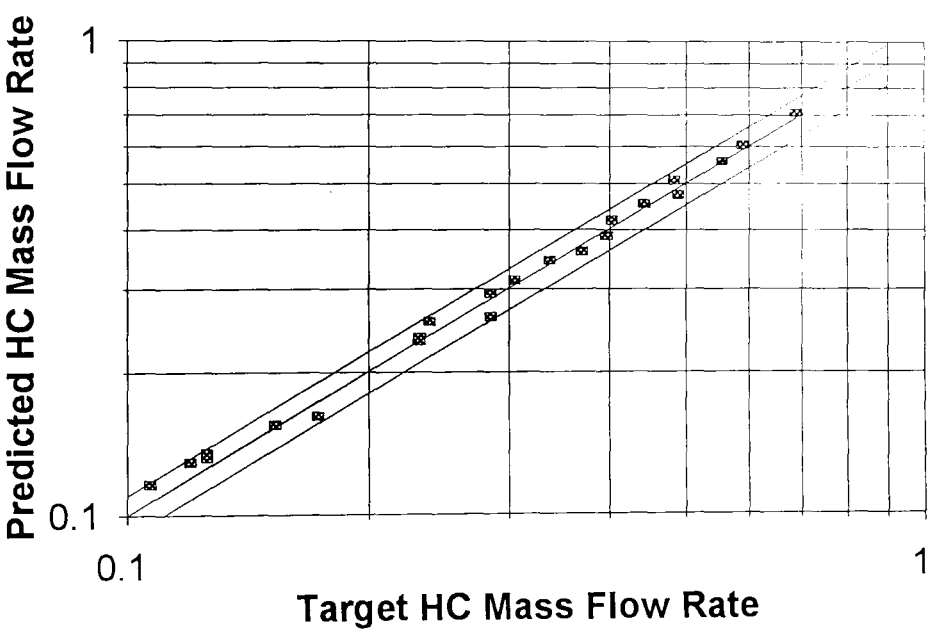

Figure 2.10
Target and network predicted HC mass flow rates (scaled 0.1 to 0.9) from speed and load inputs showing +/- 10% error bands for:
a) Training Data
b) Validation Data

CO Mass Flow Rates:

a)

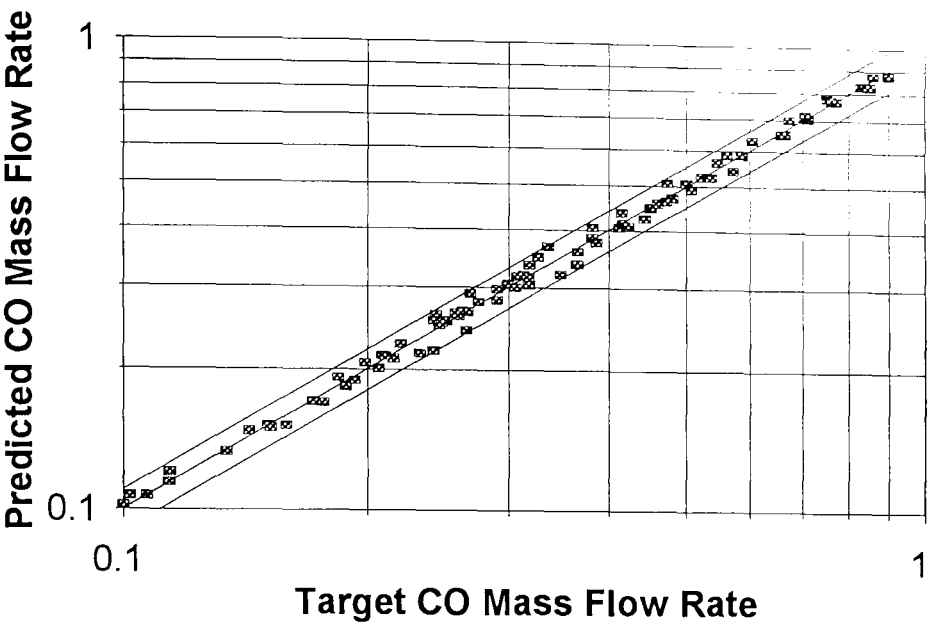

b)

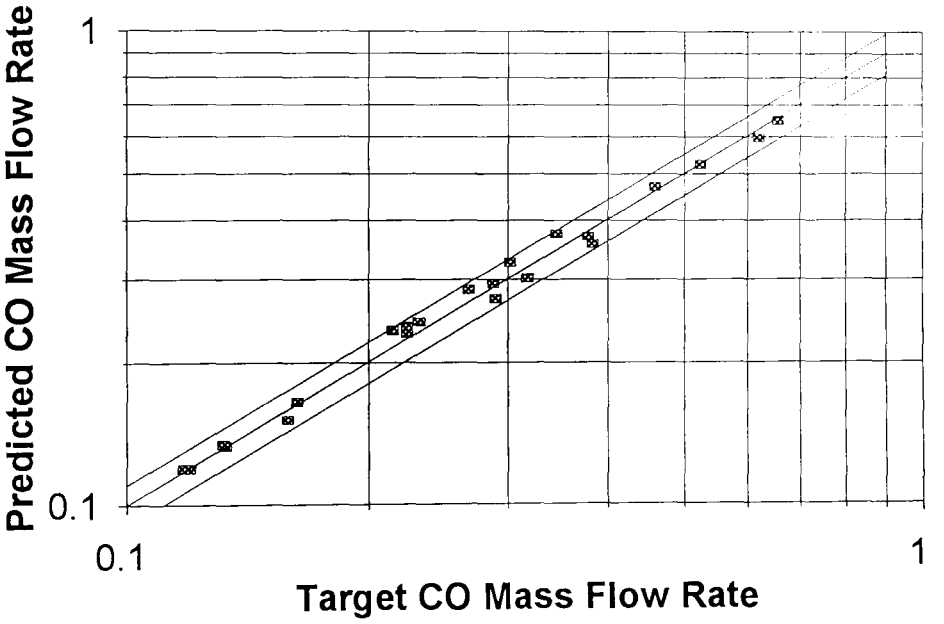

Figure 2.11
Target and network predicted CO mass flow rates (scaled 0.1 to 0.9) from speed and load inputs showing +/- 10% error bands for:
a) Training Data
b) Validation Data

NOx Mass Flow Rates:

a)

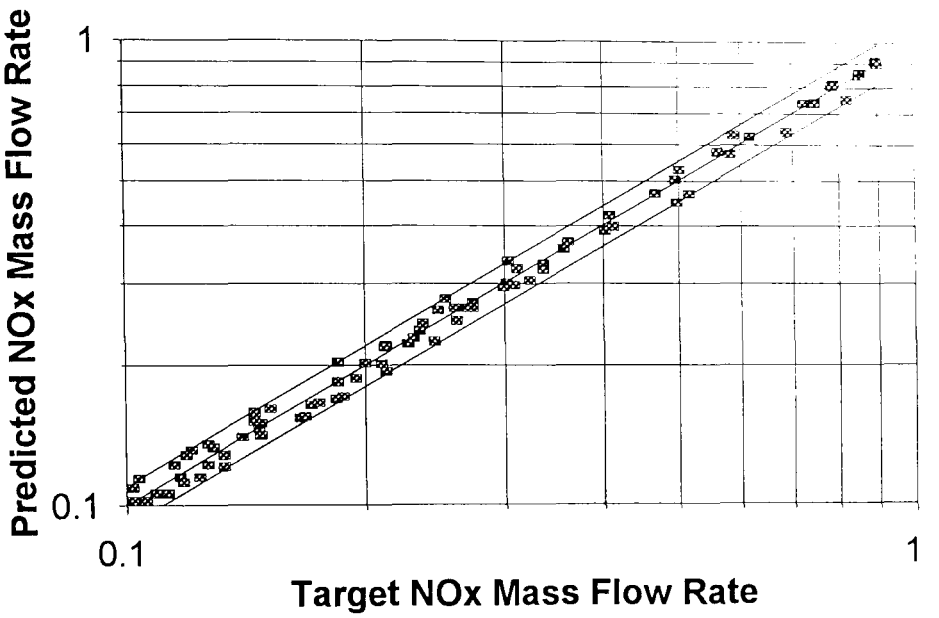

b)

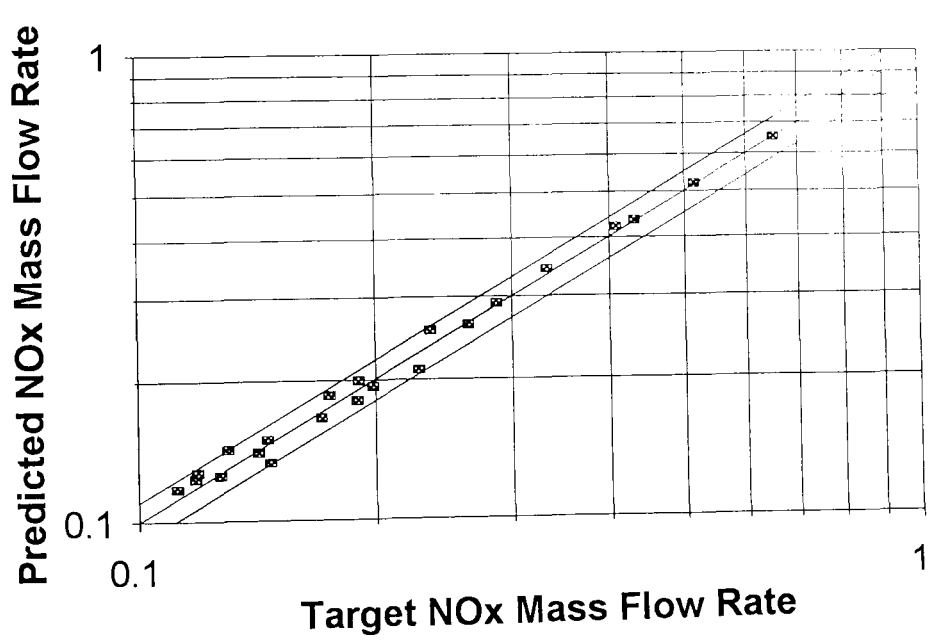

Figure 2.12
Target and network predicted NOx mass flow rates (scaled 0.1 to 0.9) from speed and load inputs showing +/- 10% error bands for:
a) Training Data
b) Validation Data

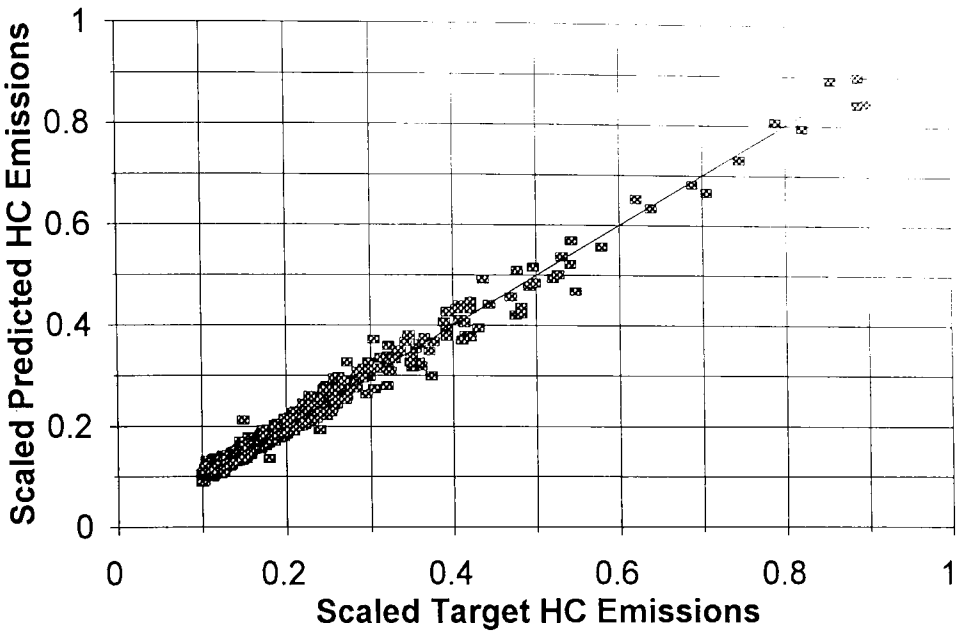

Figure 2.13
Target and predicted HC emissions (scaled 0.1 to 0.9) for 1.6 litre spark ignition engine characterised as a function of engine speed, load, AFR, spark timing and EGR rate.

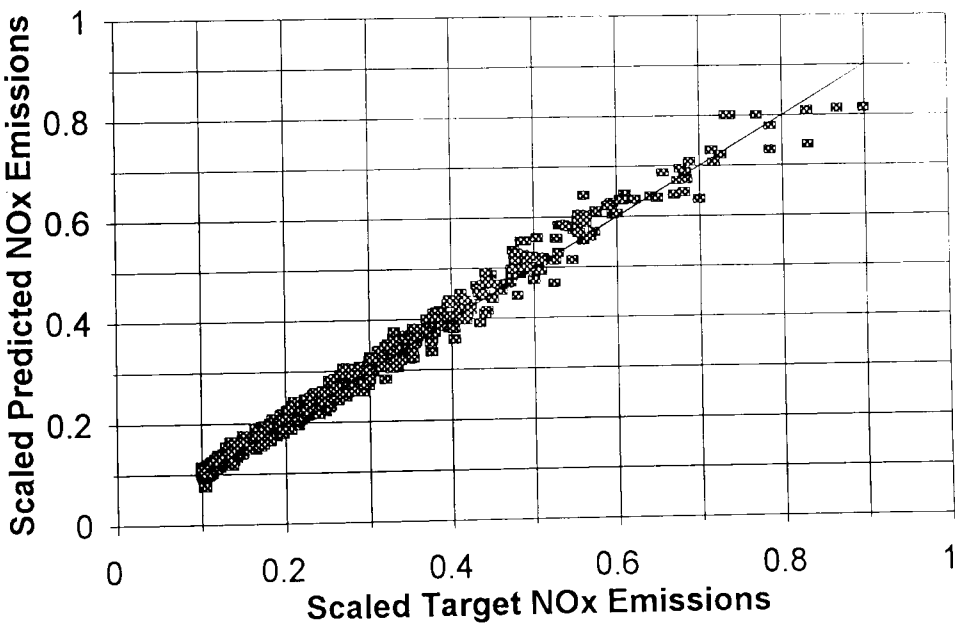

Figure 2.14
Target and predicted NOx emissions (scaled 0.1 to 0.9) for 1.6 litre spark ignition engine characterised as a function of engine speed, load, AFR, spark timing and EGR rate.

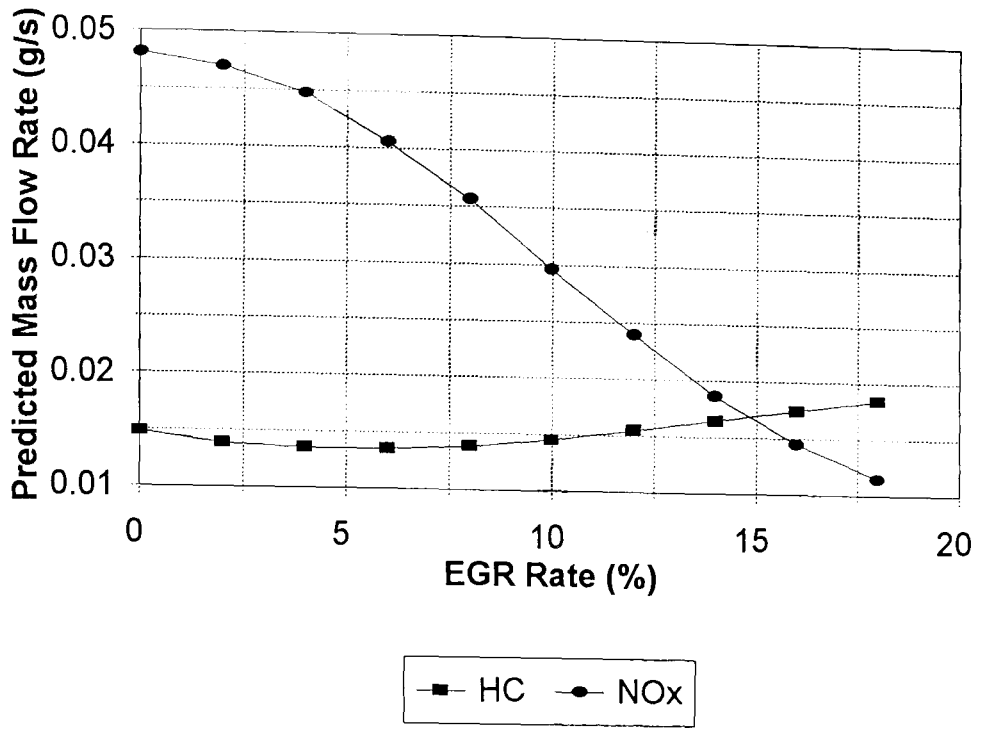

Figure 2.15
Neural network predicted effect of EGR rate on HC and NOx emissions flow rates for 1.6 litre spark ignition engine running at 2000 rpm, 50 Nm brake load, stoichiometric AFR and MBT spark timing.

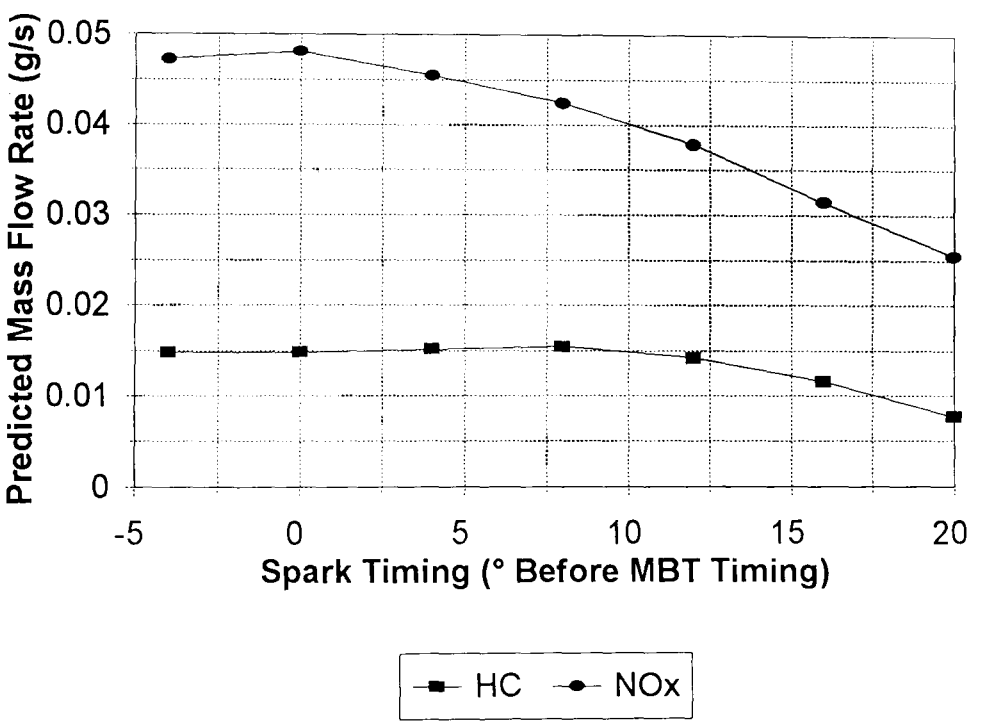

Figure 2.16
Neural network predicted effect of spark timing on HC and NOx emissions flow rates for 1.6 litre spark ignition engine running at 2000 rpm, 50 Nm brake load, stoichiometric AFR and zero EGR rate.

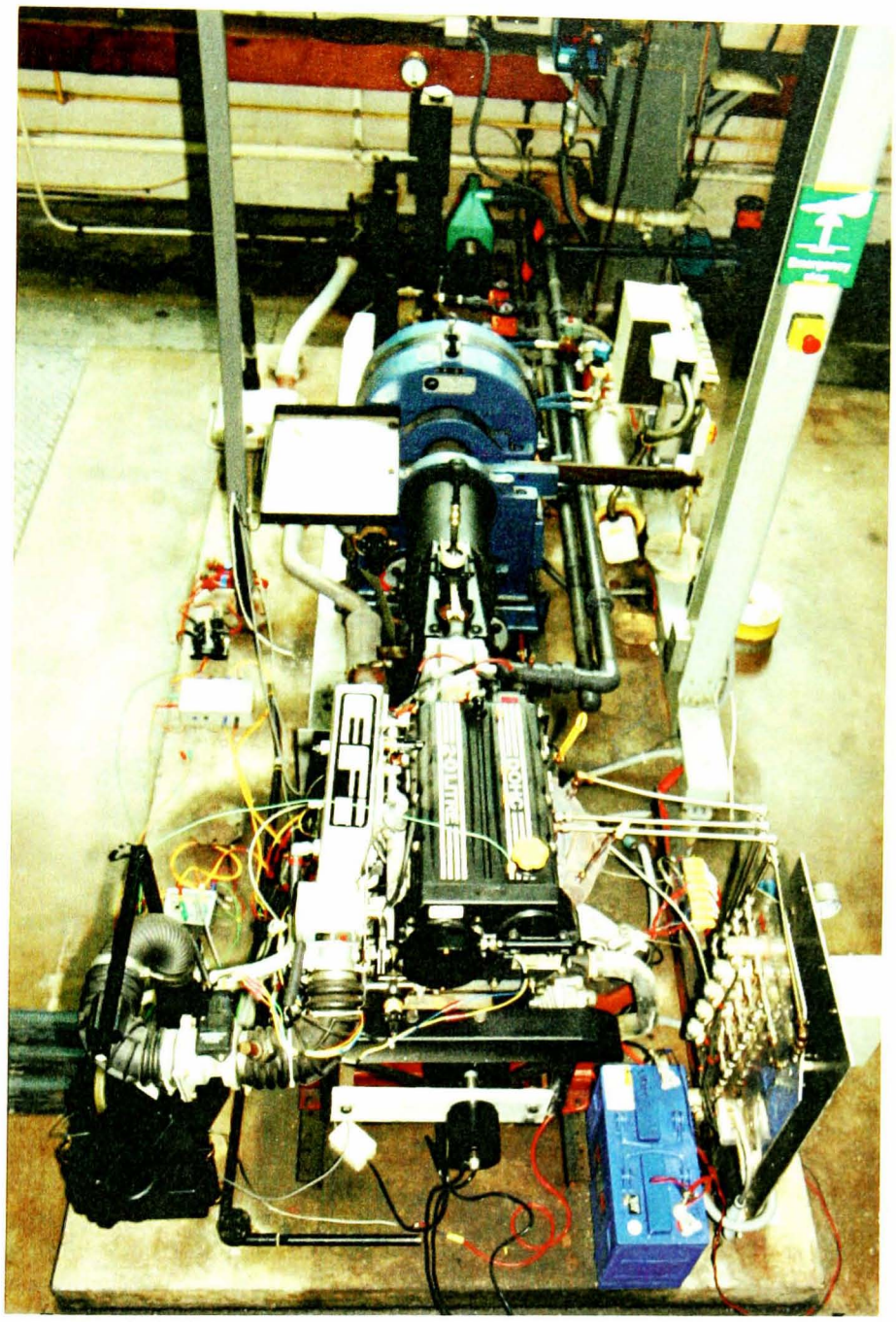

Figure 3.1
Engine Assembly and Dynamometer Mounted on the Test Bed

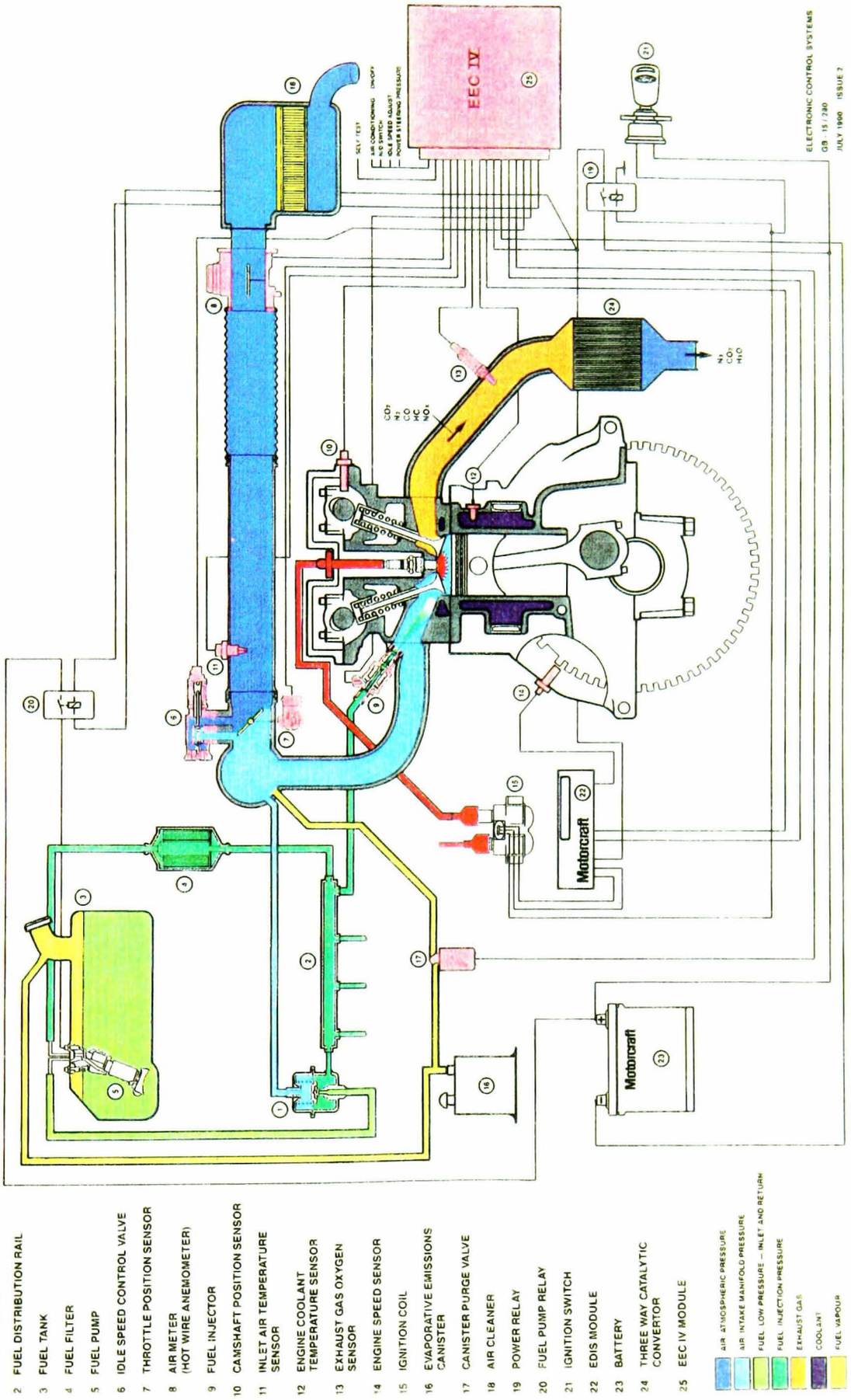

1 FUEL PRESSURE REGULATOR
2 FUEL DISTRIBUTION RAIL
3 FUEL TANK
4 FUEL FILTER
5 FUEL PUMP
6 IDLE SPEED CONTROL VALVE
7 THROTTLE POSITION SENSOR
8 AIR METER (HOT WIRE ANEMOMETER)
9 FUEL INJECTOR
10 CAMSHAFT POSITION SENSOR
11 INLET AIR TEMPERATURE SENSOR
12 ENGINE COOLANT TEMPERATURE SENSOR
13 EXHAUST GAS OXYGEN SENSOR
14 ENGINE SPEED SENSOR
15 IGNITION COIL
16 EVAPORATIVE EMISSIONS CANISTER
17 CANISTER PURGE VALVE
18 AIR CLEANER
19 POWER RELAY
20 FUEL PUMP RELAY
21 IGNITION SWITCH
22 EDIS MODULE
23 BATTERY
24 THREE WAY CATALYTIC CONVERTOR
25 EEC IV MODULE

AIR ATMOSPHERIC PRESSURE
AIR INTAKE MANIFOLD PRESSURE
FUEL LOW PRESSURE – INLET AND RETURN
FUEL INJECTION PRESSURE
EXHAUST GAS
COOLANT
FUEL VAPOUR

Figure 3.2
Schematic of the Ford EECIV Engine Management System

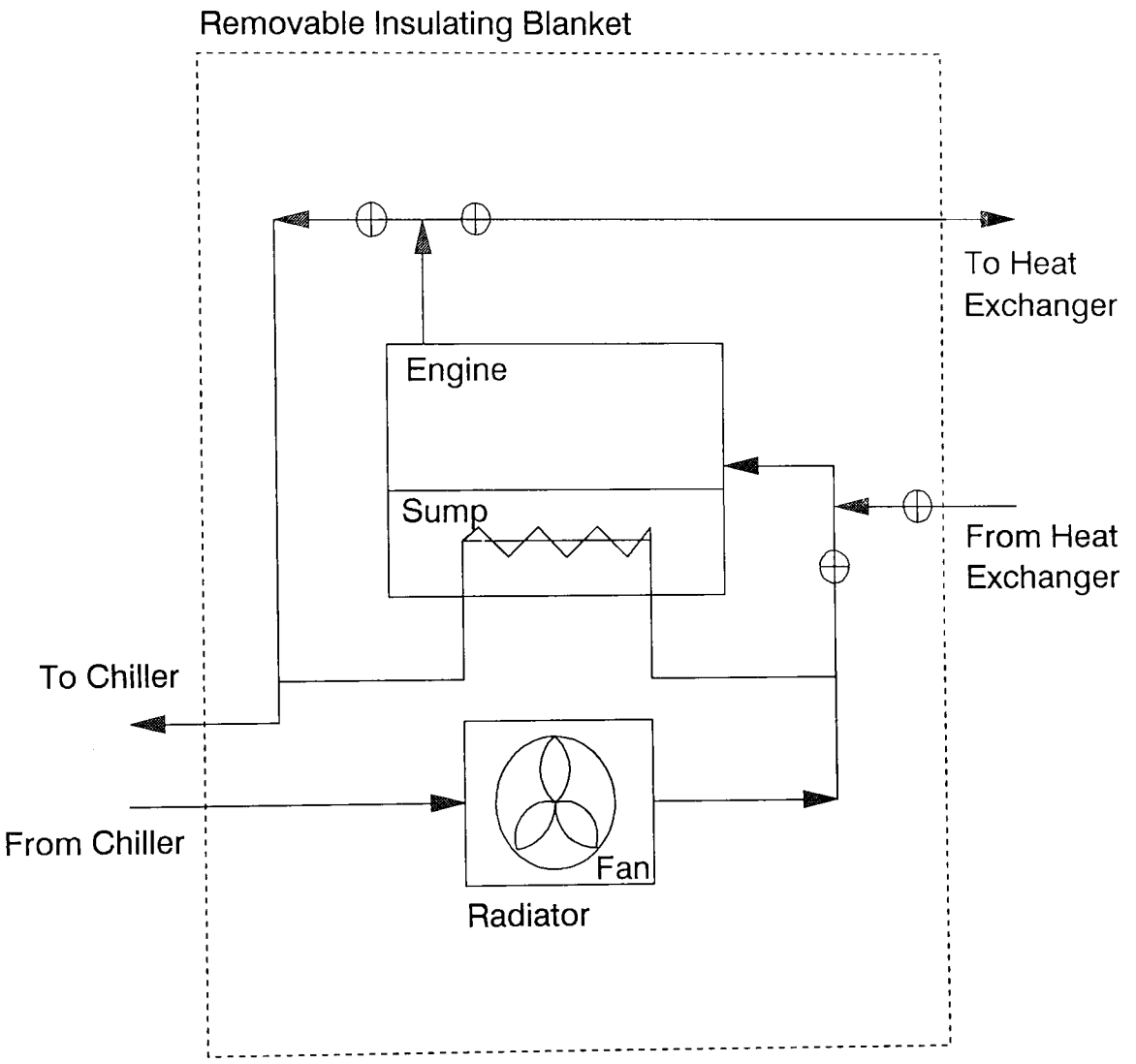

Figure 3.3
Schematic of engine cooling circuit.

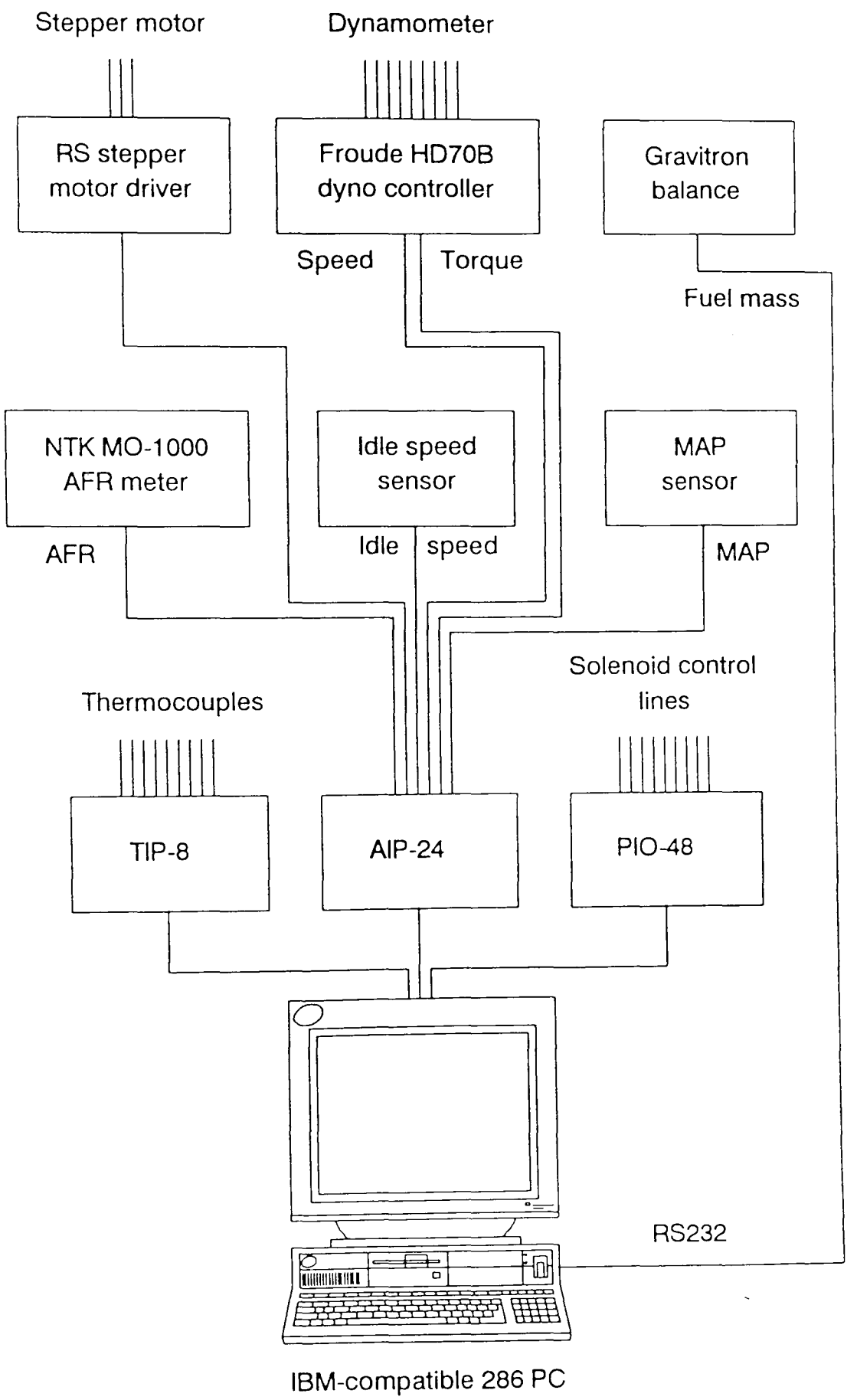

Figure 3.4
Schematic of engine rig monitoring and control facility.

a)

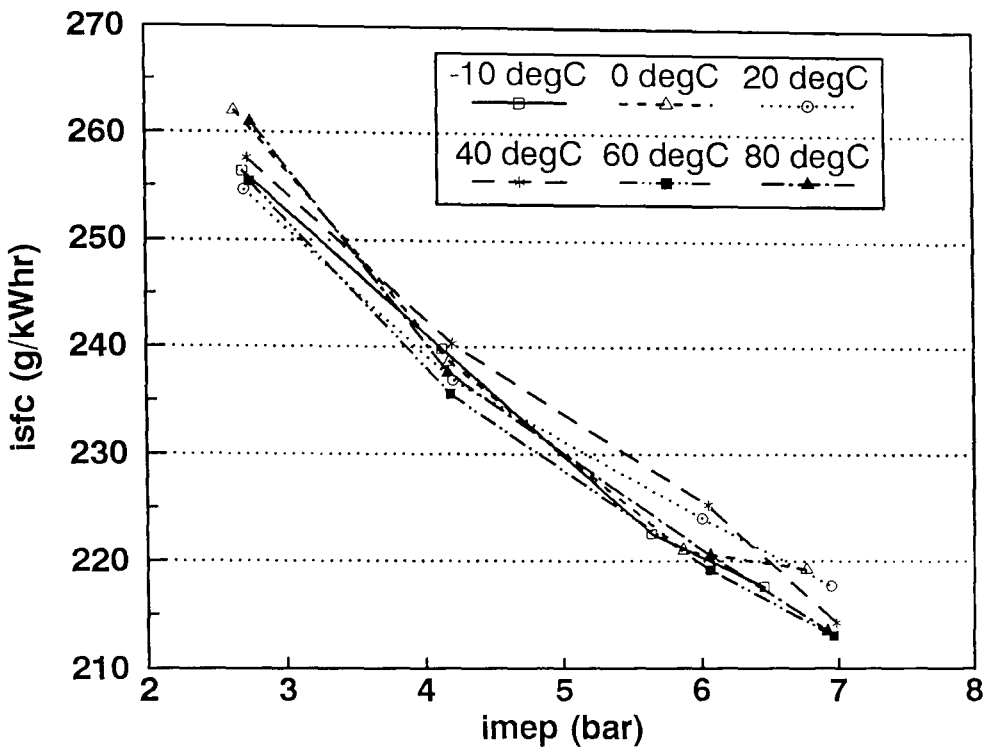

b)

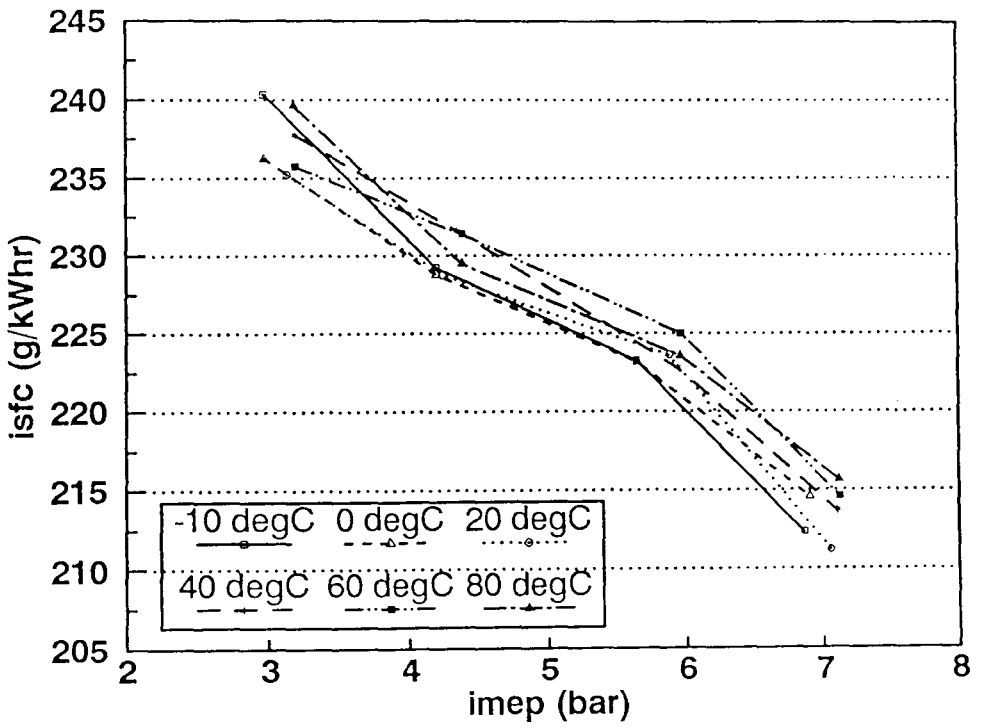

Figure 4.1
isfc plotted against imep for fixed throttle warm-up tests for 2 litre DOHC 8V engine. Tail-pipe AFR stoichiometric throughout.
a) Engine speed 1750 rpm.
b) Engine speed 2400 rpm.

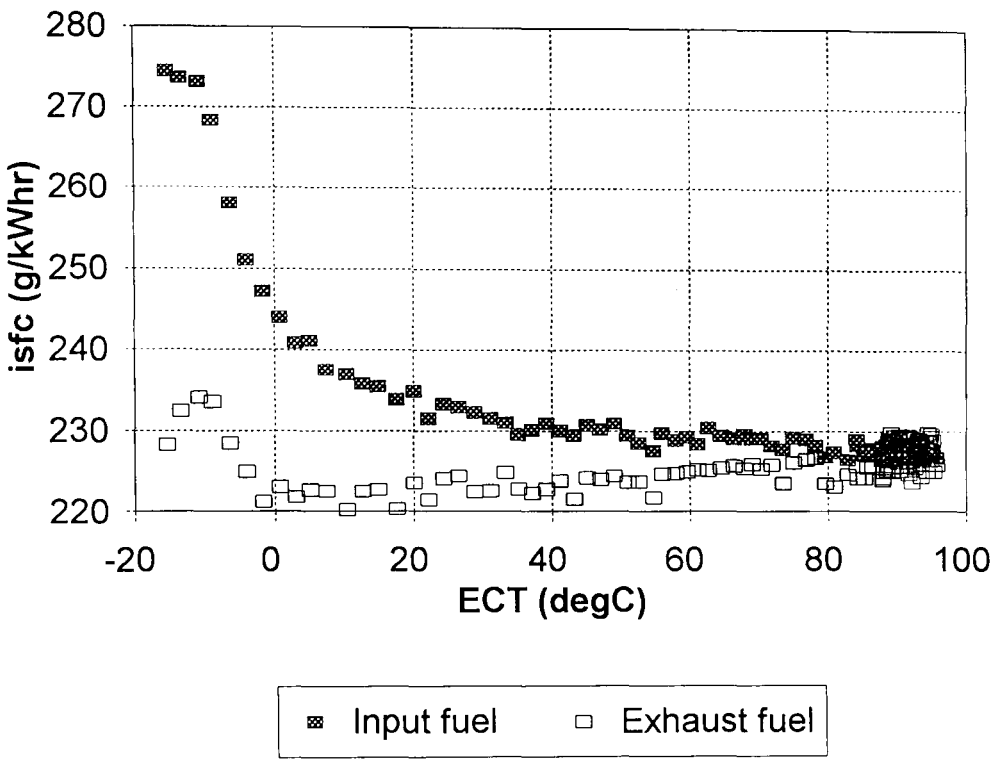

Figure 4.2
isfc determined from fuel injected and fuel detected in exhaust gases against ECT for cold-start test at 2400 rpm, imep 5.9 bar, tail-pipe AFR 14.2:1.

a)

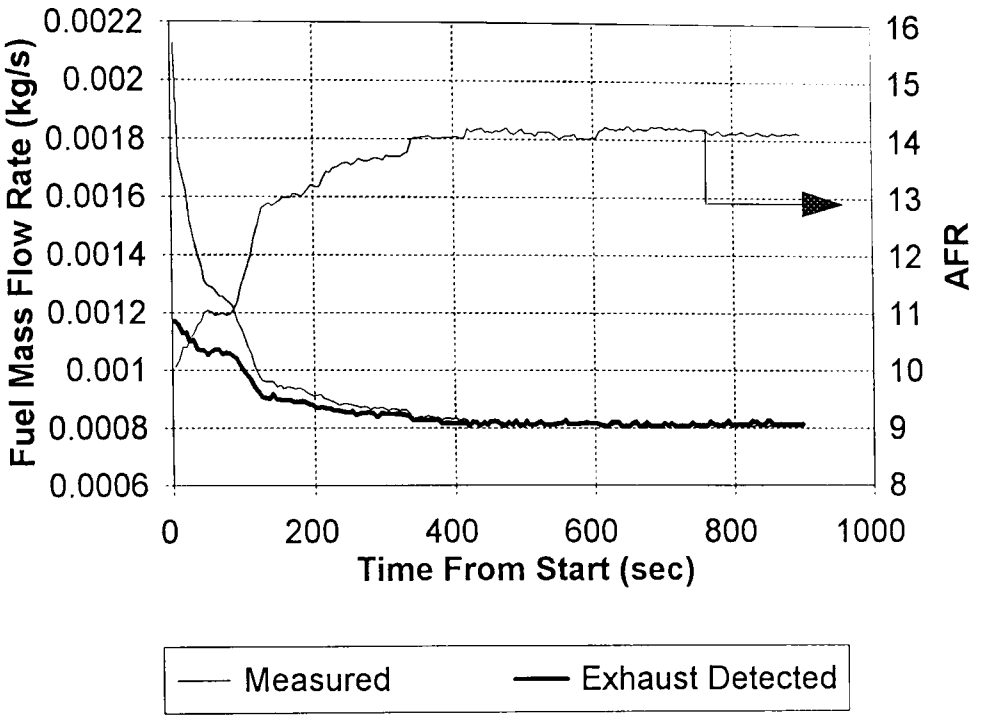

b)

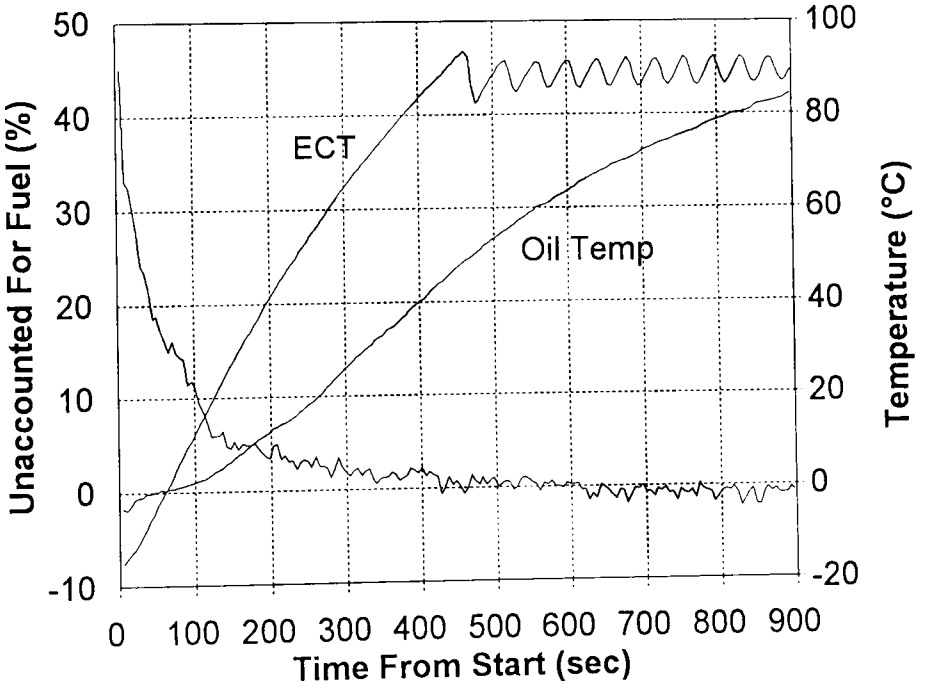

Figure 4.3
Fixed throttle warm-up test data. Test conditions:
1750 rpm, imep 4.1 bar, start temperature -15°C.
a) Measured and exhaust detected fuel mass flow rates.
b) 'Unaccounted for' fuel fraction and warm-up profiles.

a)

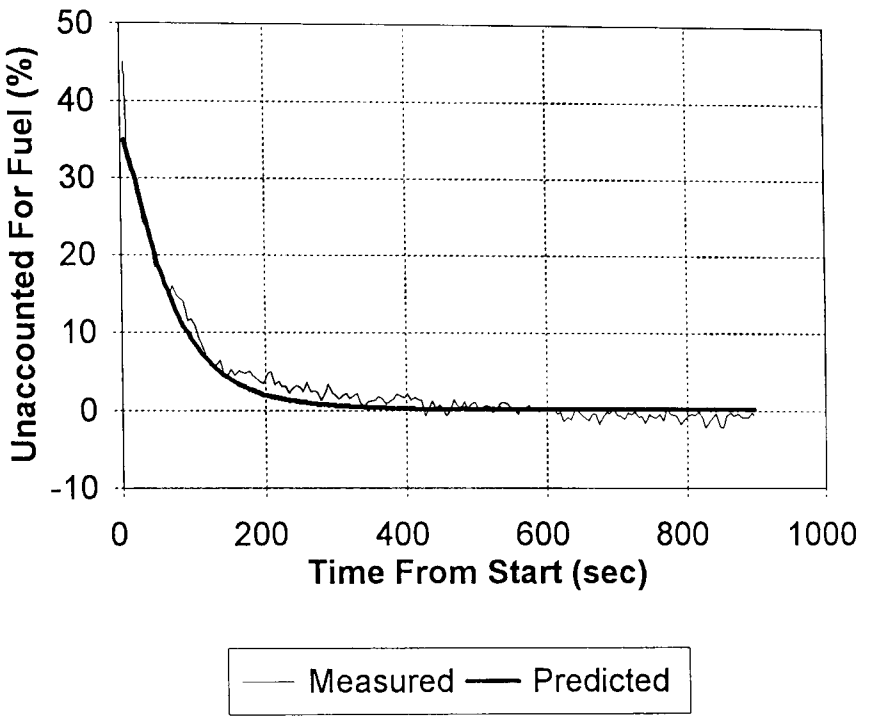

b)

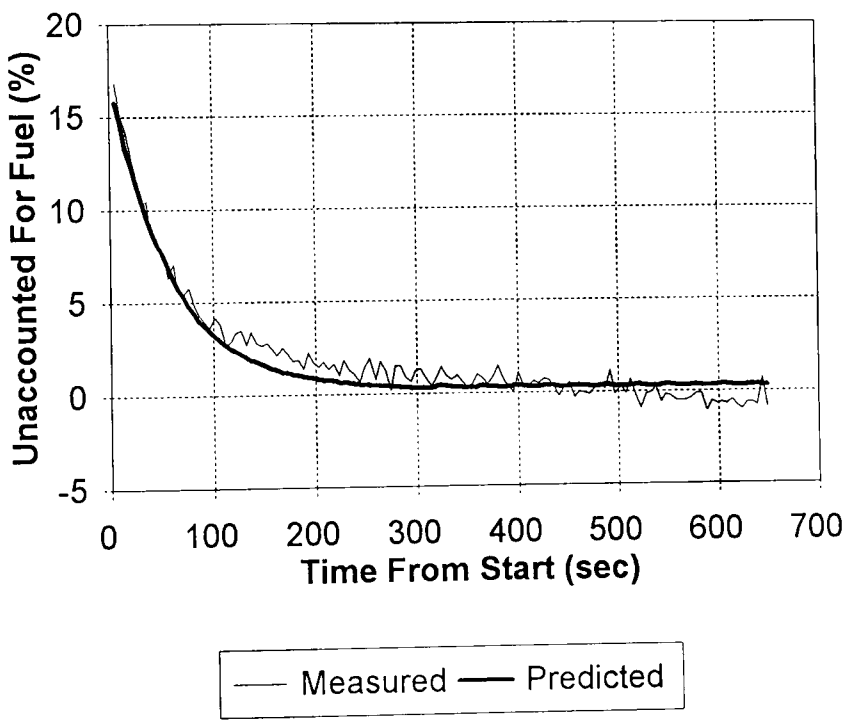

Figure 4.4
Measured and predicted 'unaccounted for' fuel during fixed throttle warm-up tests for 2 litre DOHC 8V engine.
a)1750 rpm,imep 4.1 bar,start temperature -15°C,EECIV cold-start strategy.
b)2400 rpm,imep 5.9 bar,start temperature -15°C,constant tail-pipe AFR.

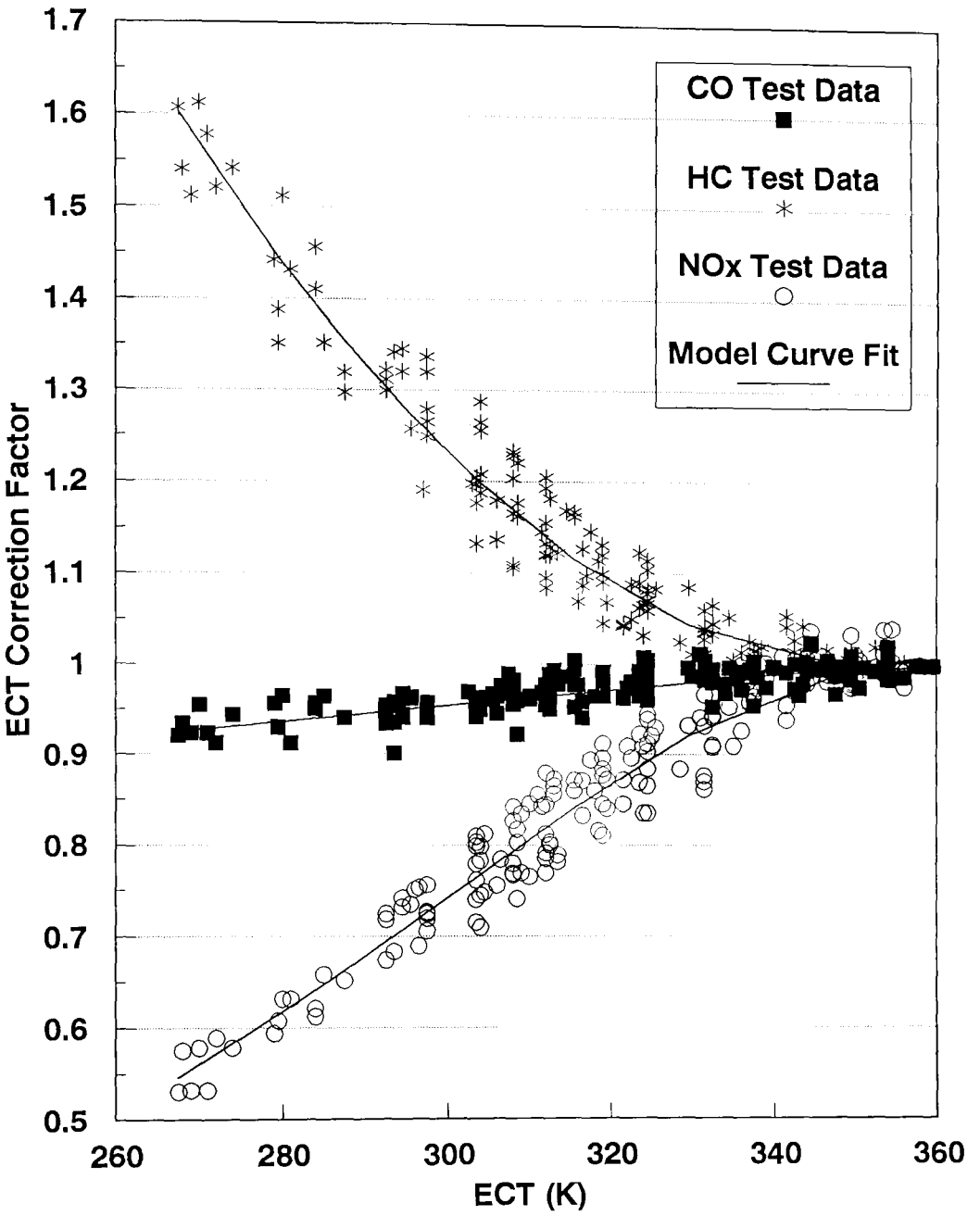

Figure 5.1
Indicated specific emissions divided by fully-warm indicated specific emissions (ECT Correction Factor) plotted against ECT. 2 litre DOHC 8V warm-up test data with range of engine speeds, imeps and AFRs (1250-2500 rpm, 2.5-7.5 bar, 12:1-17.5:1).

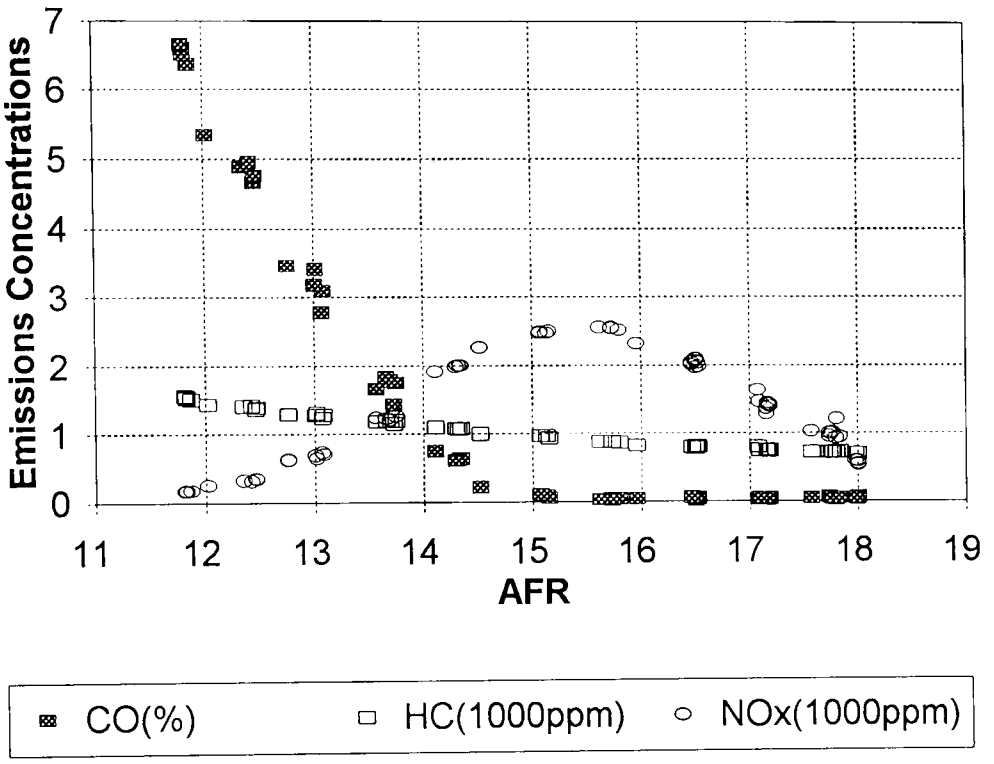

Figure 5.2
2 litre DOHC 8V engine-out emissions concentrations plotted against tail-pipe AFR. Steady-state fully-warm test conditions: 1250 rpm, 80 Nm brake load.

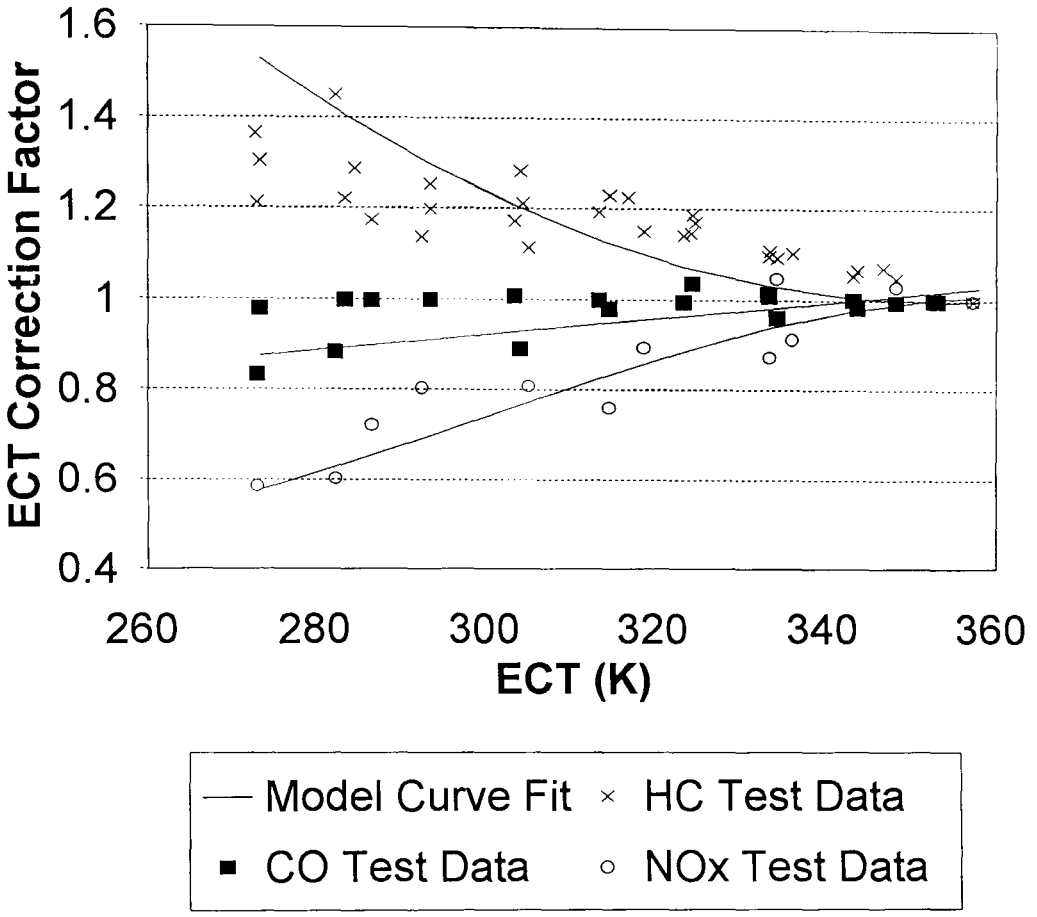

Figure 5.3
Indicated specific emissions divided by fully-warm indicated specific emissions (ECT Correction Factor) plotted against ECT. 1.8 litre Zetec engine warm-up test data at 2000 rpm, imep 8.3 bar, AFRs 12:1-17:1.

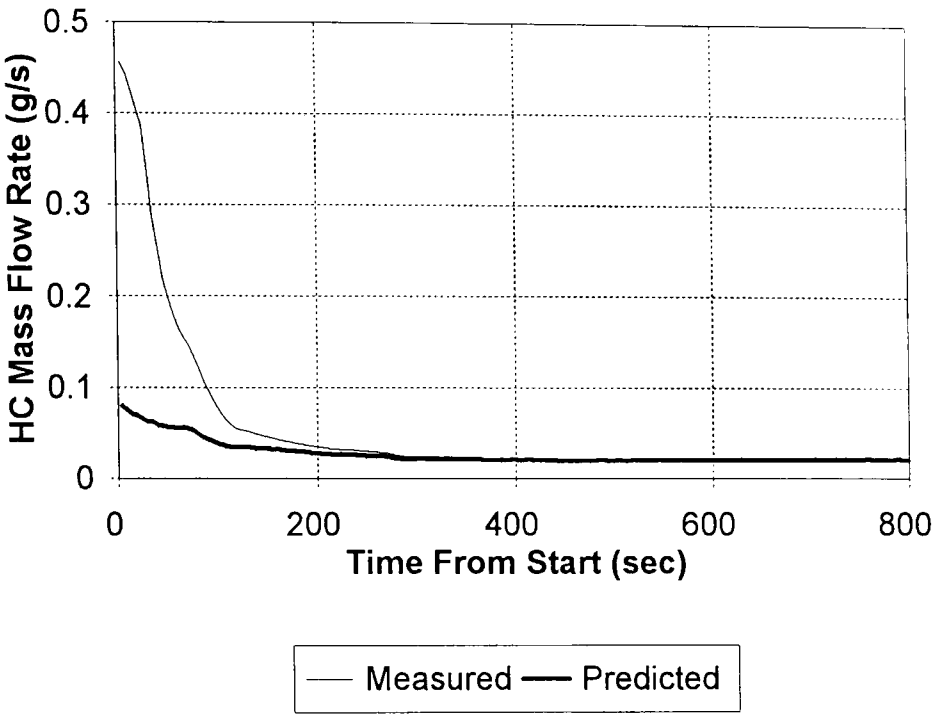

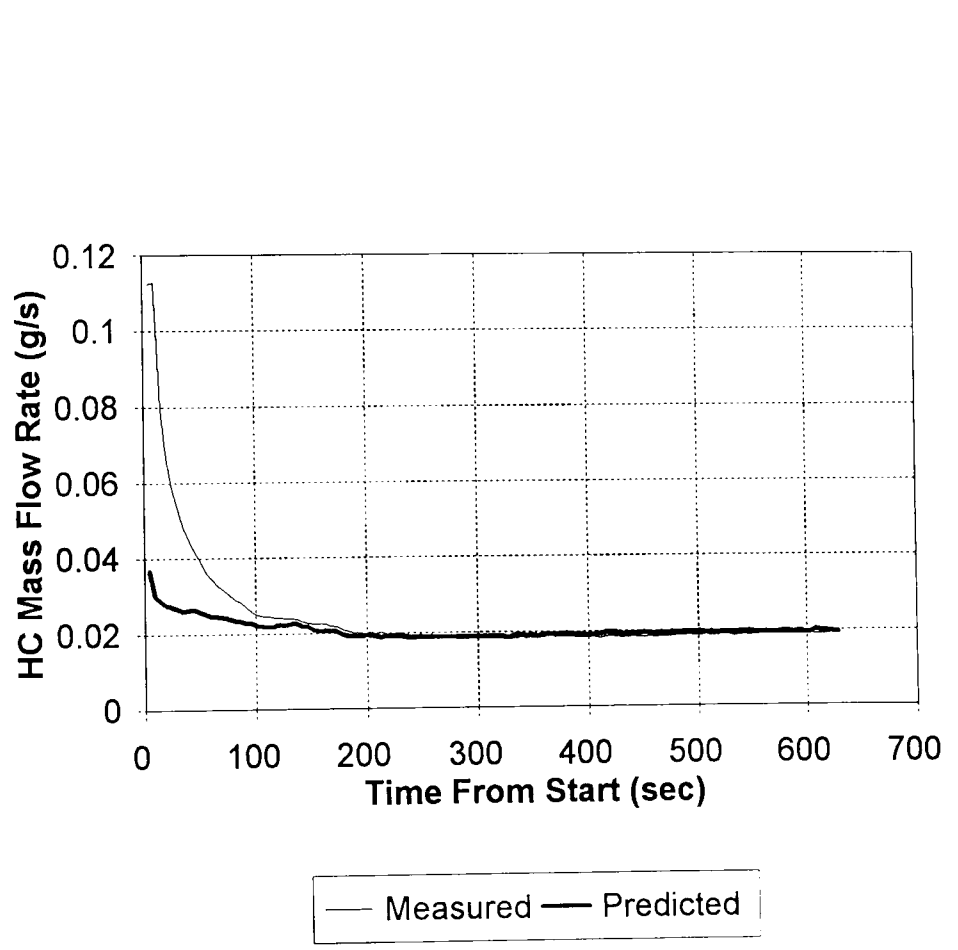

Figure 5.4
Measured and predicted HC mass flow rates during cold-starting with EECIV cold-start AFR strategy and AFR 14.5:1 at fully-warm.
1750 rpm, imep 7.3 bar, start temperature -15°C (upper)
1750 rpm, imep 5.5 bar, start temperature 20°C (upper)

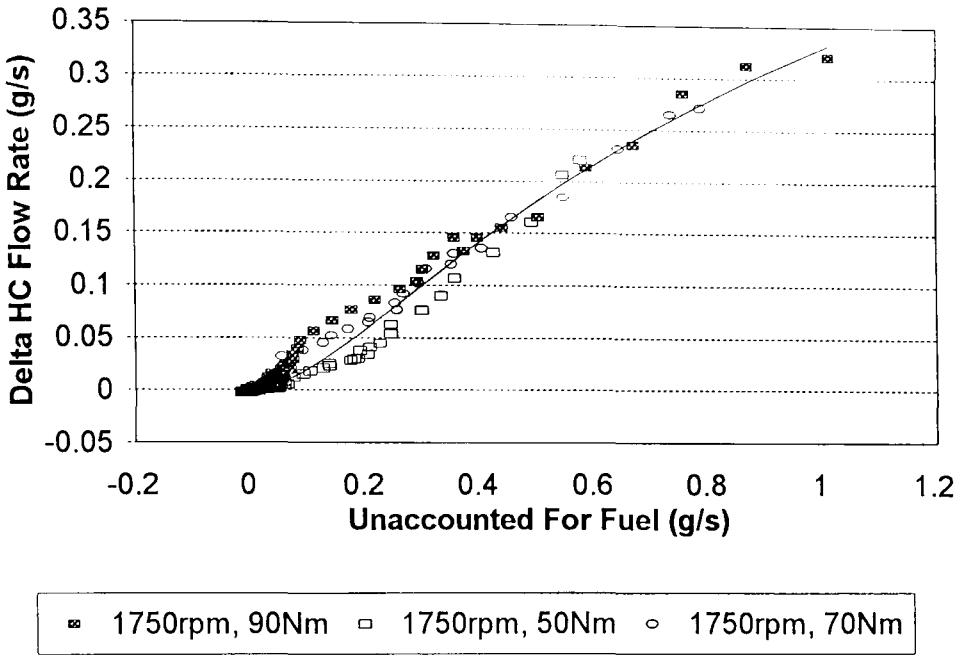

Figure 5.5
Delta HC flow rate plotted against 'unaccounted for' fuel during warm-up at 1750 rpm and three fully-warm brake loads for 2 litre DOHC 8V engine. EECIV cold-start AFR strategy and AFR 14.5:1 when fully-warm. Start temperature -15°C

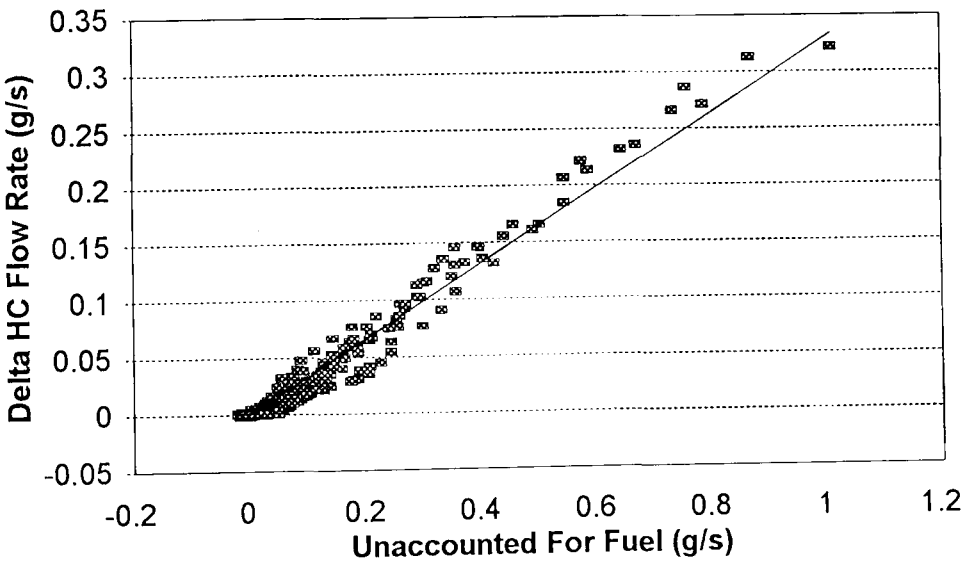

Figure 5.6
Delta HC flow rate plotted against 'unaccounted for' fuel during warm-up for 2 litre DOHC 8V engine with range of engine speeds, loads and start temperatures (1250 - 2400 rpm, 30 - 90 Nm, -15°C - +20°C).

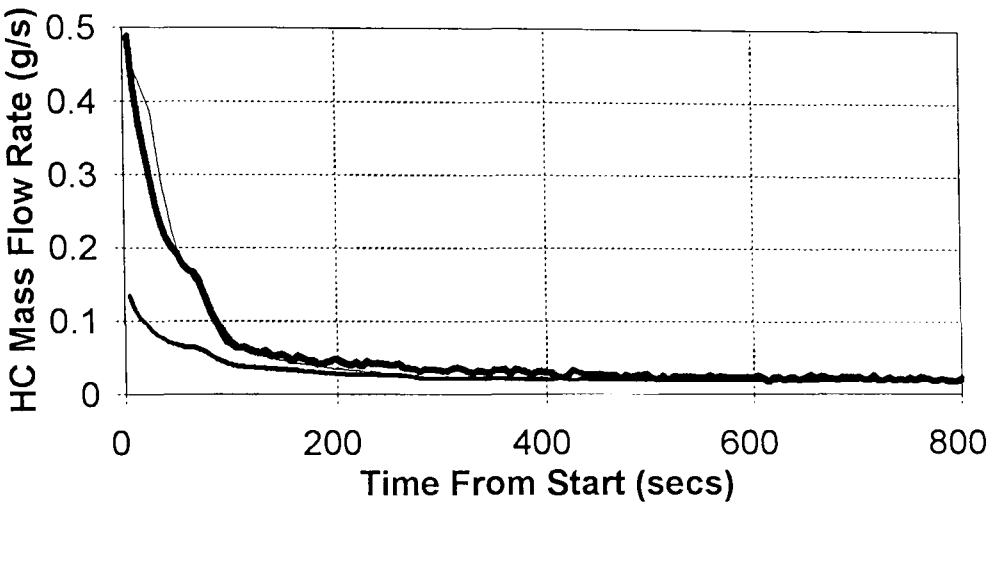

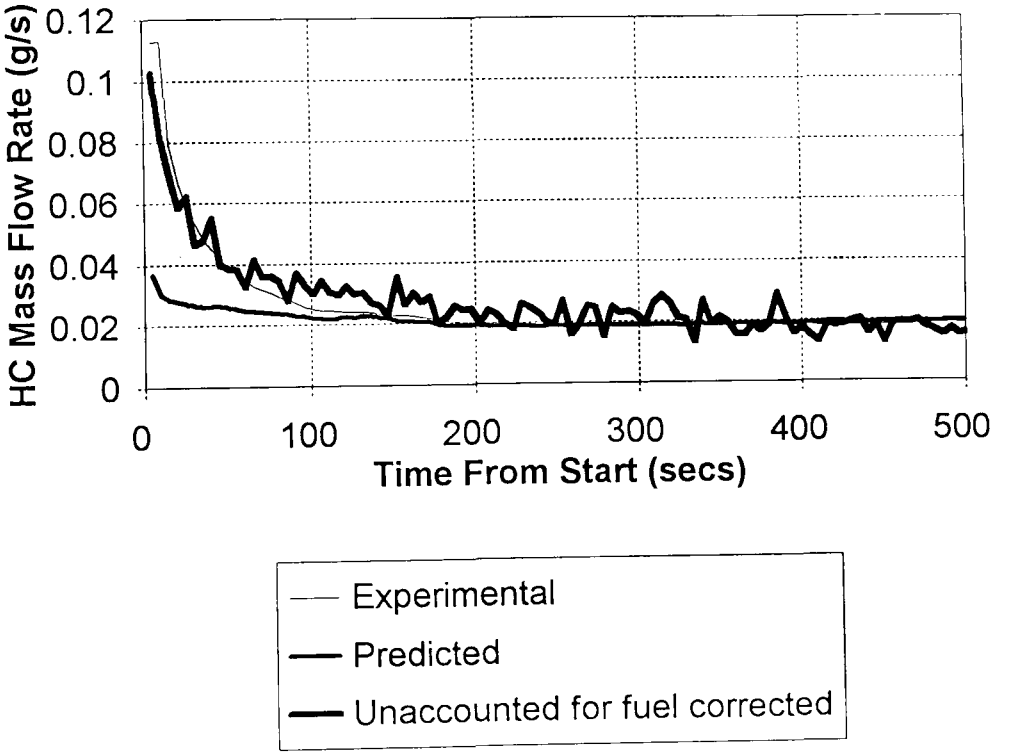

Figure 5.7
Measured, predicted and 'unaccounted for' fuel corrected HC mass flow rates during cold-starting with EECIV cold-start AFR strategy and AFR 14.5:1 at fully-warm.
1750 rpm, imep 7.3 bar, start temperature -15°C (upper)
1750 rpm, imep 5.5 bar, start temperature 20°C (upper)

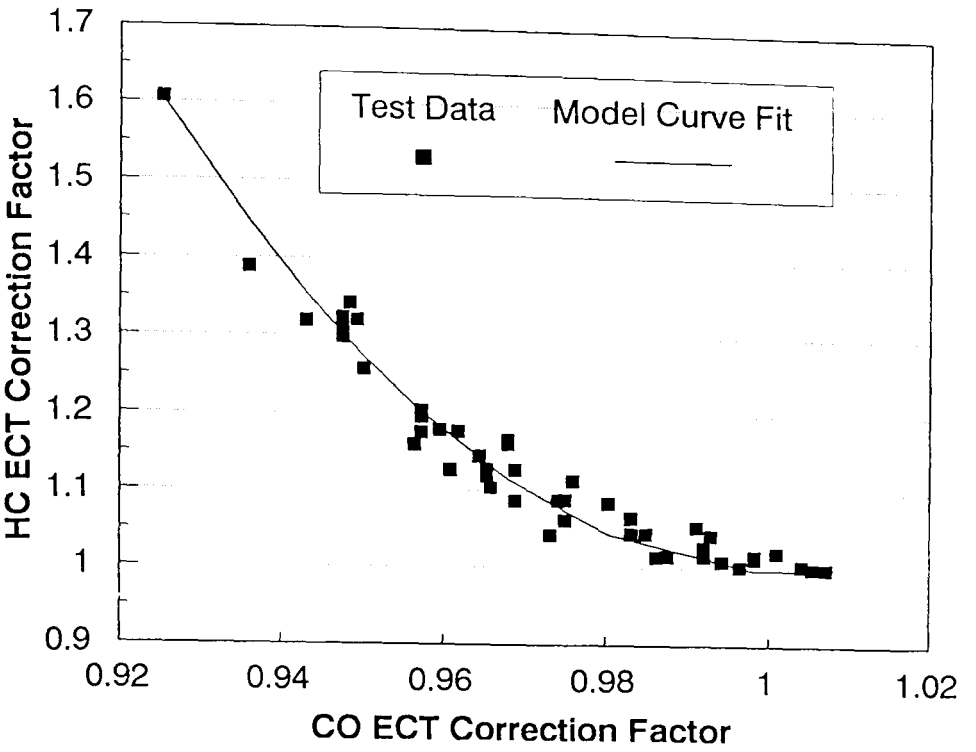

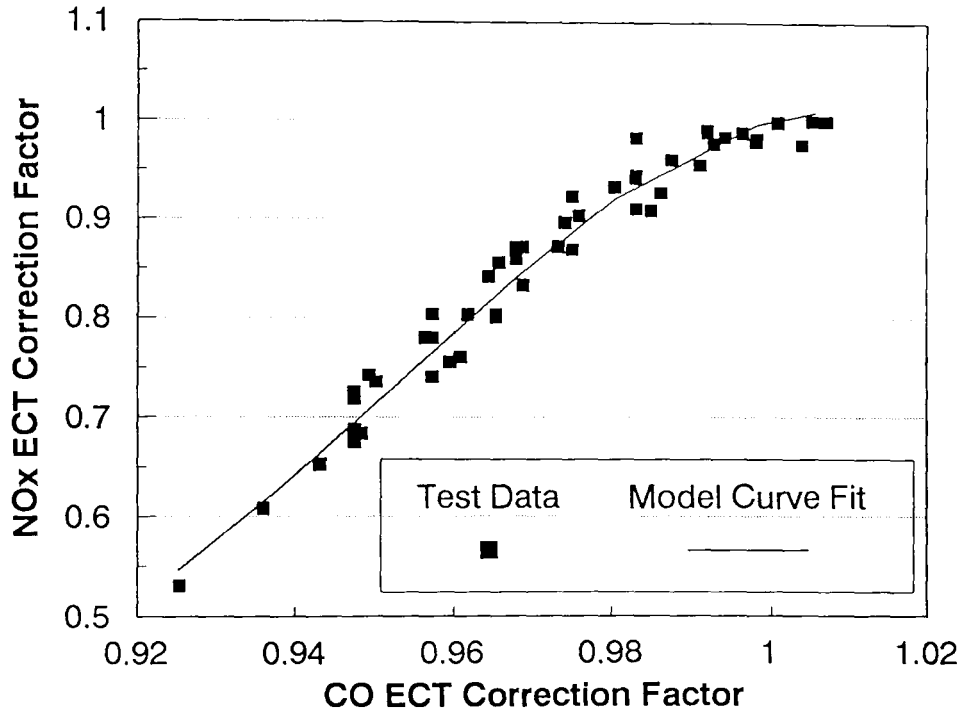

Figure 5.8
ishc ECT correction function (upper) and isno$_x$ ECT correction function (lower) against isco ECT correction function for 270K < ECT < 360 K showing typical experimental data points.

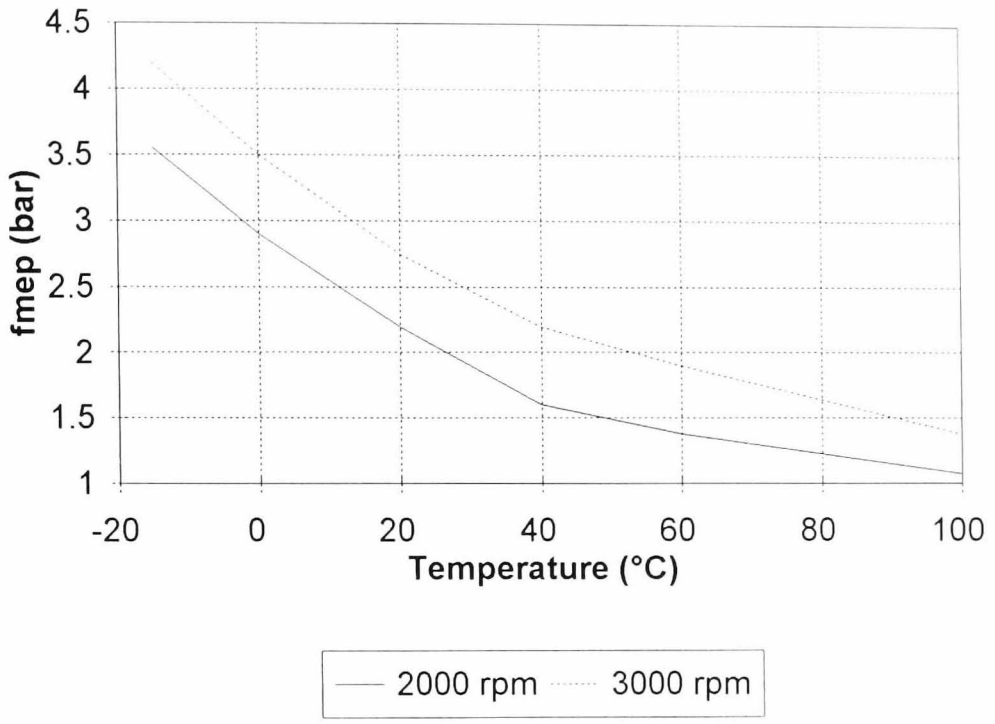

Figure 6.1(a)
Motored frictional losses for a 1.3 litre spark ignition engine at various oil temperatures [6.3].

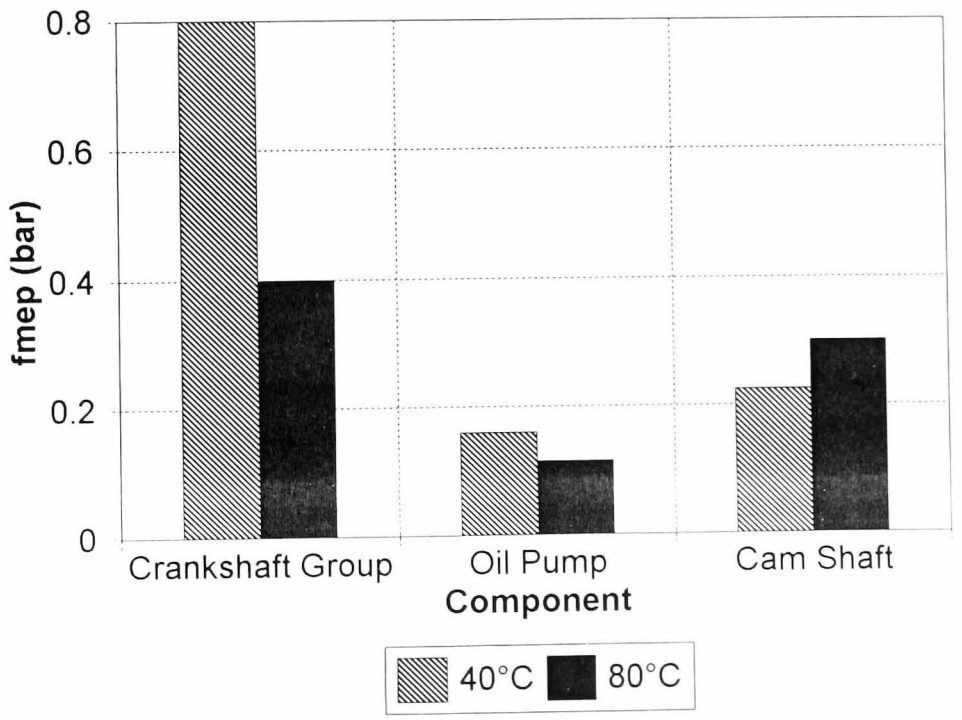

Figure 6.1(b)
Engine component frictional losses at different warm-up stages for a 1.3 litre spark ignition engine [6.3].

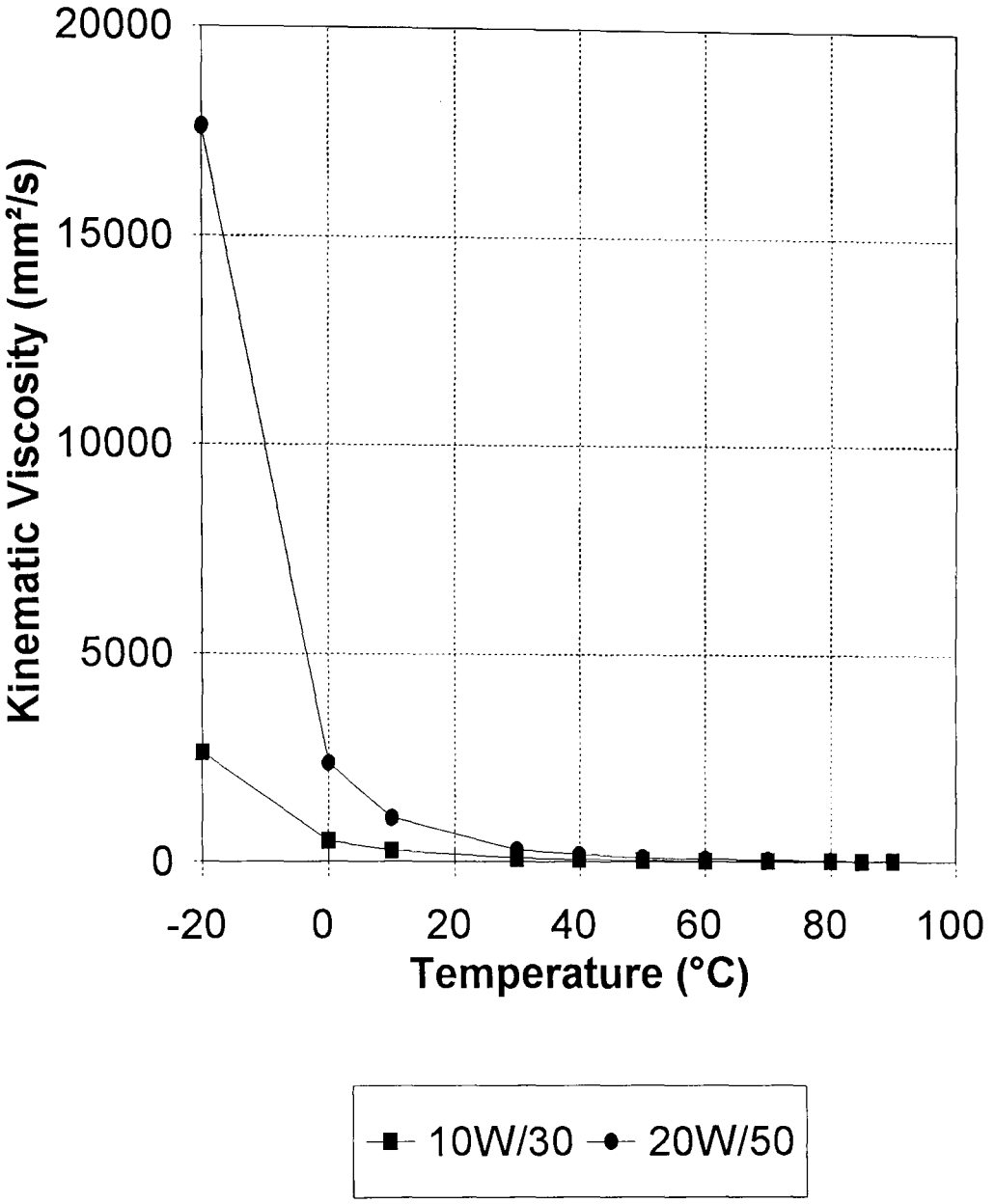

Figure 6.2
Oil viscosity variation with temperature for test oils. Oil viscosities calculated from Walther equation (6.10).

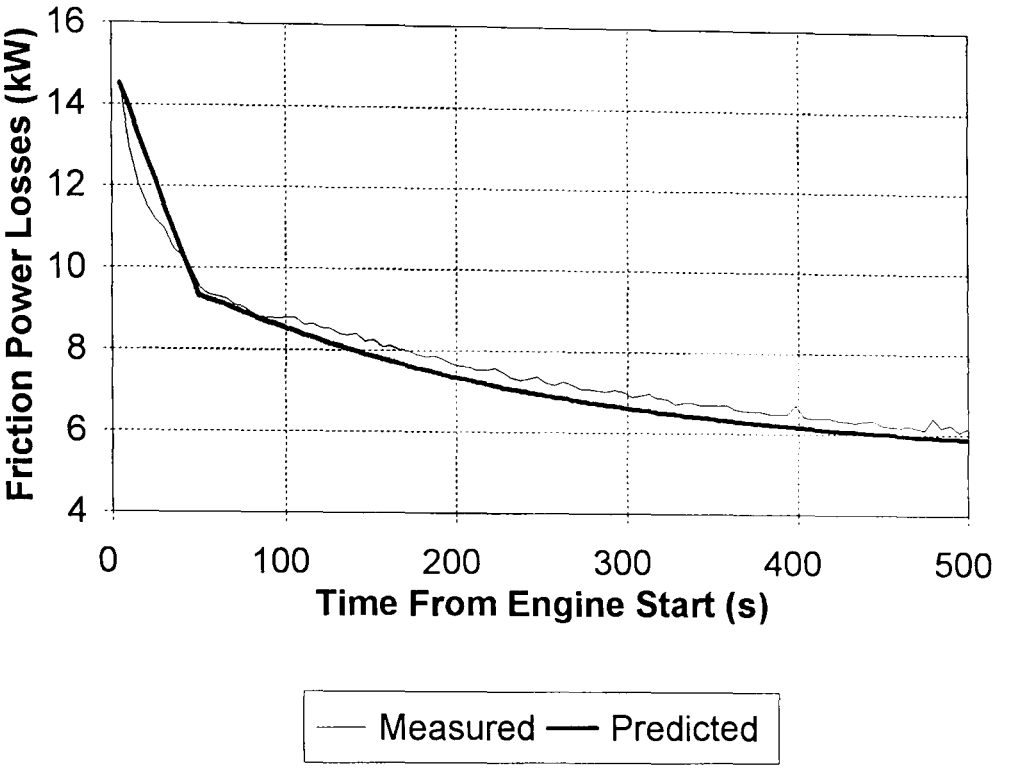

Figure 6.3
Measured and PROMETS predicted friction power losses (upper) and warm-up profiles (lower) for 2 litre DOHC 8V with SAE 10W/30 oil. Test conditions: 2800 rpm, imep 6.5 bar, start/soak temperarure 20°C.

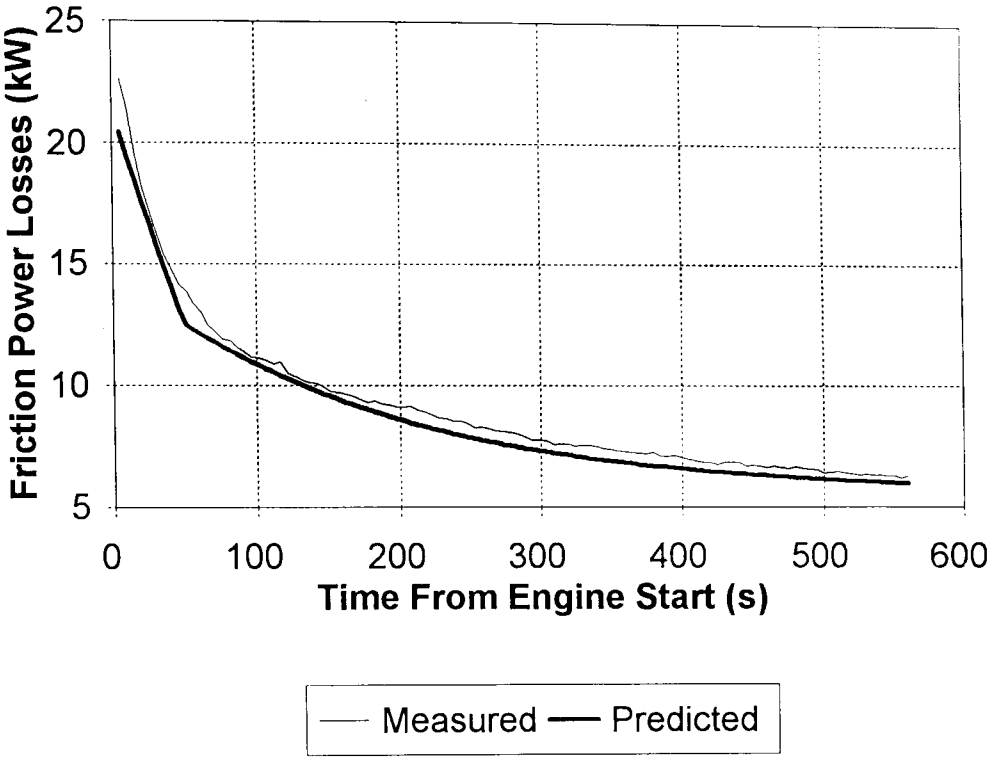

Figure 6.4
Measured and PROMETS predicted friction power losses (upper) and warm-up profiles (lower) for 2 Litre DOHC 8V with SAE 20W/50 oil. Test conditions: 2800 rpm, imep 4.1 bar, start/soak temperature -10°C.

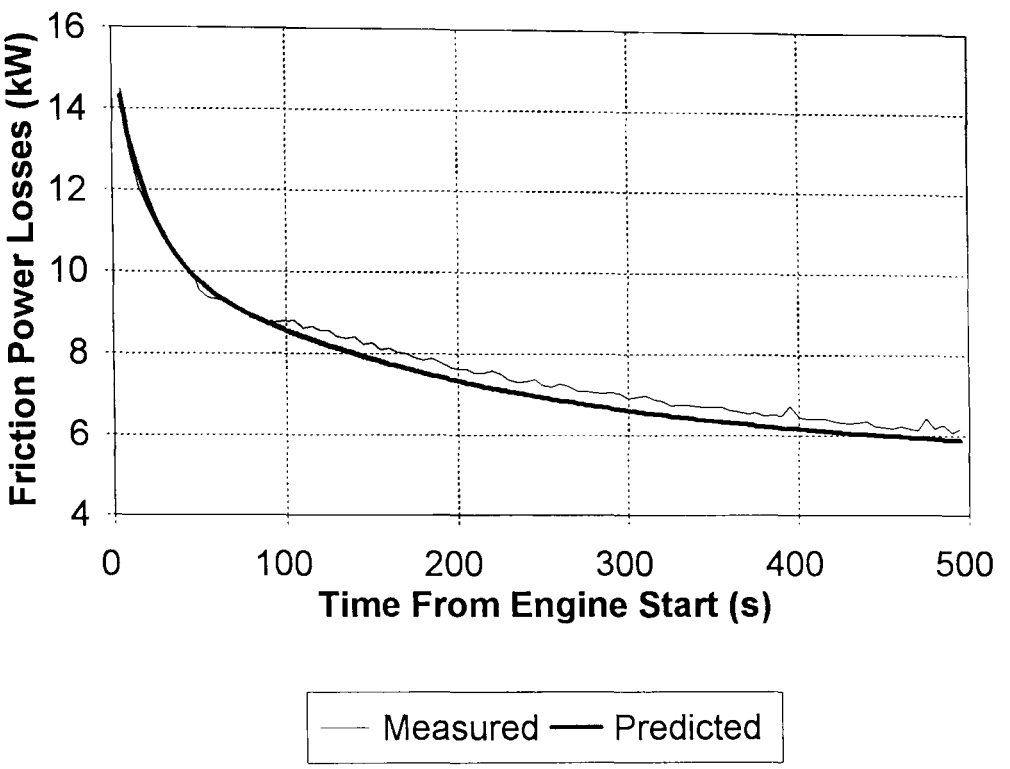

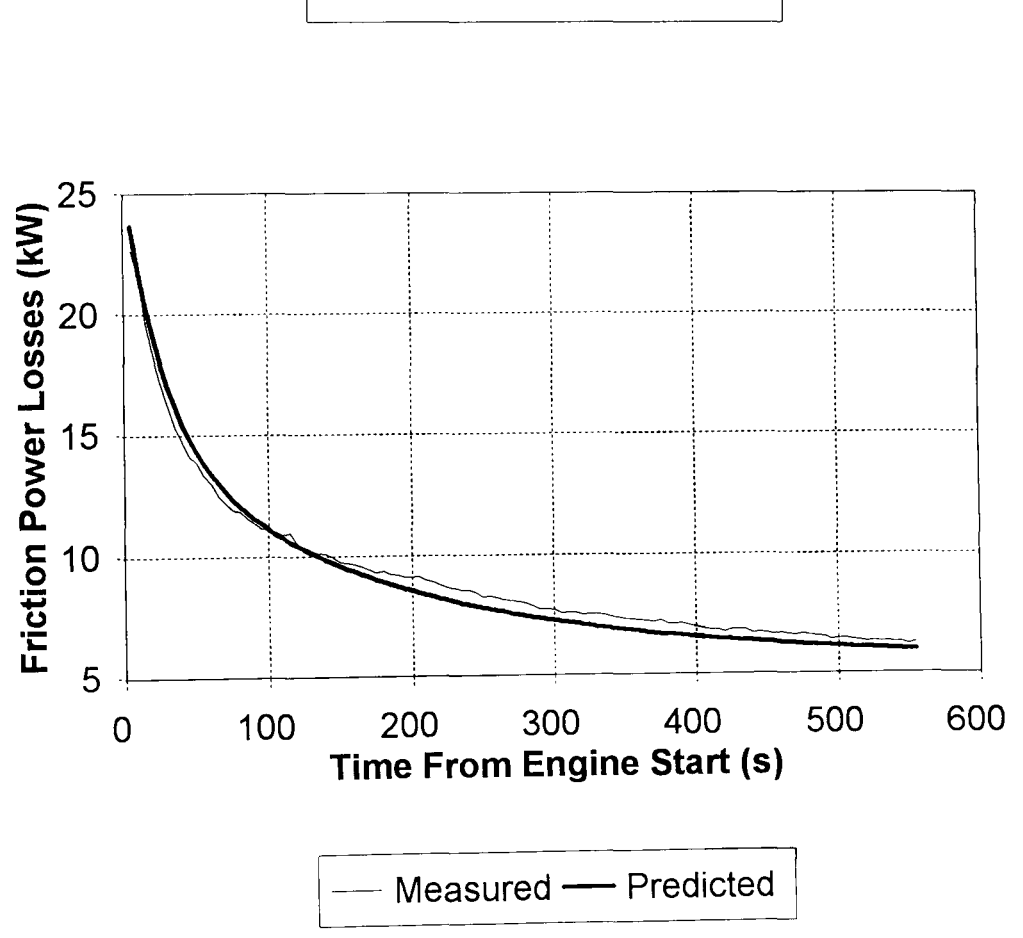

Figure 6.5
Measured and PROMETS predicted friction power losses with 20°C start (upper) and -10°C start (lower) for 2 litre DOHC 8V.
PROMETS predictions modified with exponential function (6.12).

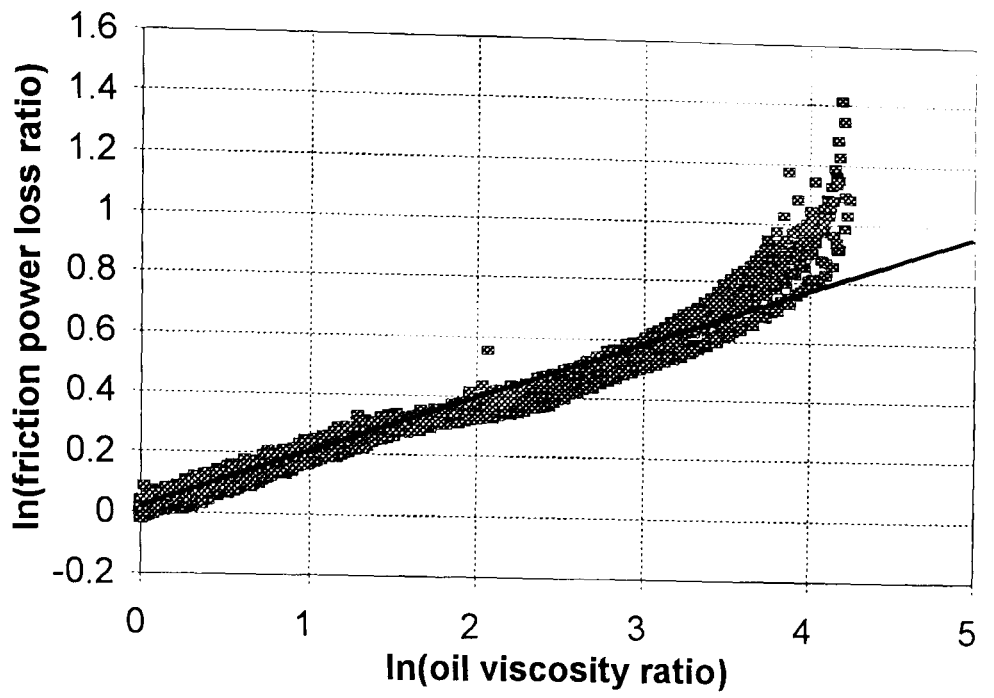

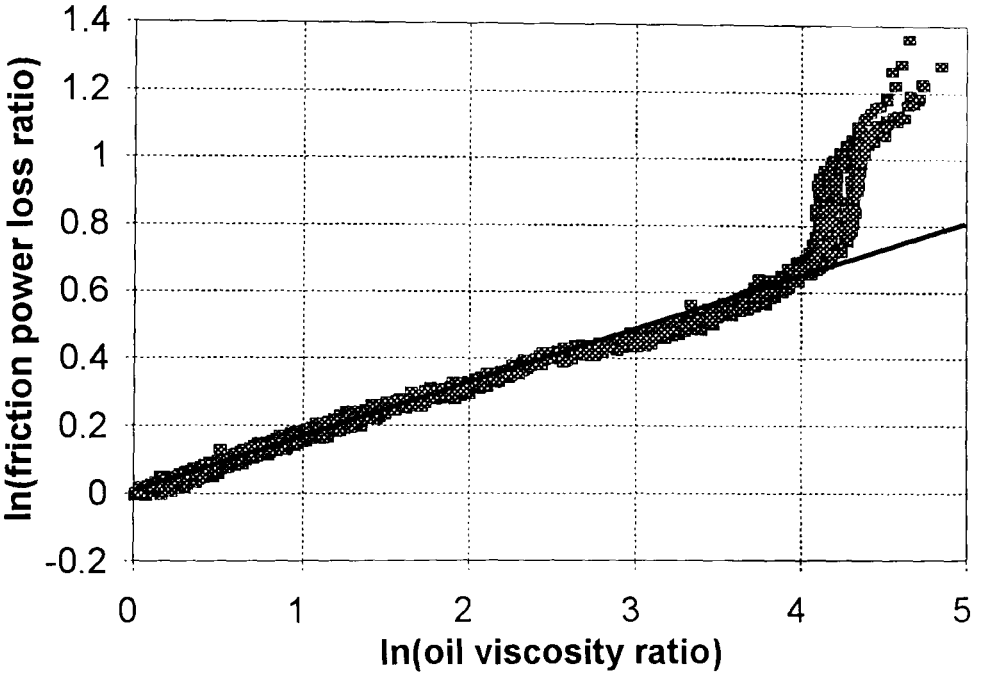

Figure 6.6
Measured friction power losses plotted against oil viscosity ratio for 2 litre DOHC 8V engine with range of engine speeds and loads and -10°C start temperature with:
a) (upper) SAE 10W/30 oil
b) (lower) SAE 20W/50 oil

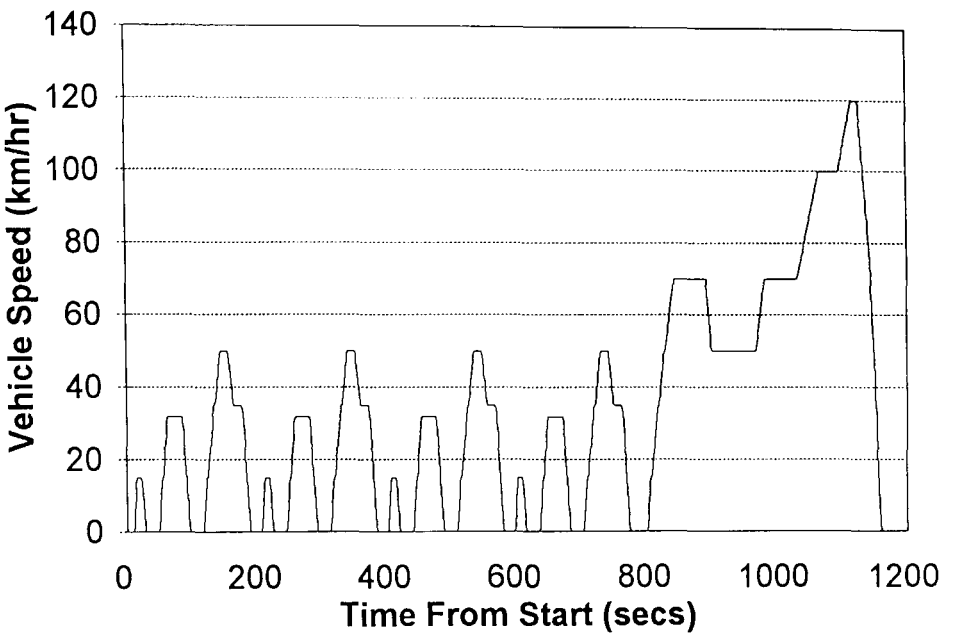

Drive Cycle Breakdown

Time(secs)	Phase
0-195	Elementary Urban Cycle No.1
196-390	Elementary Urban Cycle No.2
391-585	Elementary Urban Cycle No.3
586-780	Elementary Urban Cycle No.4
781-1180	Extra-Urban Drive Cycle

Figure 7.1
NEDC or ECE+EUDC vehicle speed vs time description

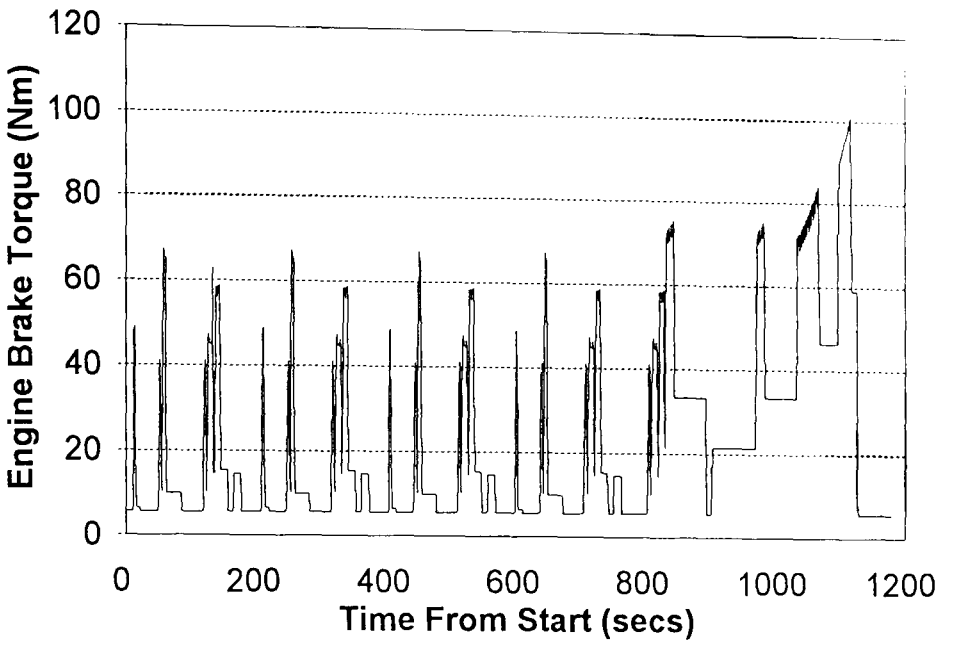

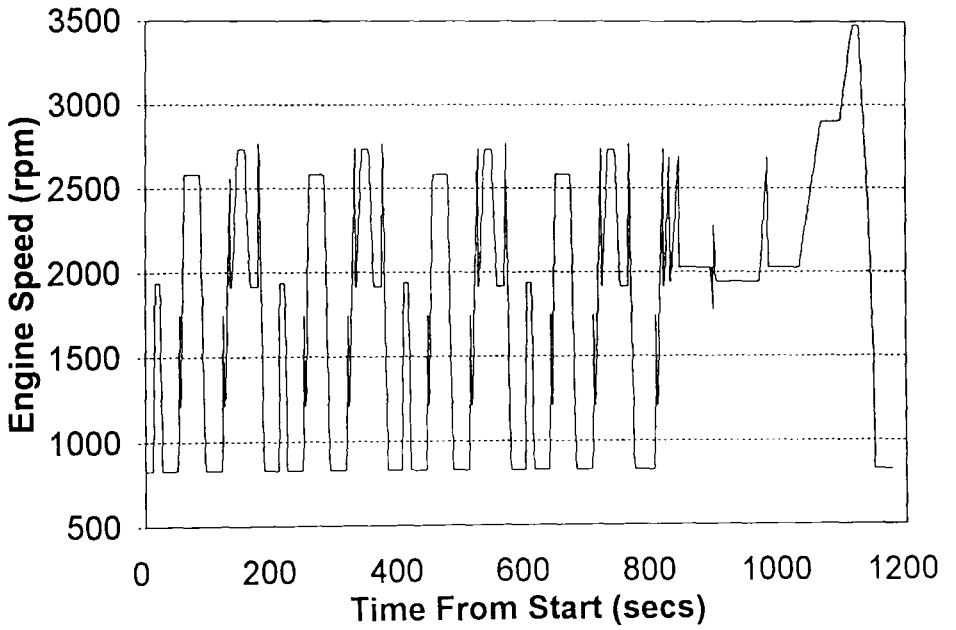

Figure 7.2
Engine brake load (upper) and speed (lower) variations over the ECE+EUDC drive cycle for 1.8 litre Zetec engine in a Mondeo.

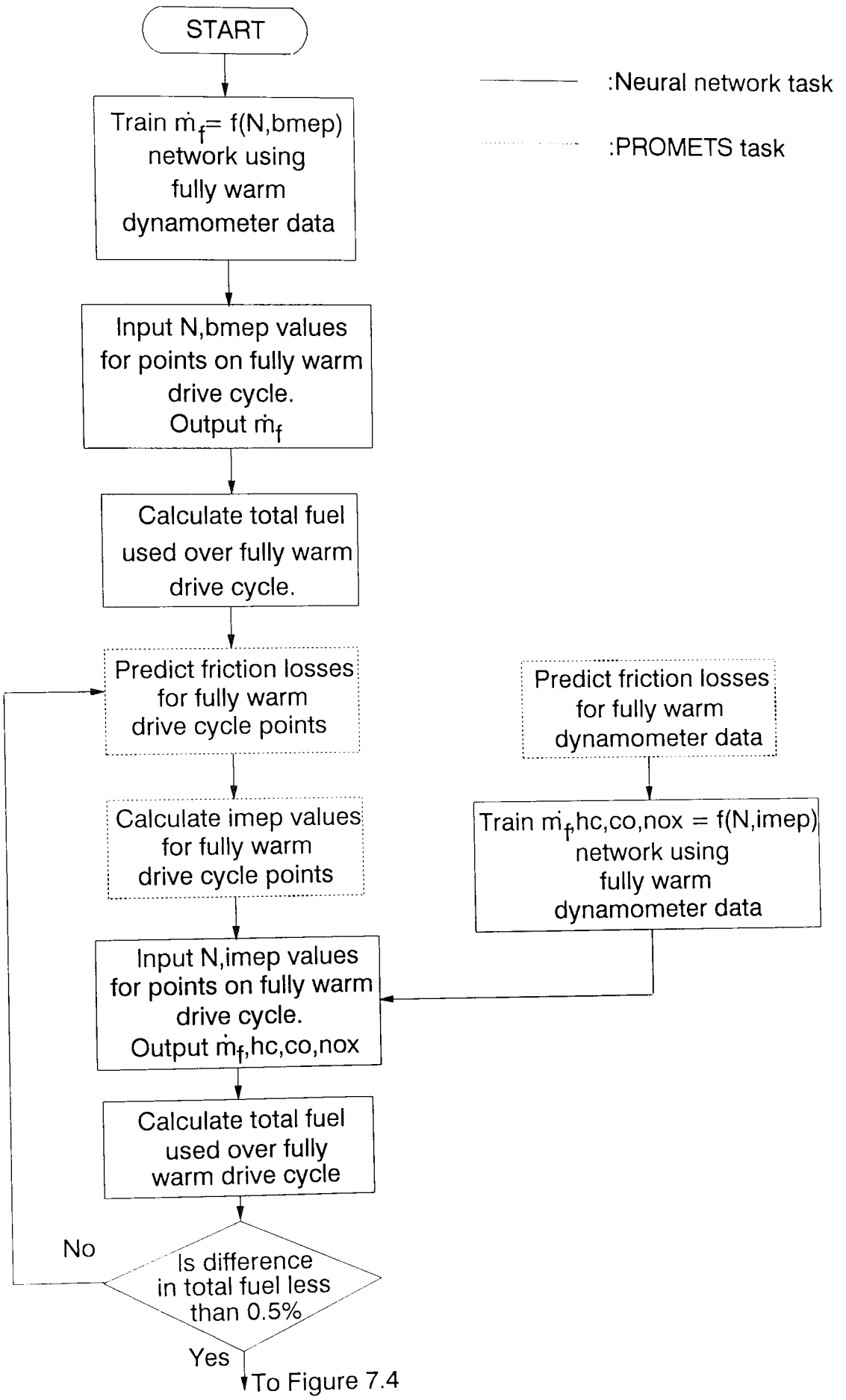

Figure 7.3
Flow chart for fully-warm drive cycle total fuel consumption prediction.

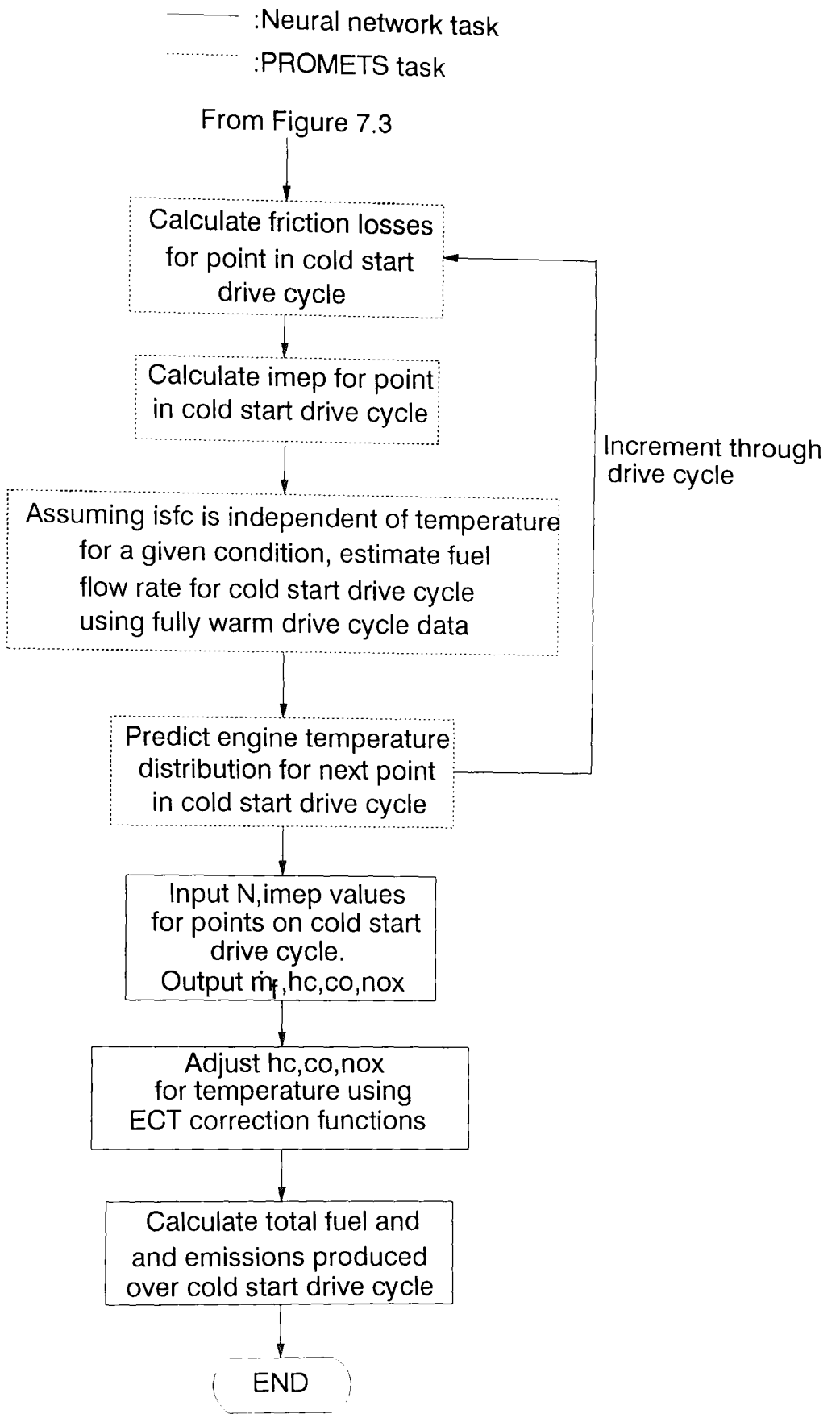

Figure 7.4
Flow chart for cold-start drive cycle total fuel consumption and emissions prediction.

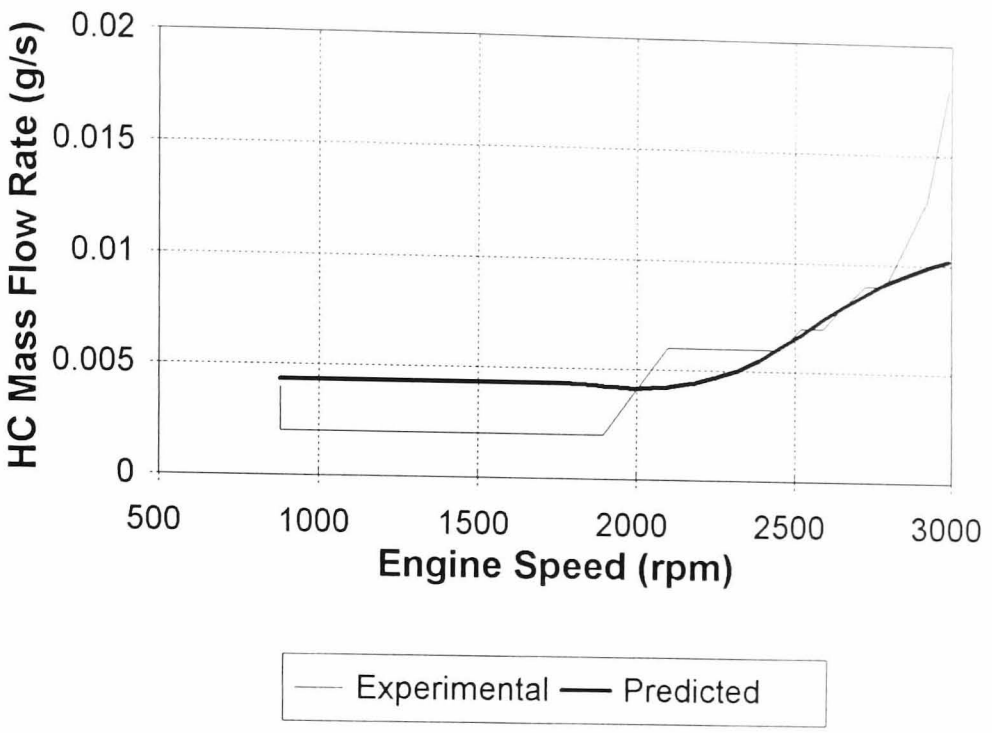

Figure 7.5
Experimental and predicted HC mass flow rates during final deceleration of ECE+EUDC drive cycle for 1.8 litre Zetec engine in a Mondeo.

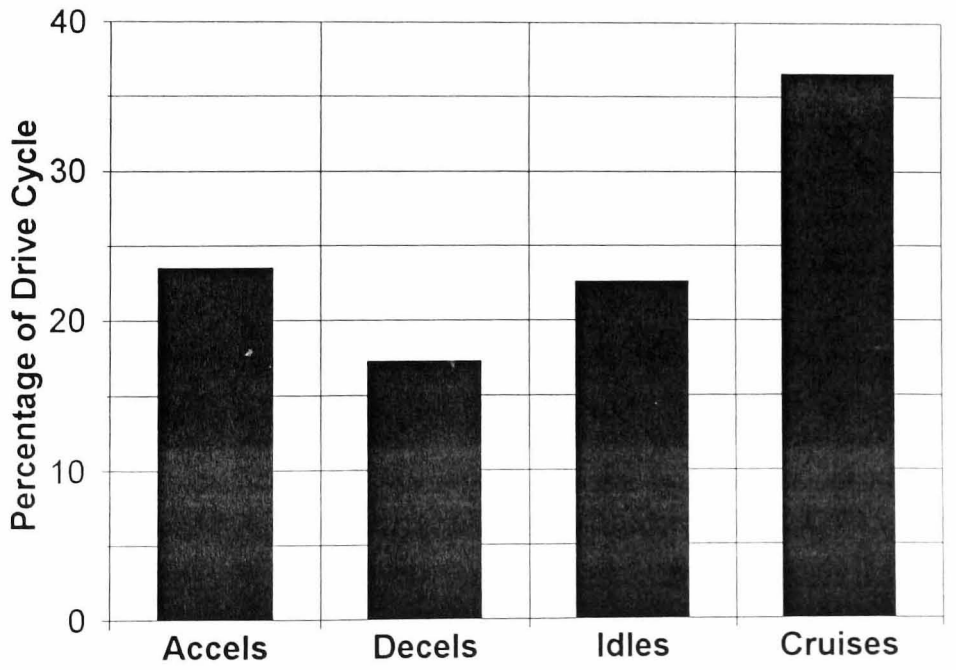

Figure 7.6
Breakdown of ECE+EUDC drive cycle into periods of acceleration, deceleration, idle and cruise.

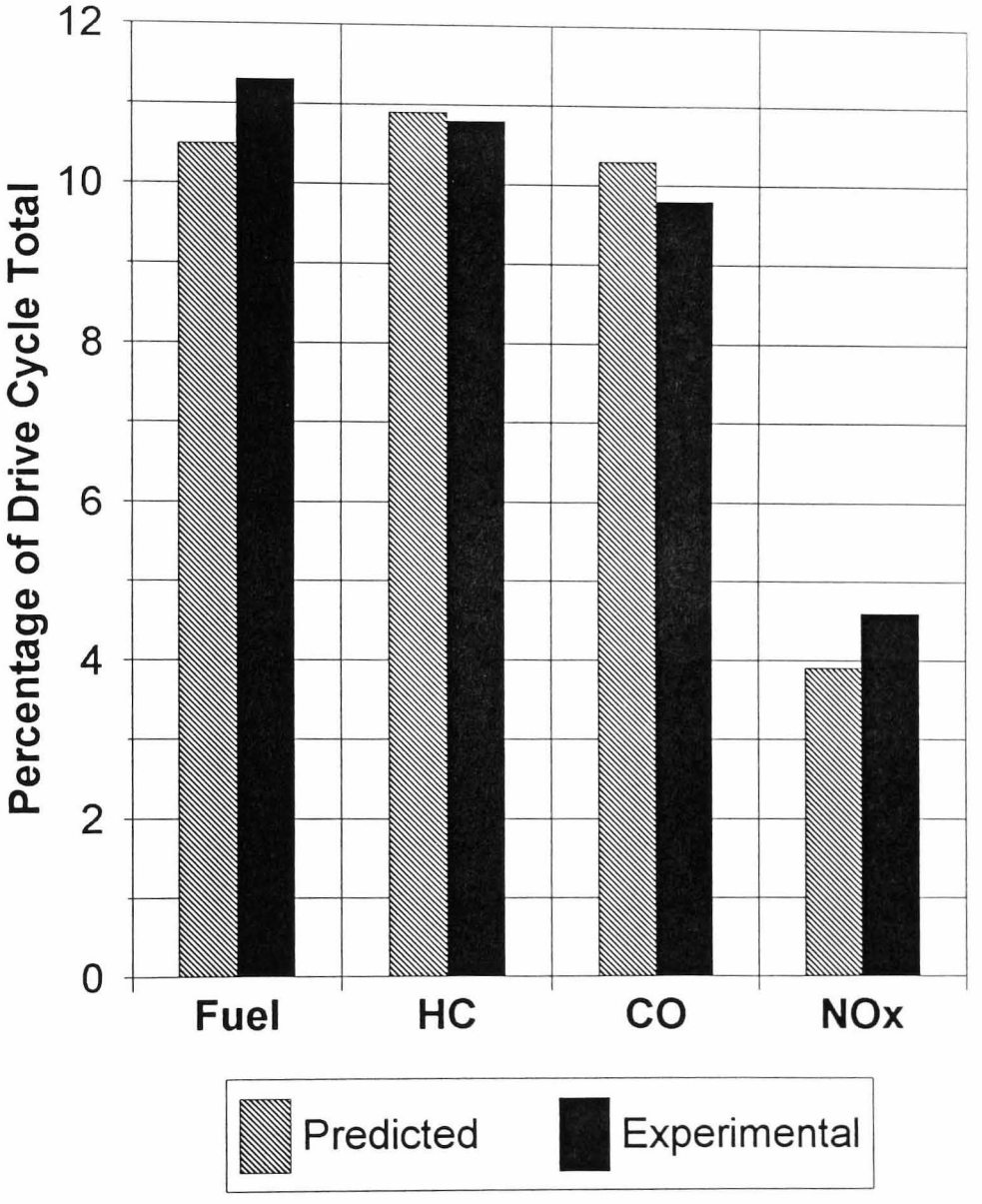

Figure 7.7
Comparison of measured and predicted fuel and emissions totals for ECE+EUDC drive cycle during periods of deceleration for 1.8 litre Zetec engine in a Mondeo.

a)

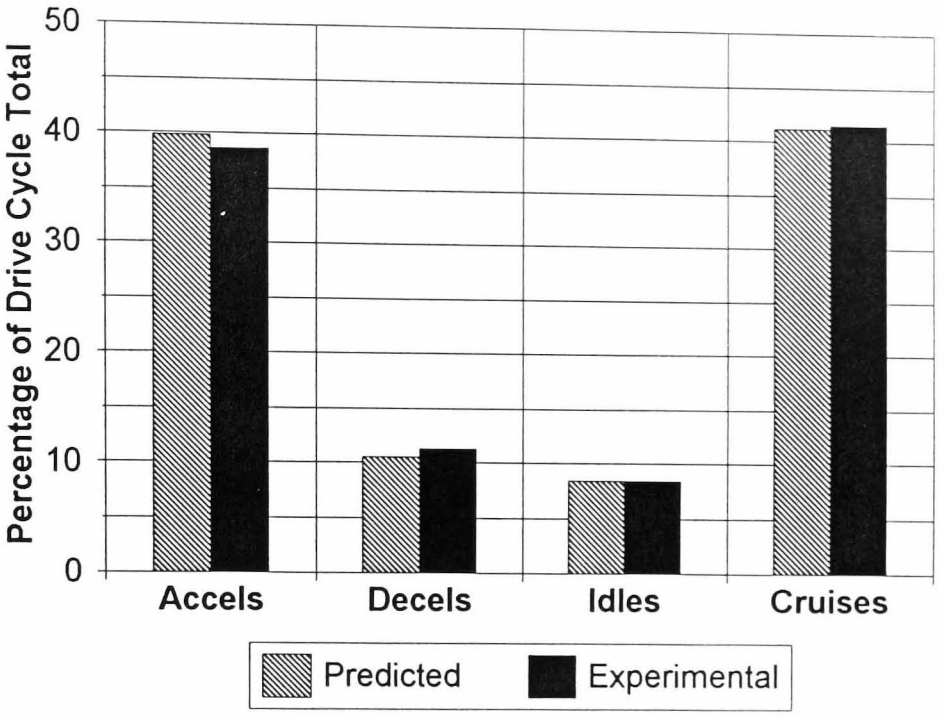

b)

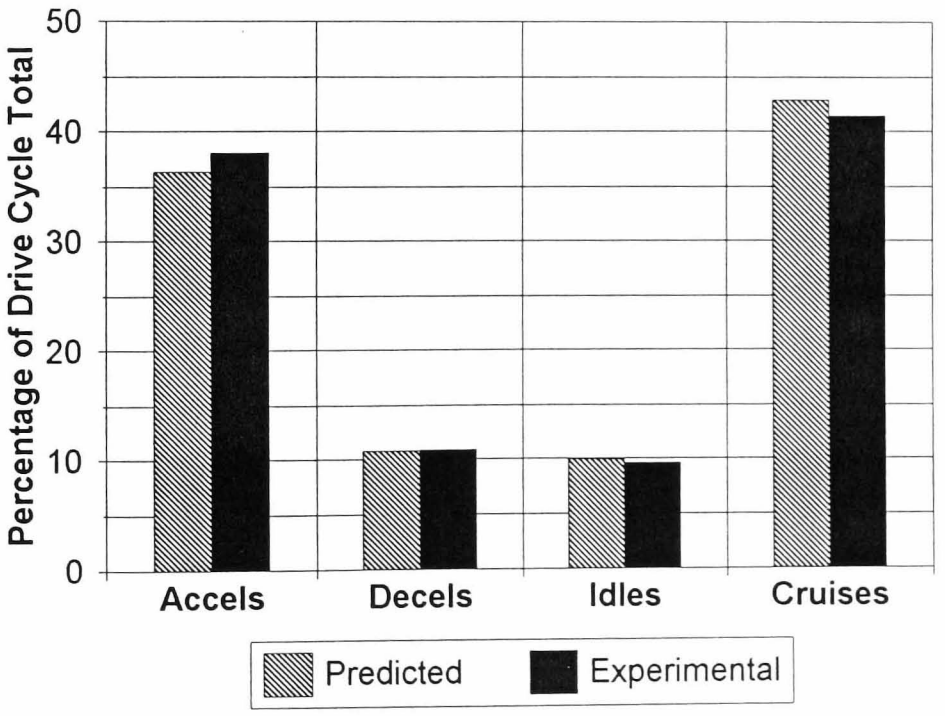

Figure 7.8
Comparison of measured and predicted flow rates during ECE+EUDC drive cycle for periods of acceleration, deceleration, idle and cruise for 1.8 litre Zetec engine in a Mondeo.
a) Fuel mass flow rates.
b) HC mass flow rates.

a)

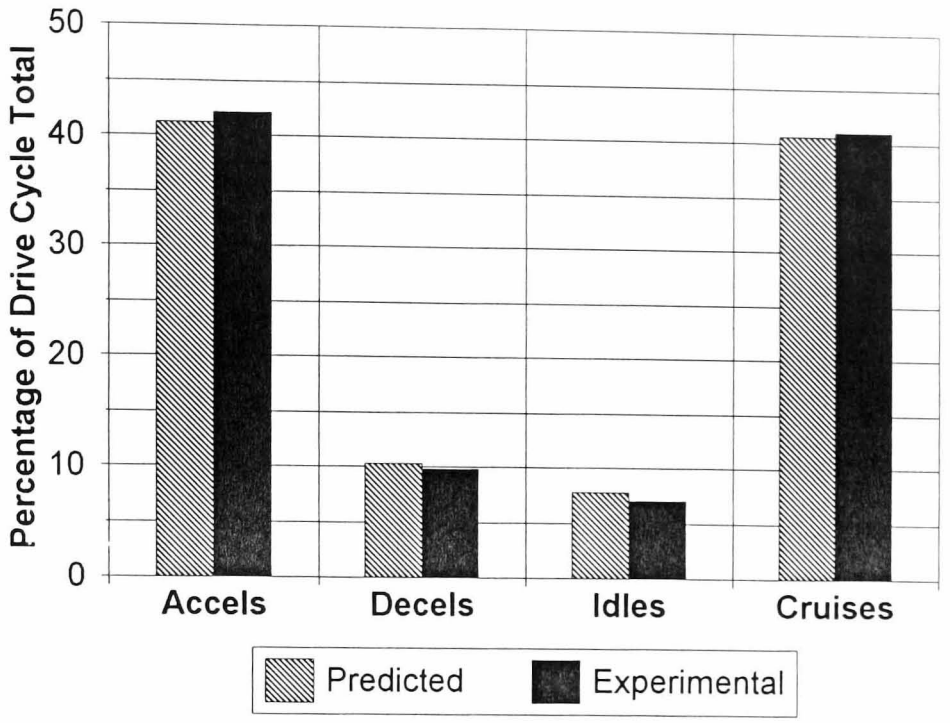

b)

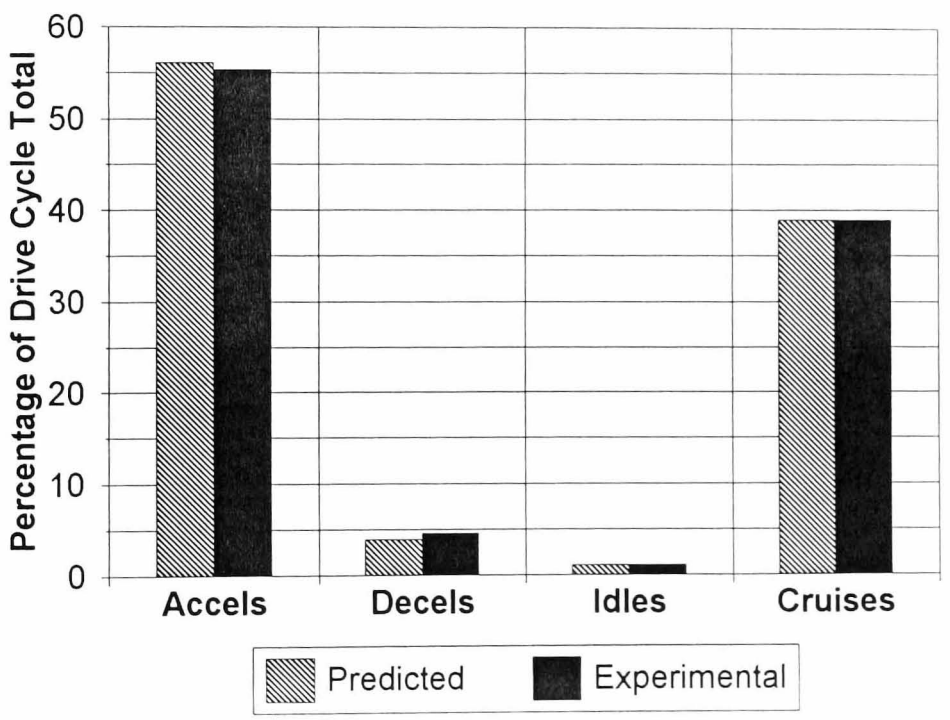

Figure 7.9
Comparison of measured and predicted flow rates during ECE+EUDC drive cycle for periods of acceleration, deceleration, idle and cruise for 1.8 litre Zetec engine in a Mondeo.
a) CO mass flow rates.
b) NOx mass flow rates.

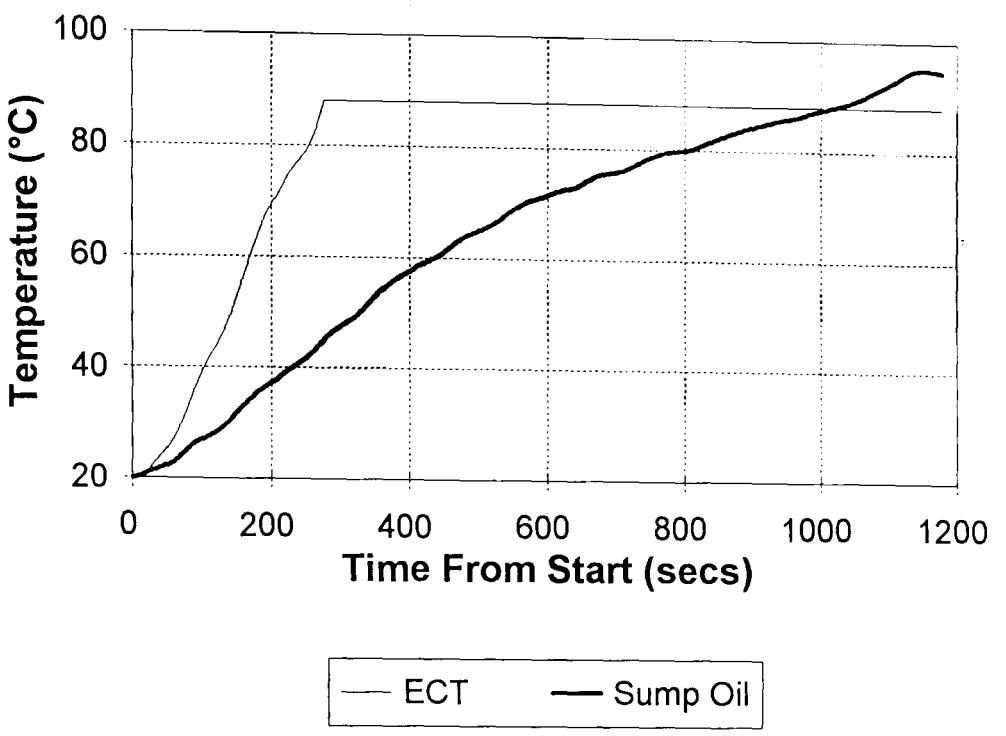

Figure 8.1
ECT and oil temperature warm-up profiles for ECE+EUDC drive cycle with 1.8 litre Zetec engine in a Mondeo and 20°C start.

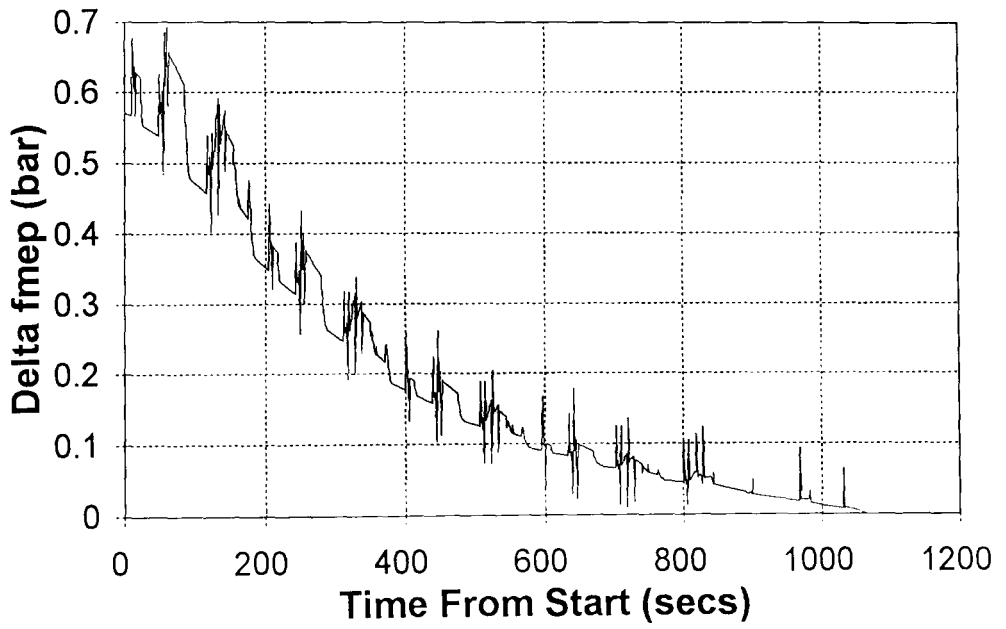

Figure 8.2
Difference between fmep during cold-started drive cycle and corresponding fmep for fully-warm drive cycle (delta fmep) for ECE+EUDC drive cycle with 1.8 litre Zetec engine in a Mondeo.

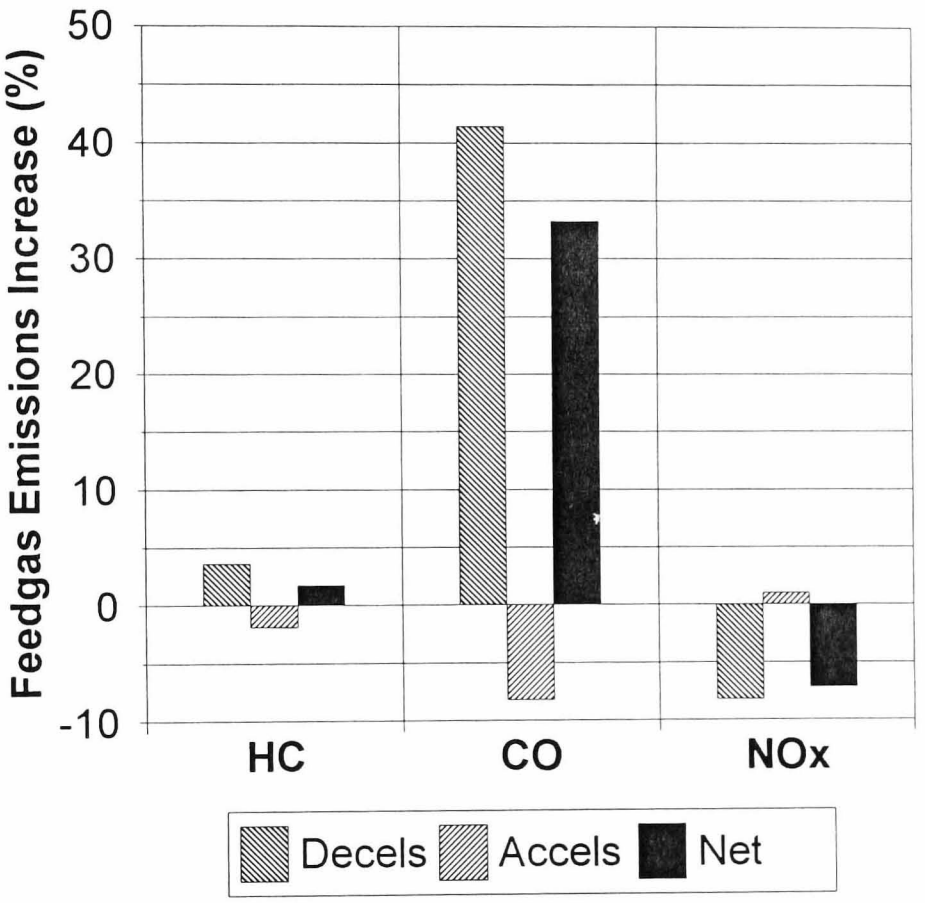

Figure 8.3
Increase in feedgas emissions due to imposed AFR excursions at transient operating points of ECE+EUDC drive cycle for 1.8 litre Zetec engine in a Mondeo.

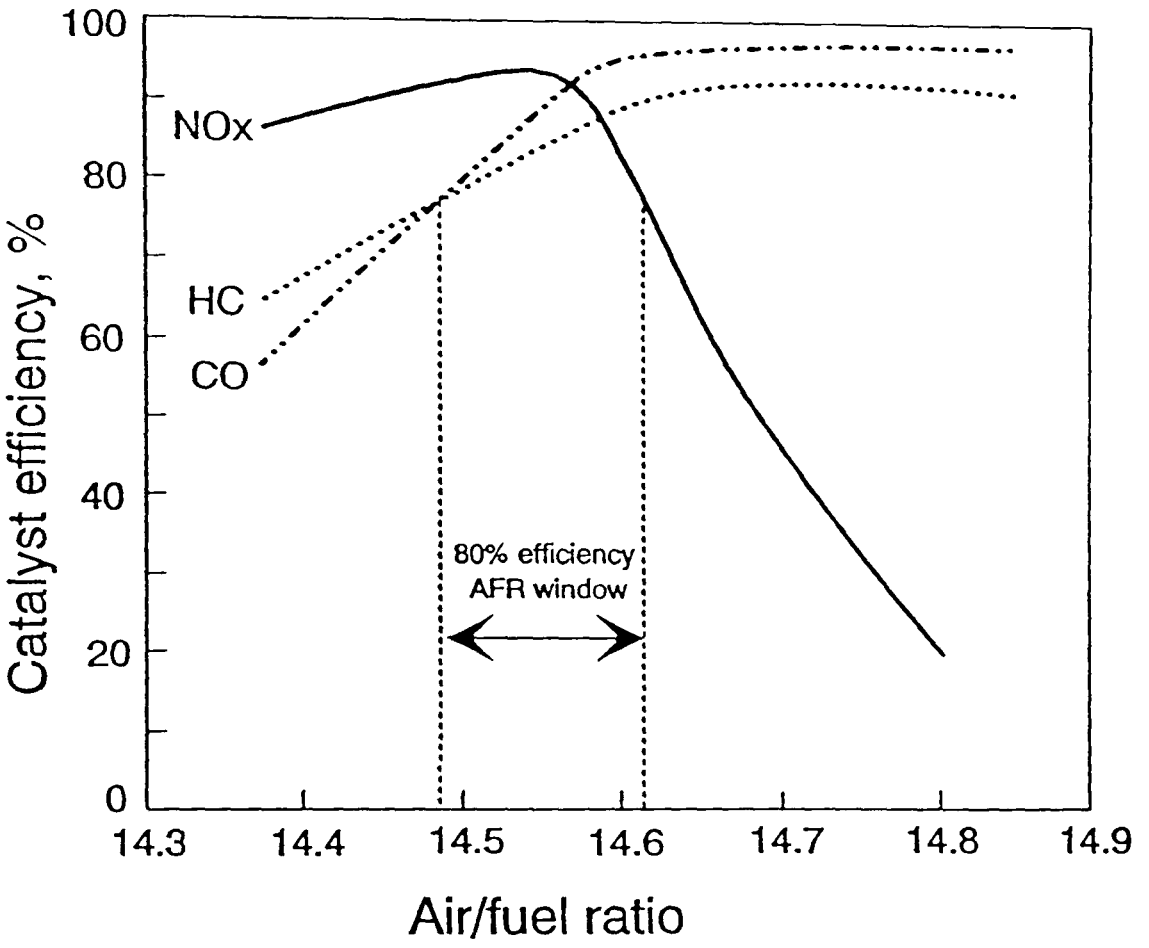

Figure 8.4
Effect of AFR on three-way catalytic convertor efficiency [8.3].

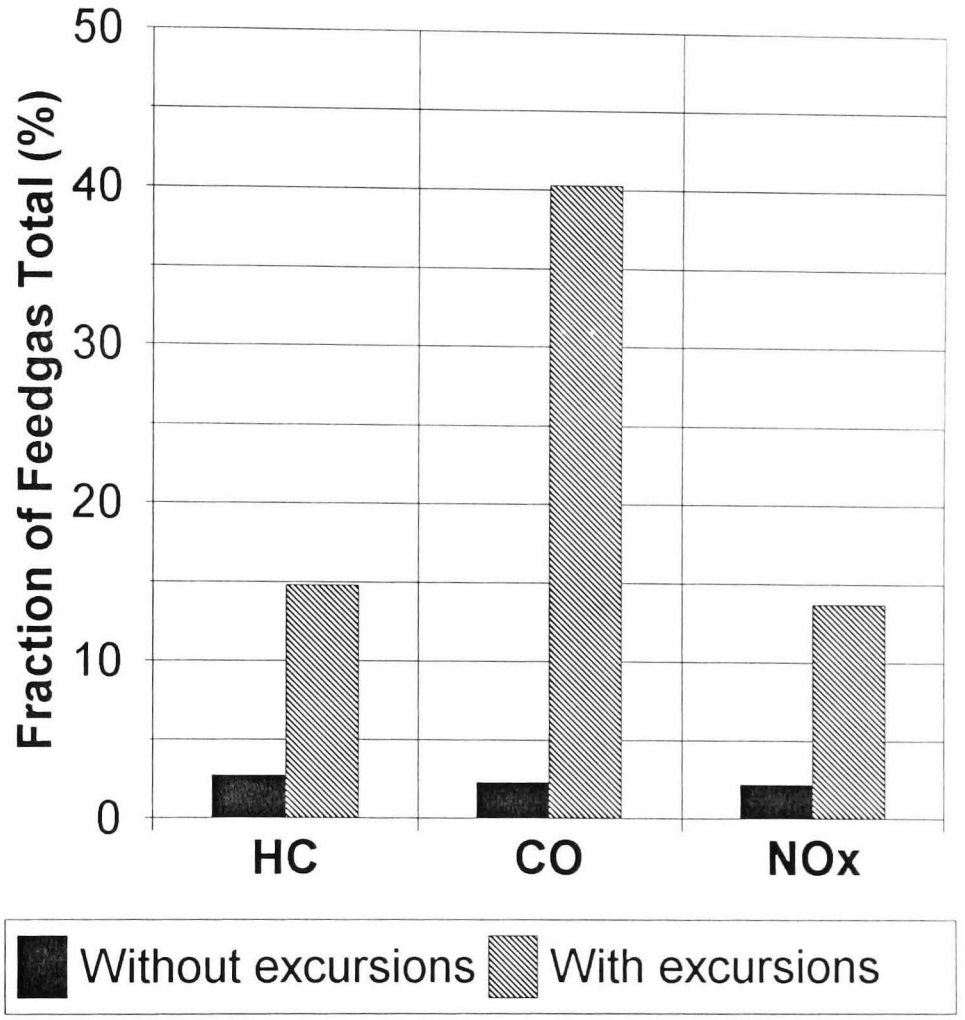

Figure 8.5
Effect of transient AFR excursions on total tail-pipe emissions as a fraction of feedgas emissions for ECE+EUDC drive cycle with 1.8 litre Zetec engine in a Mondeo.

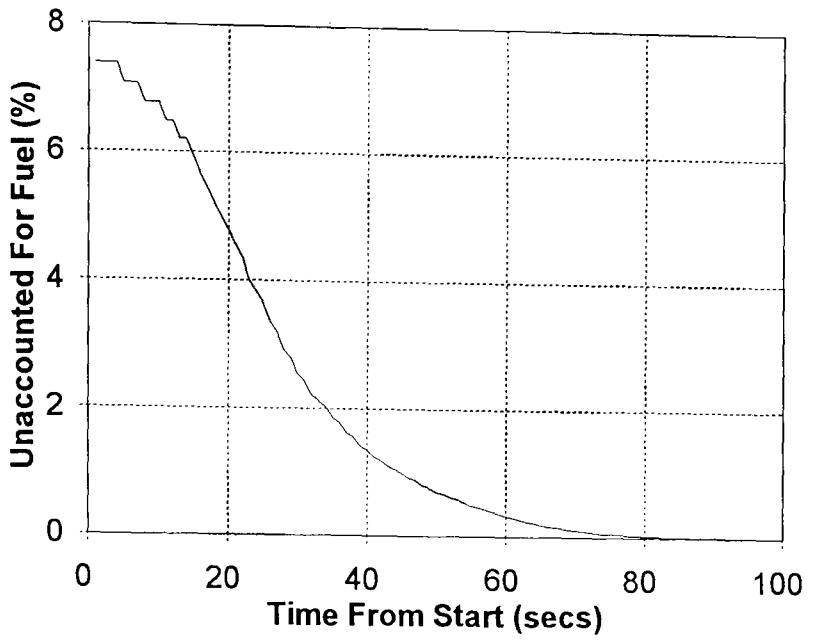

Figure 8.6
Predicted 'unaccounted for' fuel percentage for a 1.8 litre Zetec engine cold-started at 20°C and allowed to idle.

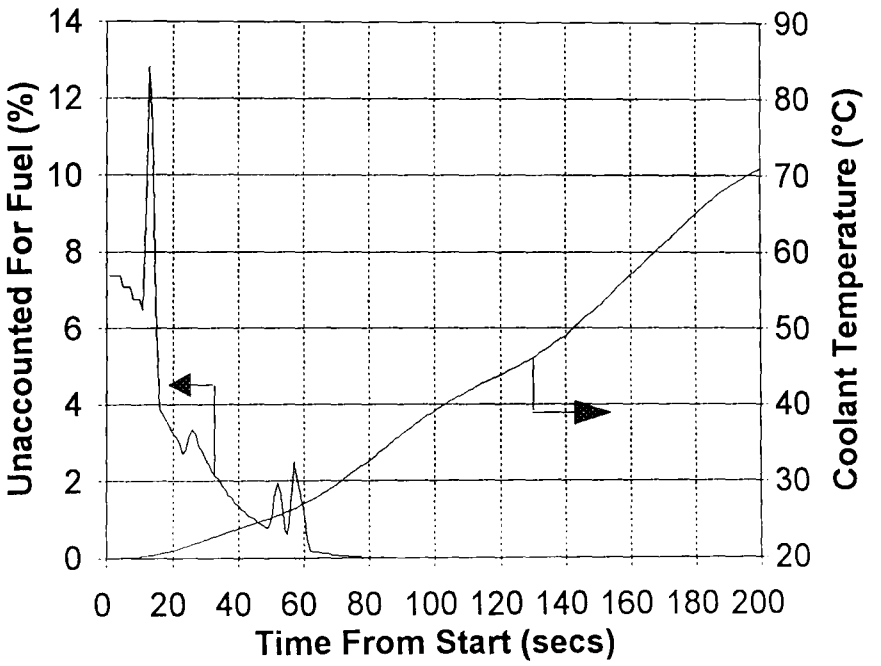

Figure 8.7
Predicted 'unaccounted for' fuel percentage for ECE+EUDC drive cycle with 20°C start and without 40 second idle conditioning period for 1.8 litre Zetec engine in a Mondeo.

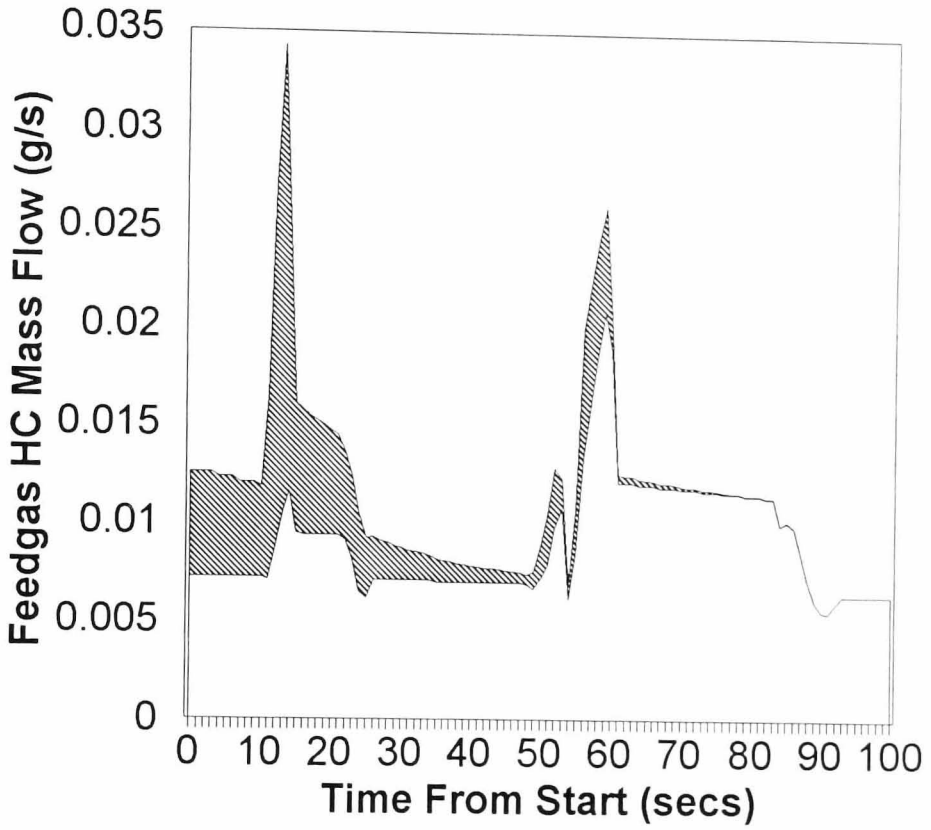

Figure 8.8

Predicted HC mass flow rate error due to 'unaccounted for' fuel (shaded) for ECE+EUDC drive cycle with 20°C start and without 40 second conditioning period for 1.8 litre Zetec engine in a Mondeo.

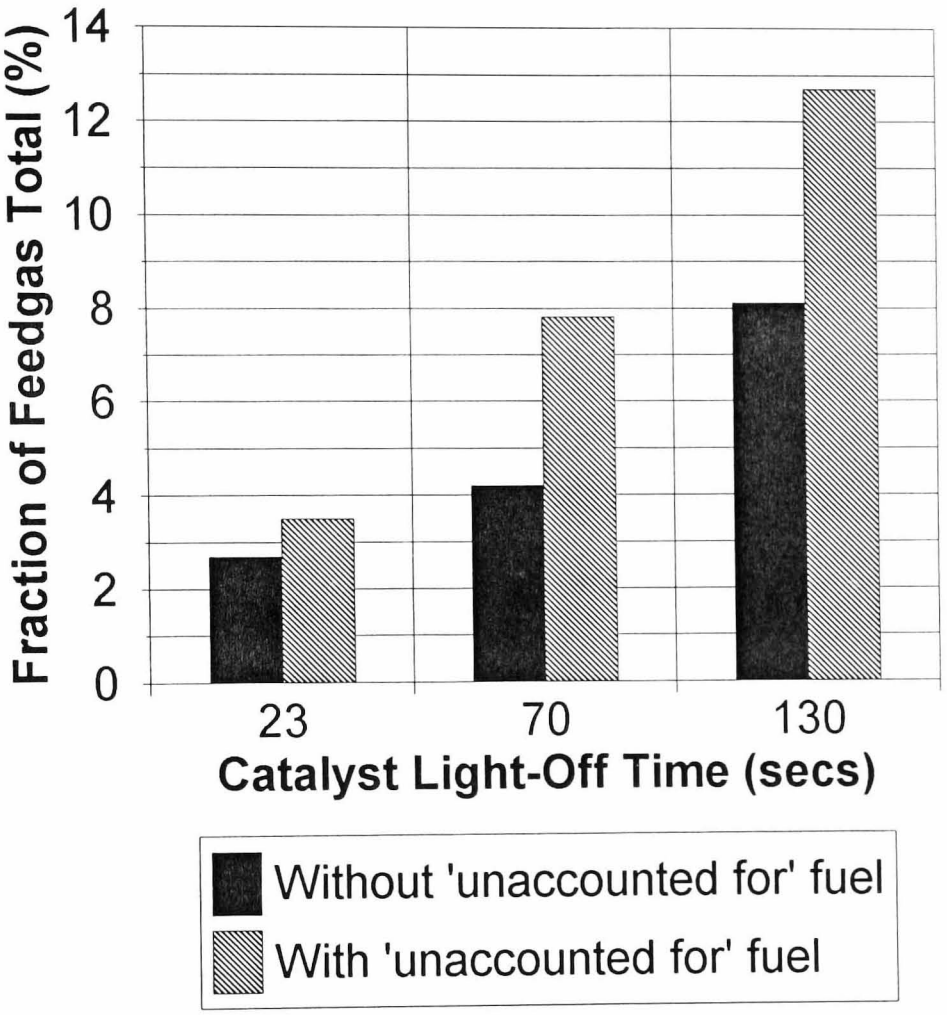

Figure 8.9
Effect of 'unaccounted for' fuel due to cold-start transient effects on tail-pipe emissions (as a percentage of feedgas totals) for ECE+EUDC drive cycle with 1.8 litre Zetec engine in a Mondeo.

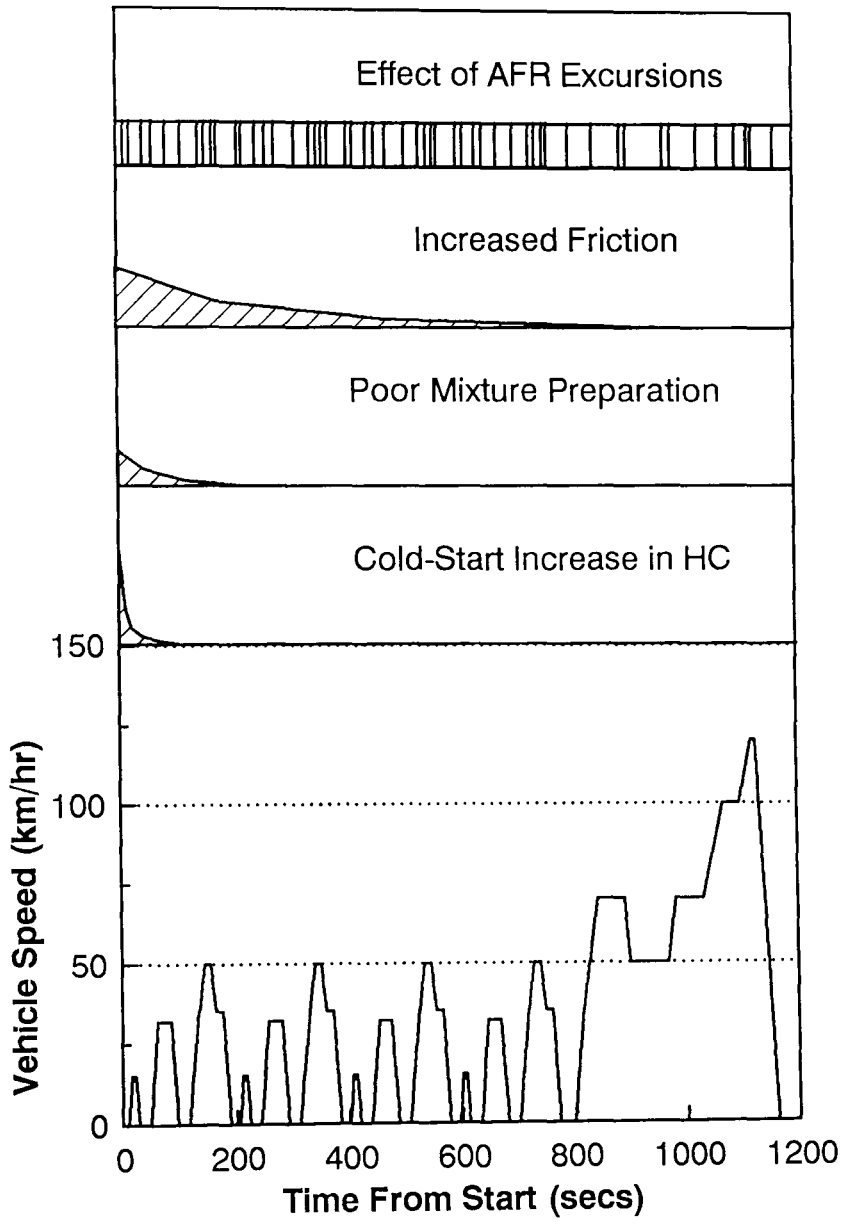

Figure 8.10
Schematic diagram showing the duration of the effects causing increased fuel consumption and feedgas emissions due to cold-starting for ECE+EUDC drive cycle with 1.8 litre Zetec engine in a Mondeo. Shaded areas indicate the relative magnitude and duration of effects.

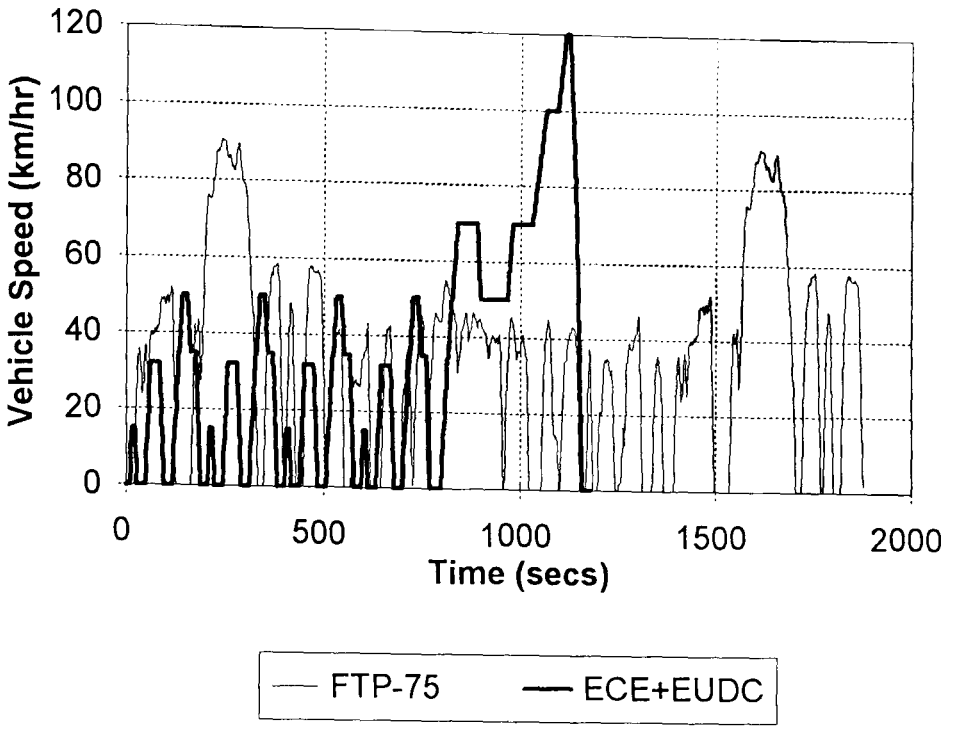

Figure 9.1
Defined second-by-second vehicle speed profiles for FTP-75 and ECE+EUDC drive cycles.

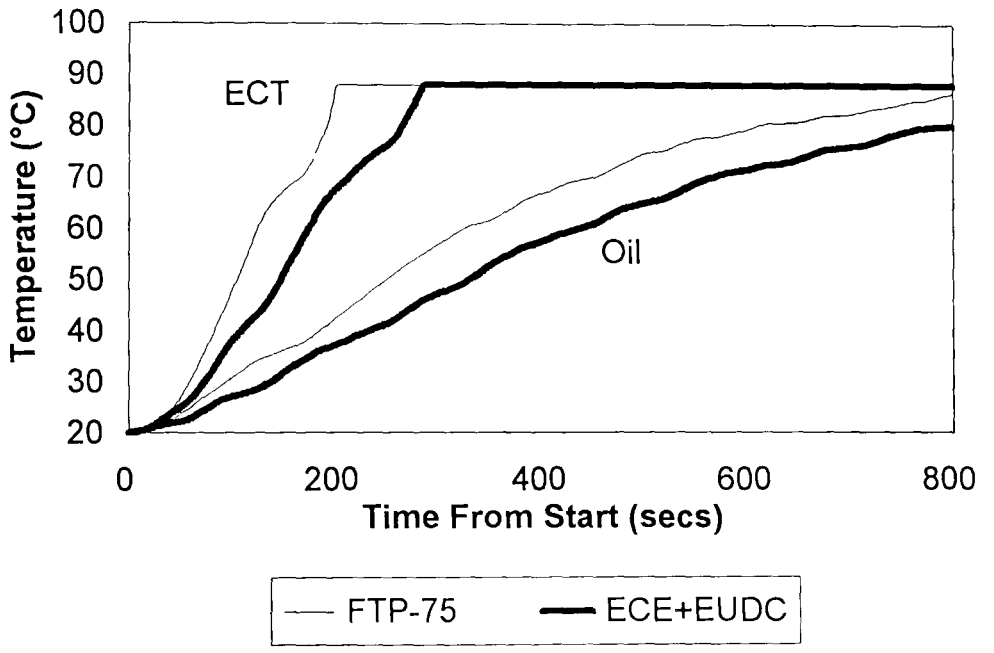

Figure 9.2
ECT and oil temperature warm-up profiles for first 800 seconds of FTP-75 and ECE+EUDC drive cycles with 20°C start temperature for 1.8 litre Zetec engine in a Mondeo.

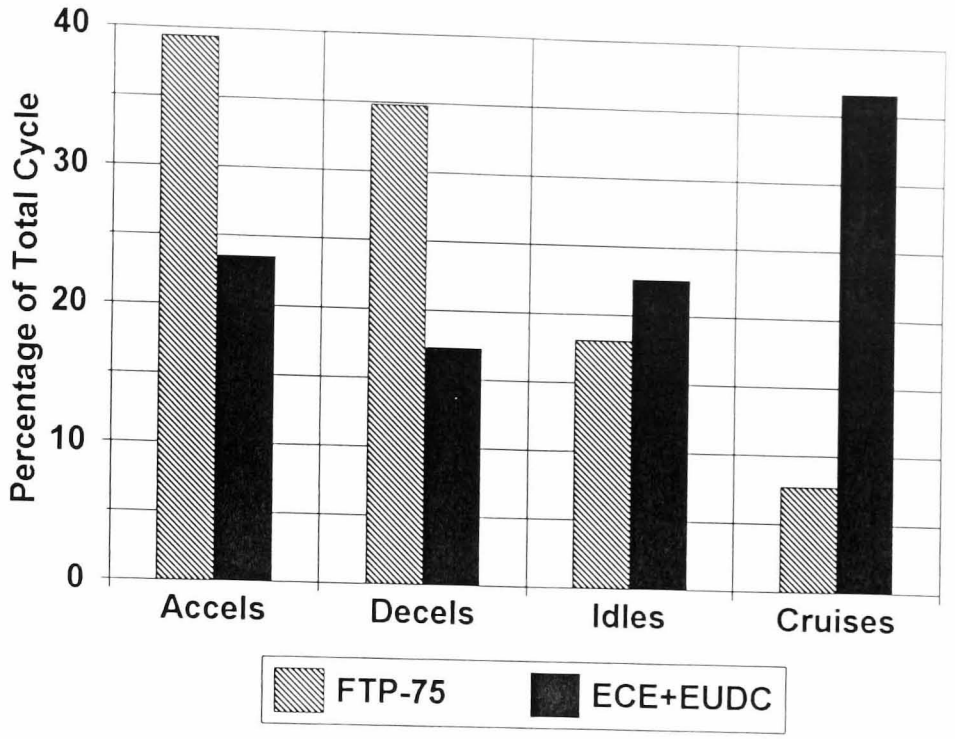

Figure 9.3
Percentage breakdown of FTP-75 and ECE+EUDC drive cycles into accel, decel, idle and cruise conditions.

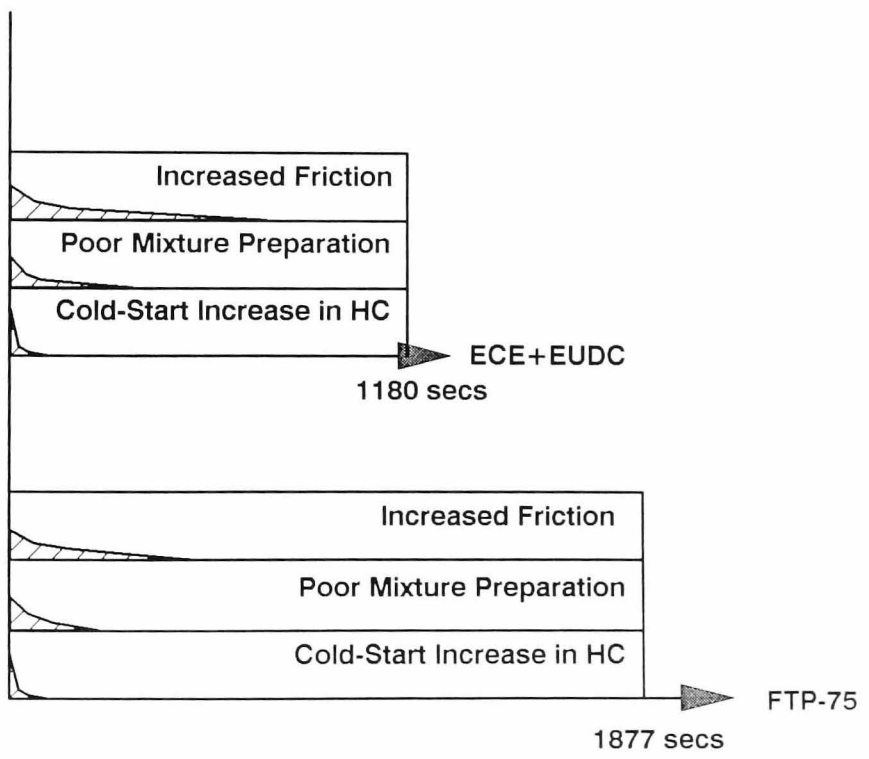

Figure 9.4
Schematic diagram showing duration of the effects causing increased fuel consumption and emissions due to cold-starting for both the FTP-75 and ECE+EUDC drive cycles.

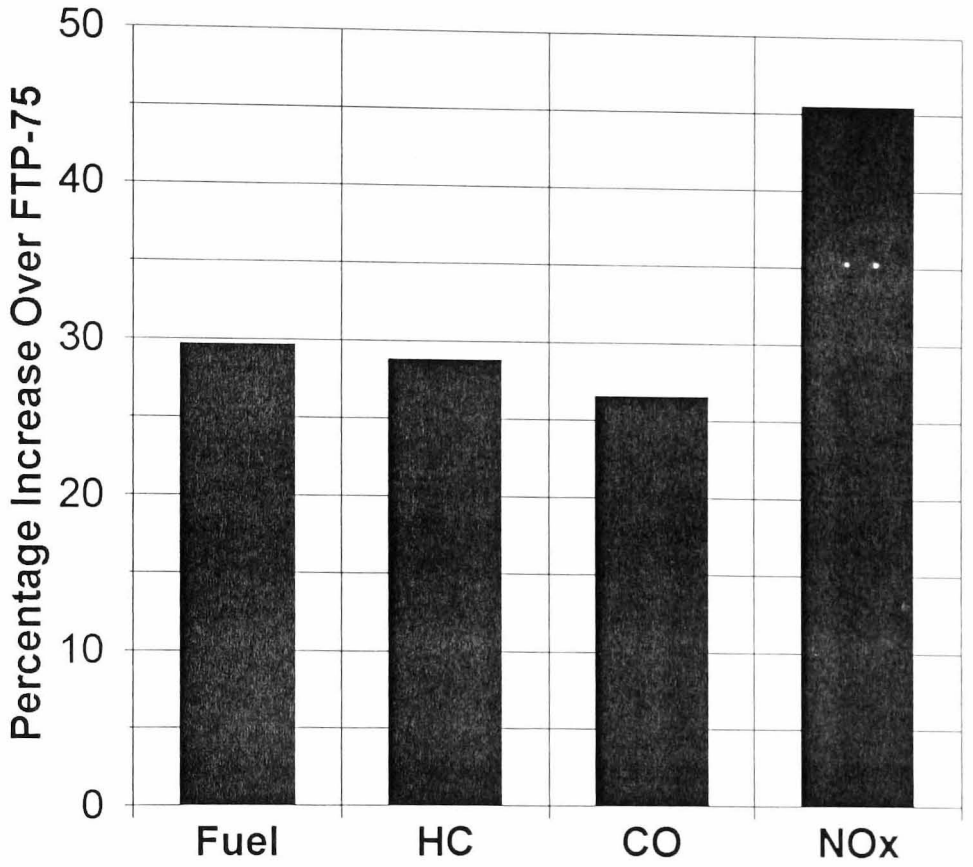

Figure 9.5
Percentage increase in fuel used and emissions produced per km for ECE+EUDC drive cycle compared to FTP-75 cycle.

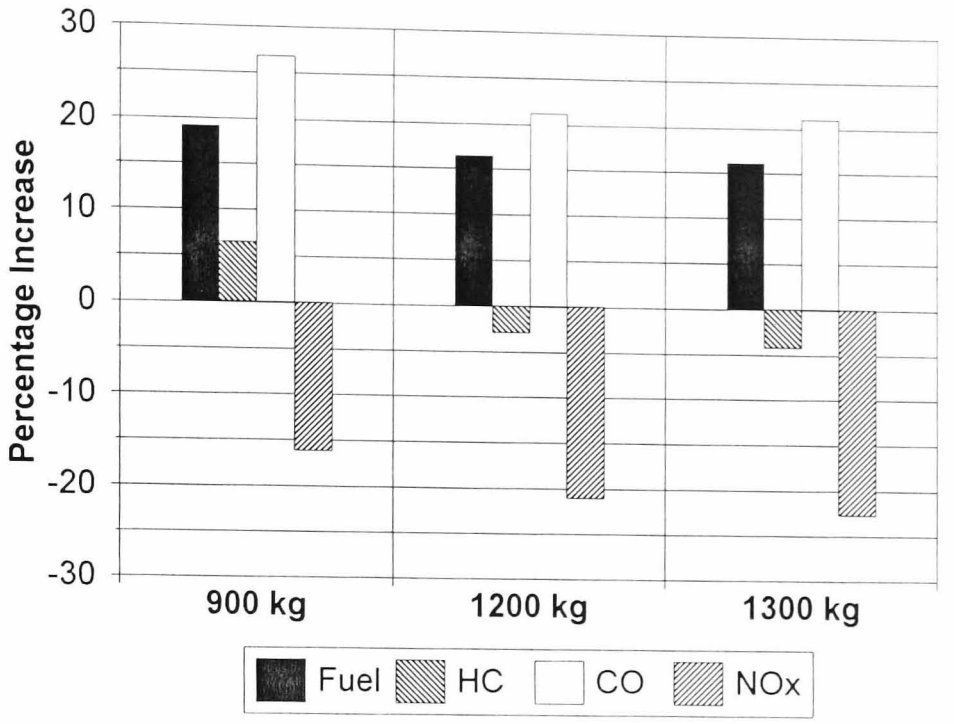

Figure 9.6
Percentage increase in total fuel consumption and feedgas emissions over ECE+EUDC drive cycle due to increasing engine size from 1.25 litres to 1.8 litres for three vehicle masses.

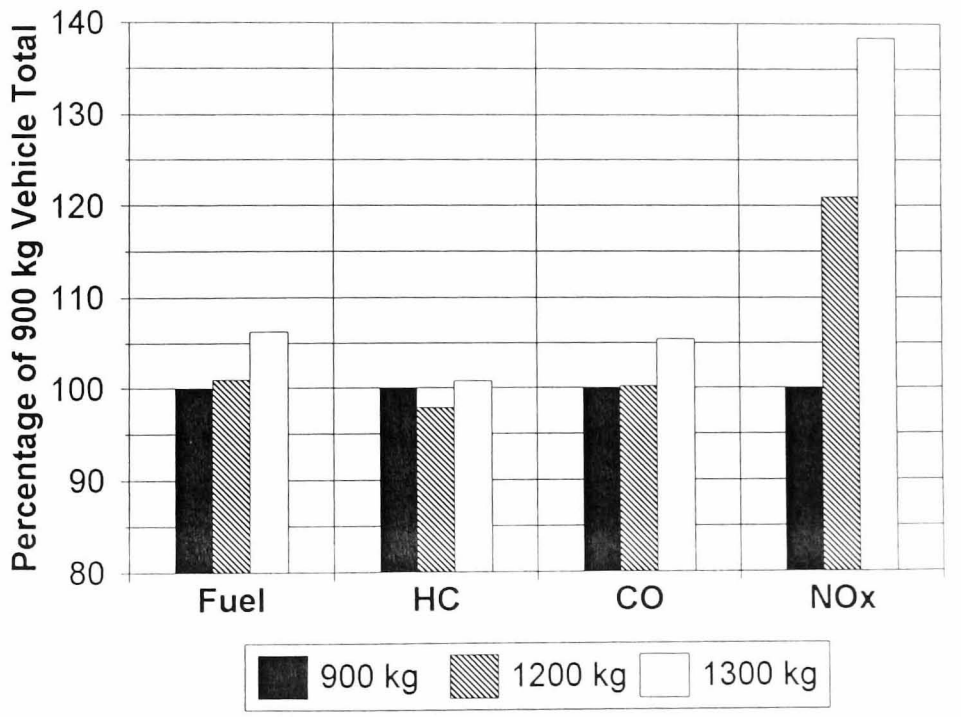

Figure 9.7
Changes in total fuel consumption and feedgas emissions over ECE+EUDC drive cycle due to increasing vehicle size relative to a 900 kg vehicle with the same 1.8 litre engine.

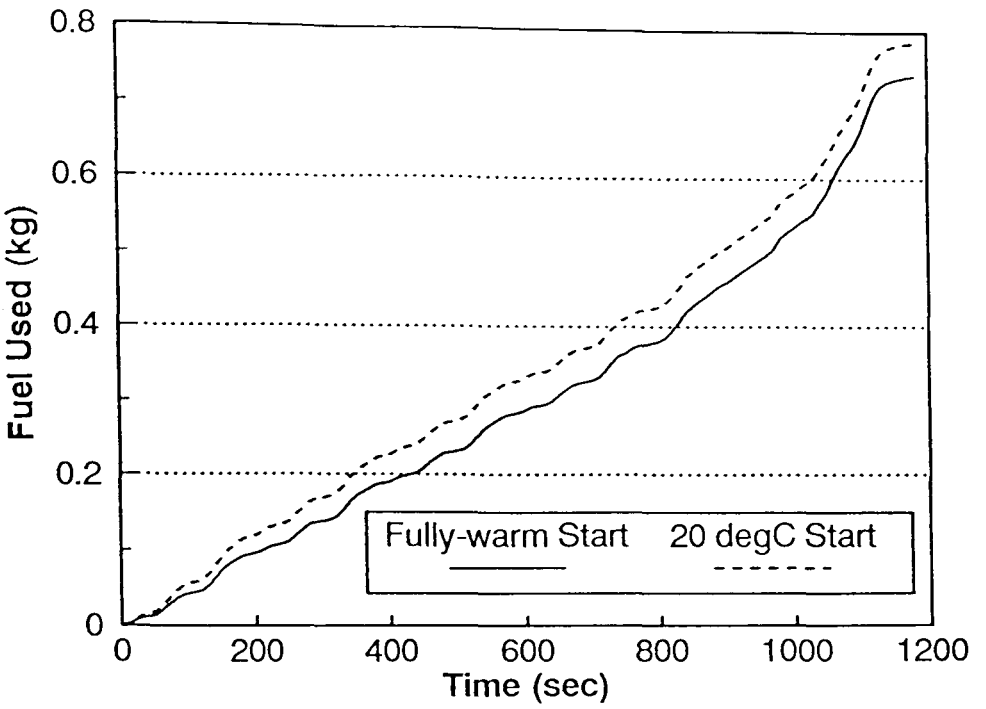

Figure 9.8
Cumulative fuel used over the ECE+EUDC drive cycle for cold-start (20°C) and fully-warm engine initial conditions for 2 litre engine in a 1200 kg vehicle.

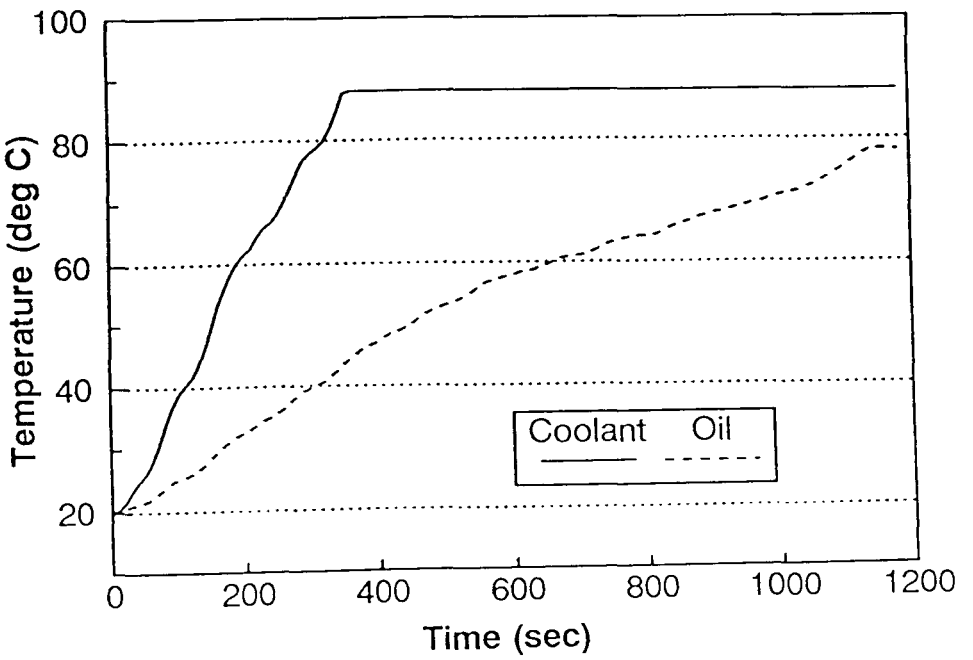

Figure 9.9
Oil and coolant predicted warm-up rate for ECE+EUDC drive cycle with 20°C start/soak temperature for 2 litre engine in a 1200 kg vehicle.

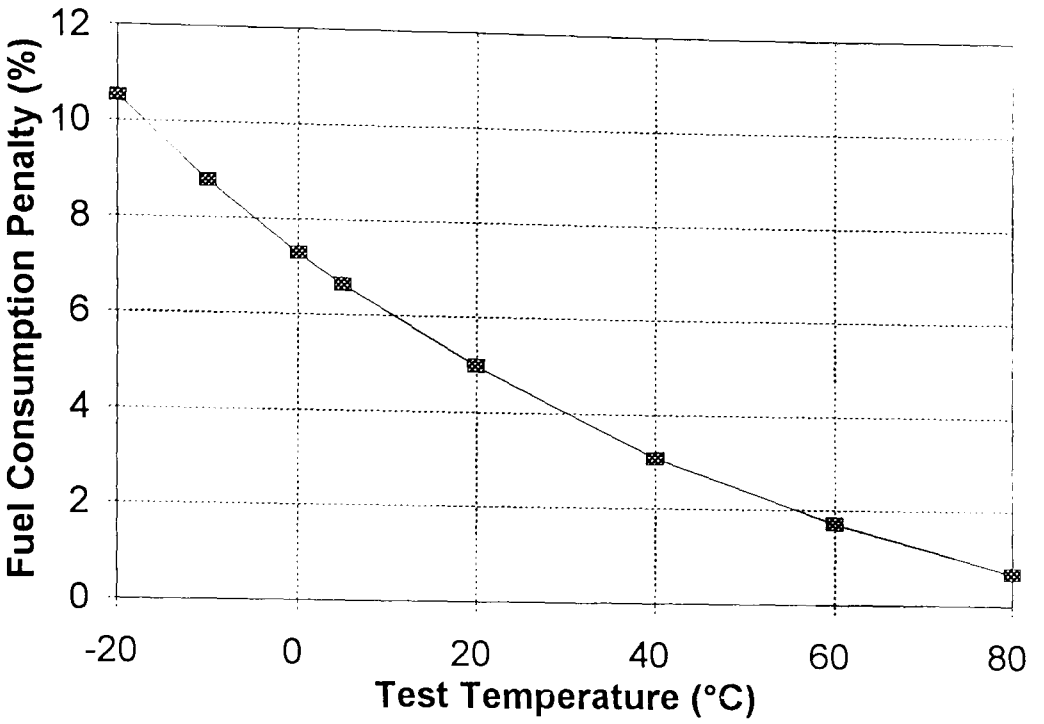

Figure 9.10
Fuel consumption penalty (percentage increase compared to value for fully-warm initial engine state) as a function of test temperature for 2 litre engine in a 1200 kg vehicle.

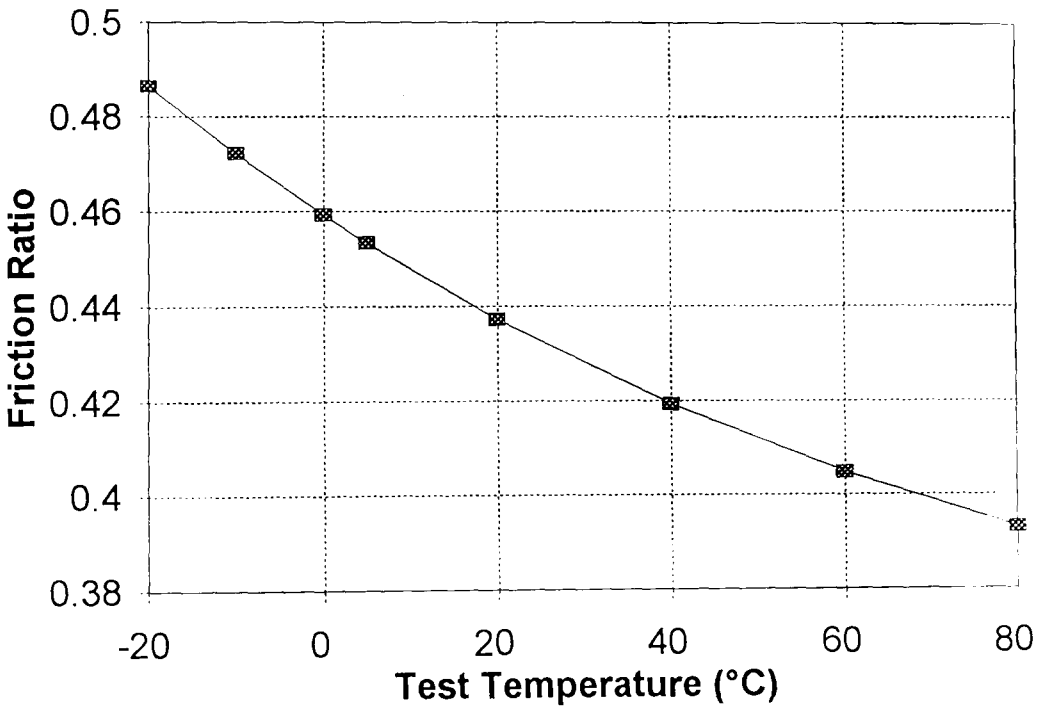

Figure 9.11
Friction ratio (defined as total friction work divided by the total indicated work summed over the drive cycle) as a function of test temperature for 2 litre engine in a 1200 kg vehicle.

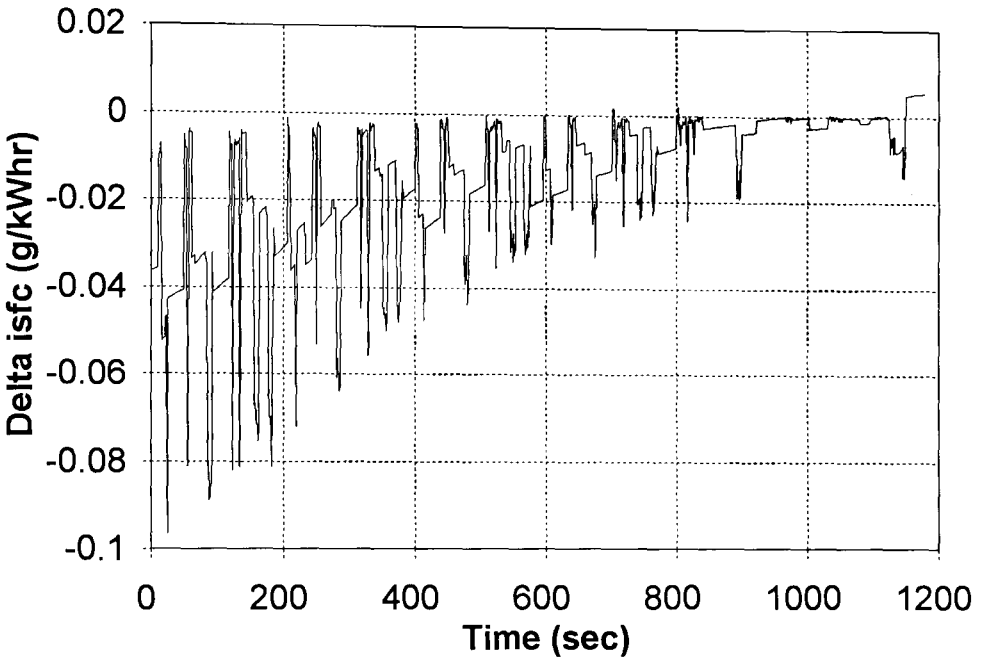

Figure 9.12
Change in isfc (Delta isfc) when start/soak temperature is reduced from fully-warm start to 20°C, as a function of time from drive cycle start for 2 litre engine in a 1200 kg vehicle.

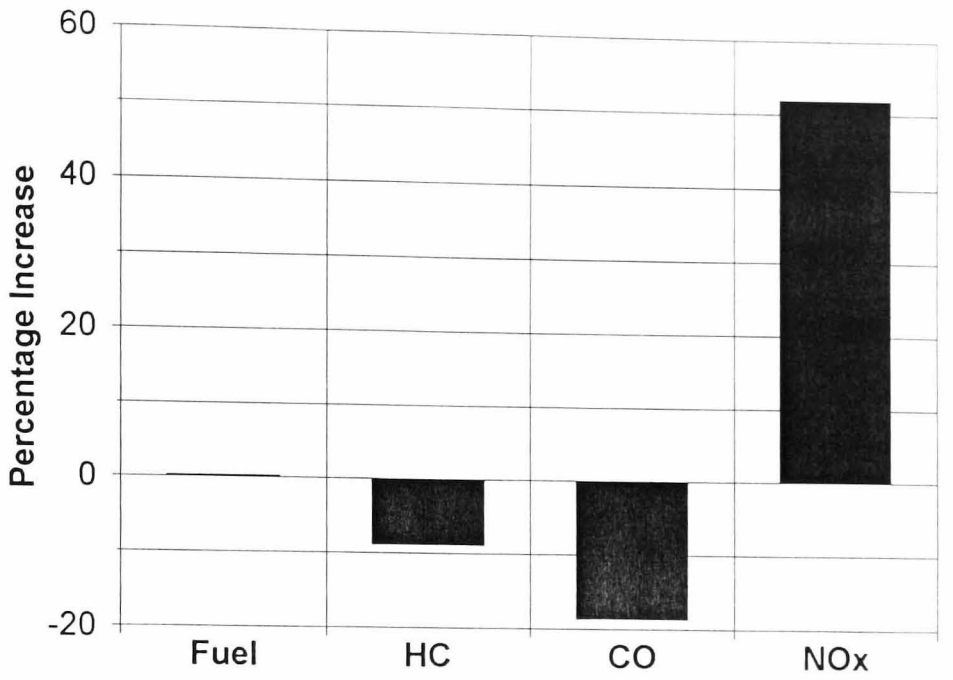

Figure 9.13
Effect of removing EGR from fully-warm engine dynamometer data on ECE+EUDC drive cycle fuel consumption and feedgas emissions.

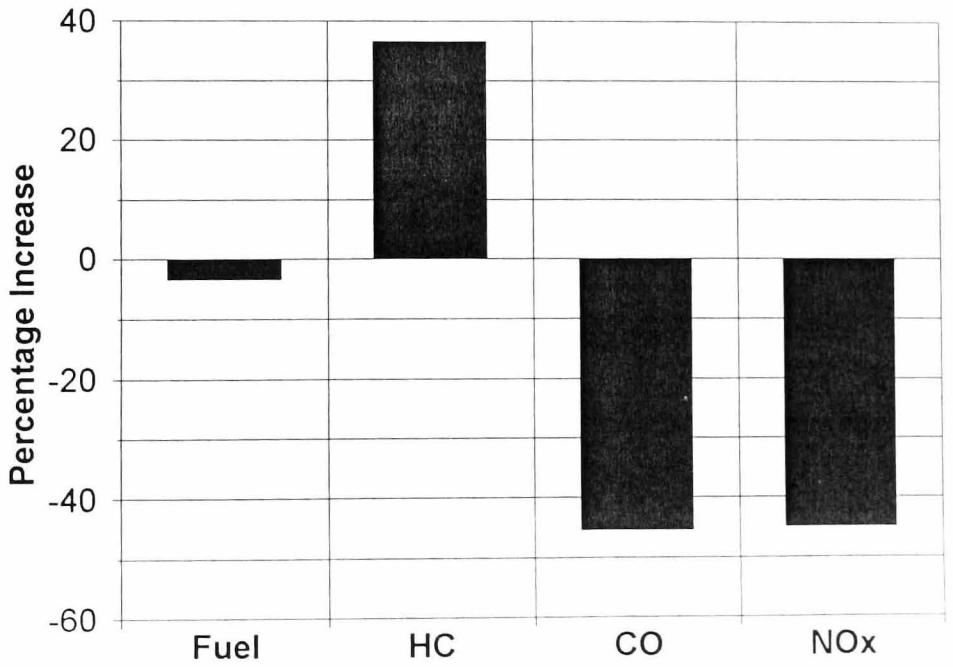

Figure 9.14
Effect on ECE+EUDC drive cycle fuel consumption and feedgas emissions of running lean of stoichiometric during cruise conditions.

Appendix A

ECT Correction Factor Modelling

A.1 Introduction

This appendix details the definition and form of the three ECT Correction Factor functions used in Chapter 5 of this thesis. For each of the three indicated specific emissions examined (isco, ishc and $isno_x$) a function relating the ratio of the indicated specific emission at a given coolant temperature to that at fully-warm coolant temperature has been defined, such that:

$$F_{ECT,T} = \frac{value_T}{value_{85°C}} \qquad (A1)$$

where $F_{ECT,T}$ is the ECT correction factor at engine coolant temperature T and value is the indicated specific emission value. All the test data correction factors were then plotted against ECT for each of the three indicated specific emissions and simple curve fitting to this data used to define three functions to predict ECT correction factors independently of engine speed, load and AFR. These functions are detailed in Table A1 and shown in Figure A1.

Table A1

ECT Correction Factor Functions

Pollutant	Function of absolute temperature (T)	Coefficients		
		a	b	c
isco	$F_{ECT,isco}(T) = a + bT$	0.39	0.001779	-
ishc	$F_{ECT,ishc}(T) = a + bT + cT^2$	11.1897	-0.05762	8.143×10^{-5}
$isno_x$	$F_{ECT,isno_x}(T) = \frac{1}{a + bT + cT^2}$	13.4620	-0.06907	9.564×10^{-5}

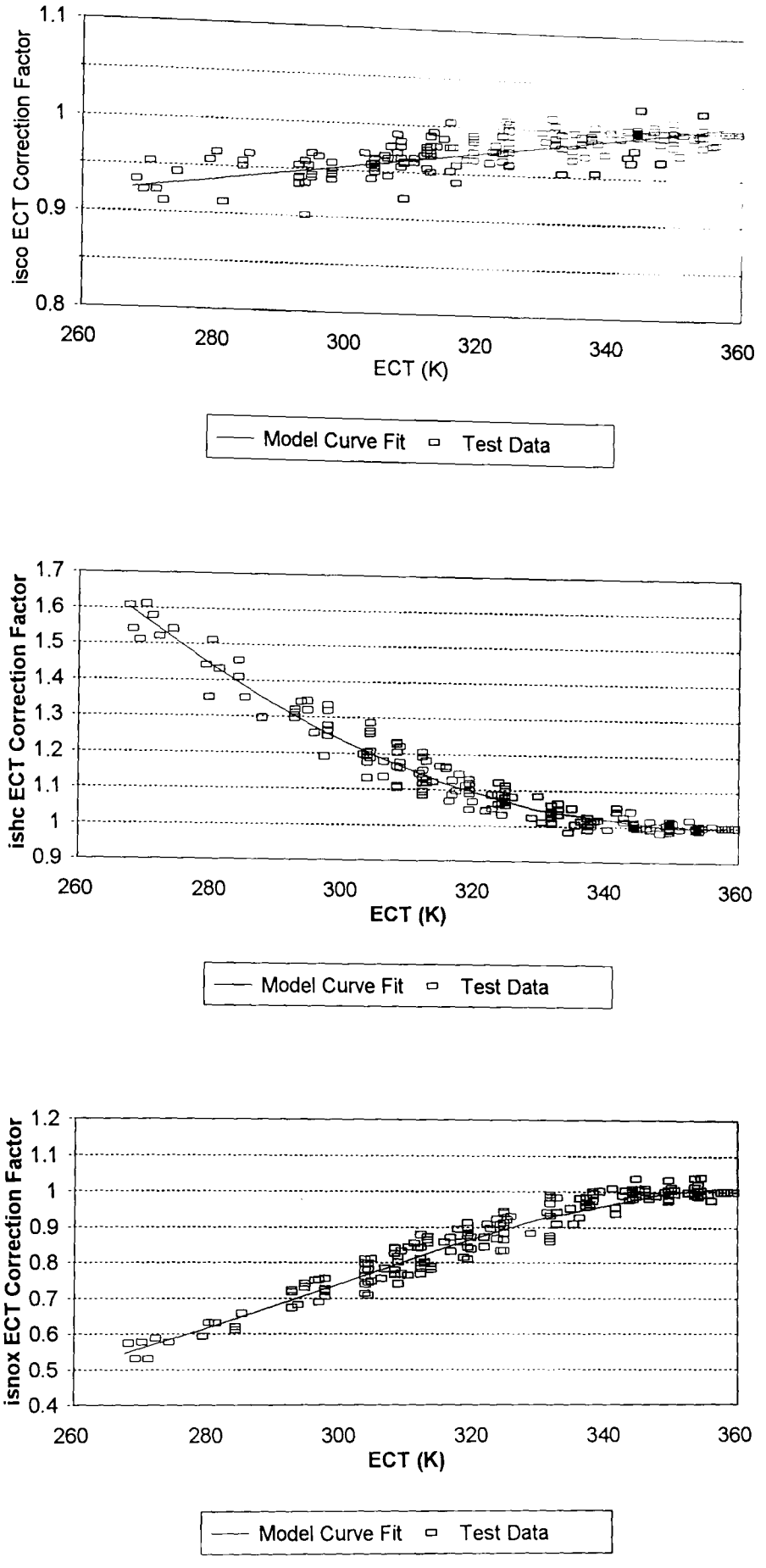

Figure A1

Indicated specific emissions divided by fully-warm indicated specific emissions (ECT Correction Factor) against ECT for 2 litre DOHC 8V warm-up test data with range of speeds, imeps and AFRs.
(1250-2500 rpm, 2.5-7.5 bar, 12:1-17.5:1)

Appendix B

Steady-State Friction Model Equations [6.9]

Table B1

Components	Description	Equation
Bearings	Main Bearing Seals	$1.22\times10^{5}\left(\frac{D_b}{B^2Sn_c}\right)$
	Main Bearings Hydrodynamic Friction	$3.03\times10^{-4}\left(\frac{ND_b^3L_bn_b}{B^2Sn_c}\right)$
	Main Bearings Turbulent Dissipation	$1.35\times10^{-10}\left(\frac{N^2D_b^2n_b}{n_c}\right)$
	Con Rod Bearings	$3.03\times10^{-4}\left(\frac{ND_b^3L_bn_b}{B^2Sn_c}\right)$
	Cam Shaft Bearings	$4.12 + 2.44\times10^{2}\left(\frac{Nn_b}{B^2Sn_c}\right)$

Table B1 (continued)

	Description	Equation
Piston	Piston Body Friction	$2.94\times10^{2}\left(\frac{S_p}{B}\right)$
	Piston Rings (without Gas Pressure Loading)	$4.06\times10^{4}\left(1+\frac{1000}{N}\right)\frac{1}{B^2}$
	Piston Rings (Due to Gas Pressure Loading)	$6.89\ \frac{P_i}{P_a}\left[0.088r_c+0.182r_c^{(1.33-kS_p)}\right]$ where $k = 2.38\times10^{-2}$ s/m

Table B1 (continued)

Components	Description	Equation
Valve Train	†Roller Follower	$C_{rf}\left(\frac{Nn_v}{Sn_c}\right)$
	†Flat Follower	$C_{ff}\left(1+\frac{1000}{N}\right)\frac{n_v}{Sn_c}$
	Oscillating Hydrodynamic Term	$C_{oh}\left(\frac{L_v^{1.5}N^{0.5}n_v}{BSn_c}\right)$
	Oscillating Mixed Term	$C_{om}\left(1+\frac{1000}{N}\right)\frac{L_v n_v}{Sn_c}$
Auxiliary Component Losses	Coolant Pump, Oil Pump and Alternator	$6.23 + 5.22\times10^{-3}N - 1.79\times10^{-7}N^2$

† For any given valve train configuration, only one of the two follower friction terms needs to predict cam follower friction.

Nomenclature for Table B1

B Bore (mm)

c Radial journal bearing clearance

C_{rf} Constant for cam roller follower friction term

C_{ff} Constant for cam flat follower friction term

C_{oh} Constant for oscillating hydrodynamic friction term

C_{om} Constant for oscillating mixed lubrication friction term

D_b Bearing diameter (mm)

D_v	Valve diameter (mm)
n_v	Volumetric efficiency
fmep	Friction mean effective pressure
L_b	Bearing length (mm)
L_s	Maximum valve lift (mm)
N	Engine speed (rpm)
n_b	Number of bearings
n_c	Number of cylinders
n_v	Number of valves
P_a	Atmospheric pressure (kPa)
P_i	Intake manifold pressure (kPa)
r_c	Compression ratio
S	Stroke (mm)
S_p	Mean piston speed (m/s)